1-21-2015 12:00 AM

Development And Study Of Measurement Methods For Jets And Bogging In A Fluidized Bed

Majid Hamidi
The University of Western Ontario

Supervisor
Dr. Cedric Briens
The University of Western Ontario Joint Supervisor
Dr. Franco Berruti
The University of Western Ontario

Graduate Program in Chemical and Biochemical Engineering
A thesis submitted in partial fulfillment of the requirements for the degree in Doctor of Philosophy

DEVELOPMENT AND STUDY OF MEASUREMENT METHODS FOR JETS AND BOGGING IN A FLUIDIZED BED

(Thesis Format: Integrated Article)

by

Majid Hamidi

Graduate Program
In
Engineering Science
Department of Mechanical and Materials Engineering

A thesis submitted in partial fulfillment of the requirements for the degree of
Doctor of Philosophy

The School of Graduate and Postdoctoral Studies

The University of Western Ontario

London, Ontario Canada

ABSTRACT

In gas-fluidized processes such as Fluid Coking™ and Fluid Catalytic Cracking, heavy hydrocarbons are converted to lighter products. In the Fluid Coking process, heavy oil feed is contacted with hot fluidized coke particles, heats up and undergoes thermal cracking. If the local concentration of liquid is very high, particles may stick together which can eventually result in process upset because of poor fluidization or even defluidization, a condition commonly known in industry as "bogging".

Coke particles in a Fluid Coker have a high dielectric constant and can concentrate an electric field within themselves. Using a capacitance sensor, the void distribution in a bed of coke particles can be visualized based on the difference in dielectric constant between coke particles and the fluidization gas. The voidage fluctuations caused by gas bubbles have been shown to change dramatically as the bed becomes bogged. Therefore, capacitance sensors are capable of predicting the bogging condition in fluid cokers. However, they should be properly designed to account for the bed geometry, the position of sensors, the temperature and the degree of electromagnetic noise in the area. This was the primary research objective for this thesis.

The first part of the thesis research focused on designing noiseless capacitance sensors that can be used to measure the liquid concentration in a fluidized bed as well as bubble properties and the length of jet cavities. The effect of bogging on the distribution of a liquid sprayed into fluidized bed was then investigated by determining the impact of bogging on the breakage rate of the liquid-solid agglomerates that are formed when a liquid is sprayed into a fluidized bed. Bubble rise velocity and frequency was measured at different locations of the fluidized bed to understand and predict early bogging.

Pressure measurements are easier to perform in industrial units than capacitance measurements. The knowledge acquired with capacitance measurements was then applied to the design of early bogging detection methods from pressure measurements. A bogging index was proposed; it uses a Kolmogorov-Smirnov test of the wavelet coefficients of pressure fluctuations and was optimised using a genetic algorithm to detect early bogging.

Detection of bogging with acoustic measurements is discussed in the next section. The speed of sound was measured at different levels of particles cohesiveness and fluidization velocities. Experimental data was compared with the results of simulations with the COMSOL acoustic toolbox.

The last part of the thesis applies the new capacitance sensors to the measurement of jet cavity fluctuations in fluidized beds. Two types of jets were investigated: the supersonic gas jets used for particle attrition in fluidized beds and the jets formed when liquid is atomized with a gas into a fluidized bed. Jet fluctuations can cause the erosion of fluidized bed internals and must be known when designing a fluidized bed. A new correlation was developed to predict the fluctuations of the jet penetration in fluidized beds. The effect of bogging on jet fluctuations was also investigated. The results of these experiments were interpreted with the previously developed correlations.

Keywords:

Fluidized bed, bogging detection, capacitance measurements, agglomerate breakage, bubble properties, wavelet analysis, supersonic jet fluctuation

CO-AUTHORSHIP

Chapter 2

Article Title:
A novel Ac-based capacitance sensor with differential noise cancelling
Authors:
Majid Hamidi, Cedric Briens, Franco Berruti, Jennifer McMillan
Article Status:
Unpublished

Chapter 3

Article Title:
Effect of fluidized bed bogging on distribution of sprayed liquid on fluidized particles
Authors:
Majid Hamidi, Cedric Briens, Franco Berruti, Jennifer McMillan
Article Status:
Published
Contributions:
Majid Hamidi conducted all experimental work, data analysis and writing. Cedric Briens, Franco Berruti and Jennifer McMillan provided guidance, supervision and revised drafts of the work.

Chapter 4

Article Title:
Early detection of defluidization using wavelet analysis of pressure fluctuations
Authors:
Majid Hamidi, Cedric Briens, Franco Berruti, Jennifer McMillan
Article Status:

Unpublished
Contributions: Majid Hamidi conducted all experimental work, data analysis and writing. Cedric Briens, Franco Berruti and Jennifer McMillan provided guidance, supervision and revised drafts of the work.

Chapter 5

Article Title: Early detection of defluidization from measured speed of sound
Authors: Majid Hamidi, Cedric Briens, Franco Berruti, Jennifer McMillan
Article Status: Unpublished
Contributions: Majid Hamidi conducted all experimental work, data analysis and writing. Cedric Briens, Franco Berruti and Jennifer McMillan provided guidance, supervision and revised drafts of the work.

Chapter 6

Article Title: Study of supersonic gas jets fluctuations in a gas-solid fluidized bed with capacitance sensors
Authors: Majid Hamidi, Cedric Briens, Franco Berruti, Jennifer McMillan
Article Status: Unpublished
Contributions:

Majid Hamidi conducted all experimental work, data analysis and writing. Cedric Briens, Franco Berruti and Jennifer McMillan provided guidance, supervision and revised drafts of the work.

Chapter 7

Article Title: Effect of bogging on gas and gas-liquid jet fluctuations
Authors: Majid Hamidi, Cedric Briens, Franco Berruti, Jennifer McMillan
Article Status: Unpublished
Contributions: Majid Hamidi conducted all experimental work, data analysis and writing. Cedric Briens, Franco Berruti and Jennifer McMillan provided guidance, supervision and revised drafts of the work.

Contributions: Majid Hamidi conducted all experimental work, data analysis and writing. Cedric Briens, Franco Berruti and Jennifer McMillan provided guidance, supervision and revised drafts of the work.

ACKNOWLEDGEMENTS

First, I would like to express my gratitude to my supervisors Dr. Cedric Briens and Dr. Franco Berruti from the Institute of Chemicals and Fuels from Alternative Resources (ICFAR) at the University of Western Ontario, for their guidance and support throughout the completion of my thesis work. Dr. Briens and Dr. Berruti kindly shared their knowledge and expertise to help on my research work, I am truly thankful for all of that. I would like to thank Dr. Jennifer McMillan, of Syncrude Canada, for providing me with valuable feedback and ensuring that my research was industrially relevant. Special thanks to Rob Taylor for his help on my experimental equipment. I also wish to acknowledge all my colleagues from ICFAR. It was great to know you all and thank you for all your help in my research work.

At last, my deepest gratitude goes to my wife, Maryam Mohagheghi Dar ranji, for her unconditional support and love. I would not have been able to pursue my education in Canada and complete my PhD degree if you had not always believed in me. I would like to dedicate this thesis to my beloved wife.

Table of Contents

LIST OF TABLES

LIST OF FIGURES

NOMENCLATURE

A Approximation wavelet component

A Wavelet scale

A_e Cross section area of nozzle exit (m^2)

a_p Particle acceleration, m/s^2

a_s Characteristic dimension, m

B Bogging index

c Speed of sound, m/s

C_{ij} Capacitance (F)

D Effective electric field length, m

D_c Bed hydraulic diameter (m)

D_i Detail wavelet component

d_w Bubble distance from the wall, cm

d_s Distance between two sources, m

d_p Particle Sauter mean diameter (m)

d_o Nozzle exit diameter (m)

d_{th} Nozzle throat diameter (m)

F Thrust of the nozzle (N)

g Normalized total free liquid

GLR Gas-to-liquid ratio, wt%

H_o Static bed height (m)

I Normalized bogging index

I_n Electrical current (A)

M Total mass, kg

m Level of oil mass fraction

$\dot{m}$ Nozzle mass flowrate (kg/s)

n Level of fluidization velocity

nw Number of wavelet octaves

p_o Pressure at nozzle throat (Pa)

p_e Pressure at nozzle exit (Pa)

Q Monopole acoustic source, N/m.kg

R Gas constant, J/mol.K

R_x Electrical resistance (Ω)

SNR_{out} Signal to noise ratio at output

T Temperature, K

t Time, s

U_s Speed of sound in particles, m/s

U_0 Speed of sound in ideal gas, m/s

U_f Fluidization velocity (superficial gas velocity), m/s

U_f Fluidization velocity (m/s)

U_{mf} Minimum fluidization velocity (m/s)

U_o Gas velocity at nozzle exit (m/s)

V_s Source voltage (V)

V_o Output voltage (V)

W Continuous wavelet transform

X Mass concentration of free liquid on a dry solids basis, wt%

z Height from gas distributor (m)

Z Specific acoustic impedance, Ns/m^3

Z_x Electrical impedance (Ω)

α Natural frequency of agglomerate breakage, Hz

α_{jet} Nozzle inclination angle (degree)

γ Ratio of specific heat constants

γ_i Power of wavelet octave

ε Voidage

v Particle velocity, m/s

ξ Particle displacement, m

ρ Density, kg/m^3

ρ_e Gas density at nozzle exit (kg/m^3)

ρ_f Fluidization gas density (kg/m^3)

ρ_g Gas density, kg/m^3

ρ_p Particle density, kg/m^3

Ψ Mother wavelet function

ω Angular frequency, rad

SUBSCRIPTS

br breakage

cal *calculated*

L injected liquid

S dry coke

e evaporated

CHAPTER 1: INTRODUCTION

1.1. Present Thesis Work

Fluidized beds have been in use for decades and have been applied to numerous industries due to their excellent gases and solids mixing, and rapid mass and heat transfer. Fluid Coking as an application of fluidized beds is a continuous process for heavy oil upgrading. The main objective of the thesis is to develop a method to detect early bogging in the Fluid Coking process, using non-invasive methods that can be used in industrial fluidized bed. Analysis of the effect of bogging on jet penetration and its fluctuations is the other objective of the thesis.

After a general introduction to the Fluid Coking process, this chapter reviews published, experimental studies on bogging detection in fluidized beds. The research objectives of this thesis are then presented.

1.2. Fluid Coking Process

Canada has the third largest oil reserves in the world behind Saudi Arabia and Venezuela. Out of the total oil reserves, 170 billion barrels are bitumen from the oil sands, which are currently recoverable and are located in Alberta (Syncrude Canada, 2011). Oil sands contain a mix of clay material, water and a form of heavy oil called bitumen. Bitumen, in its raw form is a dark-colored, asphalt-like oil, that requires upgrading to enable its transportation by pipeline and to be used by conventional refineries.

Heavy oil such as bitumen can be upgraded into synthetic crude oil using Fluid Coking^{TM} which is a thermal, non-catalytic conversion process. Fluid Coking is prefered for upgrading bitumen because of its high flexibility, reliability, continuous operation and low greenhouse gas emissions. Syncrude Canada Ltd. has the three largest Fluid Cokers in the world and is one of the largest producers of crude oil in Canada (Syncrude Canada, 2011).

The Fluid Coker that is used by Syncrude Canada is a two vessels system, including a fluidized bed burner and a fluidized bed reactor, as shown in Figure 1.1 (House, 2007).

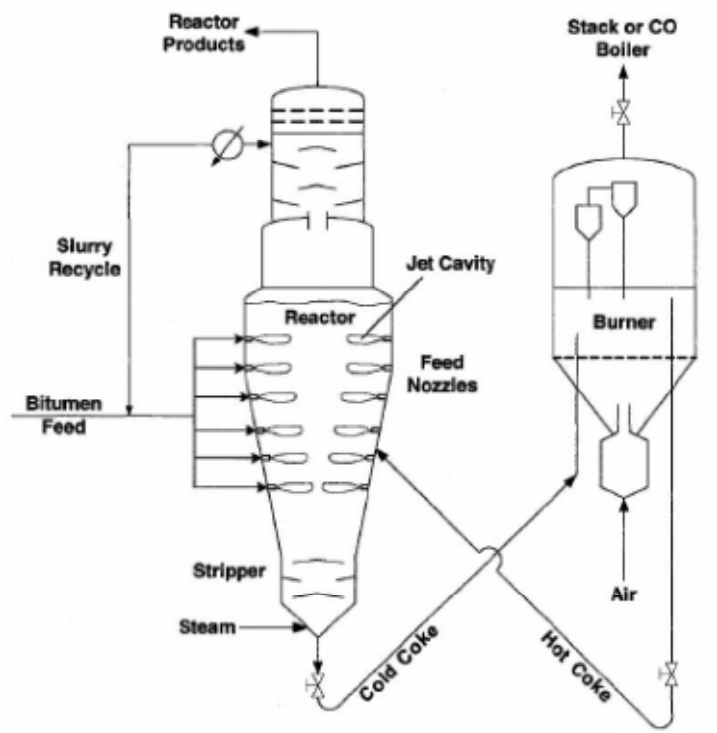

Figure 1.1: The fluid coking process (adapted from House, 2007)

During the process, the fluidized bed burner heats up coke particles to temperatures ranging from 600 to 680 °C while they are transported to the top of the reactor section where they are contacted with bitumen feed, at a temperature ranging from 300 to 400°C.

The coker reactor as the primary equipment in the bitumen upgrading can be divided into three sections: stripper section, reaction section and scrubber section. There are some liquid-gas nozzles in the reaction section to atomize the bitumen and to quickly and uniformly spray it over the individual particles for a stable reaction rate. In the Syncrude fluid coker, these spray nozzles use 600 psig steam to atomize and spray the bitumen into the reactor dense coke bed. Bitumen then thermally cracks on the surface of the hot coke particles, at a temperature ranging from 510 to 550 °C. Vapours released from the thermal cracking of bitumen first go through the cyclones located at the top of the reactor

to remove the entrained coke particles which are sent back to the dense bed into the stripper section. The average superficial velocity of the rising gases is ranging from 0.3 m/s to 1.0 m/s depending upon the coke size to maintain fluidization (Pfeiffer, 1959).After passing the cyclones, the released vapours flow through the condenser to be processed into the shipping section downstream. Coke particles losing heat in the cracking process move down the reactor and circulate back to the reactor after reheating in the burner.

1.3. Problem statement

Industrial fluidized beds are often used for continuous operation, with particles added to or removed from the fluidized bed continuously. In a continuously operating fluidized bed, alteration of hydrodynamic behaviour may occur over time due to imposed or unwanted changes. Changes in fluidization velocity or particle size distribution are examples of imposed changes. Unwanted changes are usually due to formation of cohesive particles, agglomeration or sintering of particles. Formation of cohesive particles can be a serious problem in processes such as thermal cracking of bitumen to naphtha, drying of freshly produced polymers or food and coating of particles for pharmaceutical use. The problem can be worse if the liquid feed rate is sufficiently high that it can result in process upset and defluidization, a condition commonly known in industry as bogging. In Fluid Cokers, bogging can lead to complete unit shut down and clean-out. Therefore, it is important to detect early bogging to prevent unit upset and shut down.

Bogging is a gradual phenomenon. In a wet bed, the minimum liquid concentration above which bed bogging occurs depends on each practical application. The distribution of injected liquid on fluidized coke particles is critical to the operation of commercial Fluid Cokers (Briens, 2003). It is important to determine how bogging can impact this distribution. Therefore, the characterization of early bogging by directly investigating its impact on the breakage kinetics of the wet agglomerates is of crucial importance and very useful for developing effective bogging detection methods.

Bogging also affects the liquid feed jet length and fluctuations in the fluidized bed and results in less liquid-solid mixing. The analysis of the effect of bogging on gas jet and gas liquid jet length and fluctuations is also important to determine the impact of bogging on liquid-solid mixing and yield of the reaction especially in Fluid Cokers.

2. Choice of measurement techniques and analysis methods

In methods reviewed in this section, one or more process parameters are measured during fluidized bed operation. These methods could, therefore, be applied as an online bogging detection system.

Other methods have been published that could not be applied to the routine monitoring of commercial reactors. Positron Emission Particle Tracking (Bridgwater, 2004) is based on tracking a radioactive particle coated with a positron emitter tracer and requires adding radioactive particles to the bed. The "falling ball method" (McDougall, 2005) in which the velocity of a ball falling from the top to the bottom of the bed is measured, characterizes the fluidity of the fluidized bed.

In contrast, most of the bogging detection methods that have been proposed in the literature are concerned with the measurement of process variables that can be applied to large industrial fluidized beds. Examples of these methods are measurement of temperature or pressure (Werther, 1999). In addition, the capacitance measurement based on the designed noiseless circuit described in chapter 2, could also be applied to industrial fluidized beds.

2.1.a. Electrical Capacitance Tomography

Electrical capacitance tomography (ECT) is a measurement method based on the change in the electrical capacitance due to variations in the distribution or concentration of dielectric materials in a given volume. Using the measured capacitance, an image of material distribution can be reconstructed. compared with other tomography methods, ECT is fast (300 frames/s was used in this thesis), low cost, non-invasive, without radiation and can withstand high temperature and pressure in the fluidized bed. The hardware of an ECT system can be designed based on charge/discharge or AC based

circuits with advantages and disadvantages associated with each of those (Yang, 1996). ECT can be used to monitor different processes including fluidized beds, fluidized bed dryers, gas-solids pneumatic conveying and gravity flows. No studies has been reported using ECT directly for bogging detection but there are publications, reviewed below, in which ECT has been applied to identify flow dynamics and liquid concentration that are closely related to bogging.

2.1.a.1. Flow dynamics measurements

Wang et al. studied bubbling and slugging flow regimes in a circulating fluidized bed with a square cross-sectional area using the ECT technique (Wang, 2006). The frequency spectrum, probability density function, and autocorrelation function of the solid holdup fluctuations as well as bubble diameter were calculated under different regimes to investigate chaotic particle behaviours in the fluidized bed. The dominant frequency of bubbles near the wall and near the center of the bed was also obtained by fitting the power spectra as power-law.

Zhao et al. used ECT sensors to obtain the solids distribution in a downflow fluidized bed equipped with specially designed solid distributor (Zhao, 2010). Using reconstructed images, the spatial and temporal characteristics of solids distribution were calculated. Their results showed that their new distributor provided a more uniform solids distribution at the inlet of the downer.

Du et al. analysed and monitored flow dynamics of fluidized beds using the ECT technique (Du, 2004). Choking phenomenon in a circulating fluidized bed for group A and B particles was studied. Using 3D ECT to study solid distribution of FCC catalyst particles (group A particles) in the riser, they found that when the air velocity was lower than the transport velocity, there were double solids ring flow structure and three-region flow structure (solids cluster at the core, solids ring close to the wall and a dilute gas ring region between them). When the air velocity was increased, during choking transition, the solids cluster in the center disappeared suddenly and the flow structure changed to two-region flow (dilute phase at the core and dense phase at the wall region). For sand particles (group B), when the air velocity was lower than the transport velocity, wall

slugs and gas intervals were formed, whereas at higher air velocity, open slugs with particle clusters inside them were observed in the riser.

The studies cited above showed that the ECT technique is a robust method for analysis of material distribution and its movement in a fluidized bed. The technique can therefore be used to measure bubble properties and to detect defluidization in a fluidized bed.

2.1.a.2. Liquid concentration measurements

ECT has been used to detect rapid changes in the hydrodynamic regime of dryers. Chaplin et al. utilized an ECTmethod to measure moisture content in a fluidized bed dryer (Chaplin, 2005). Results were validated with X-Ray tomography that showed that the ECT data were fairly accurate when the moisture content was less than 5 wt%.

Wang et al. utilized ECT for online monitoring of solids moisture in a batch fluidized bed (Wang, 2009). They found that the moisture content only affected the adjacent electrodes. With compensating the measurement error caused by temperature variations, operation efficiency was improved with applying a single closed loop control strategy to process where the data from ECT was used to control actuators.

In summary, the ECT technique was shown to detect local concentration of liquid in the fluidized bed when there was a considerable difference between the dielectric constant of the liquid and the dielectric constant of the other materials.

2.1.b. Pressure measurement

Differential and absolute pressure measurements are the most frequently measured and analyzed parameters influidized beds. Pressure reflects closely the hydrodynamics of fluidized beds. The analysis method can be categorized as linear or non-linear methods. Average pressure drop measurements provide information on global properties of a fluidized bed such as bed height and density while the high frequency components of measured pressure yield useful information on flow characteristics in the fluidized bed.

2.1.b.1. Linear methods

Kai et al. analysed the average deviation of differential pressure fluctuations (standard deviation divided by the average) in a fluidized bed (Kai, 1987). Bubble size was

measured as well using an optical probe in the bed. They observed that the standard deviation of differential pressure fluctuations was correlated with fluidization regime and fluidization quality when fluidization quality was decreasing as the bubble size was increasing. However, the signal was strongly correlated with fluidization velocity as well.

The variance of high-frequency pressure fluctuations was used for bogging warning (Chirone, 2006). A steady decrease in variance of high-frequency (100 Hz) pressure fluctuations observed during combustion of pine seed shells in fluidized beds with internal diameters of 10 and 37 cm. However, the effect of changes in fluidization velocity on this method was unknown.

Daw et al. patented a technique called "Fluidization quality analyzer" to determine fluidization quality by measuring high-frequency pressure drop over the whole or part of the fluidized bed (Daw, 1995). The pressure signal was amplified by a "buffer amplifier" and processed by a low-pass filter, a differentiator, a rectifier and a PID-controller that compared the signal to a predefined set point and regulated a control valve to adjust the gas flowrate being fed to a fluidized bed. The system was not designed directly to detect bogging but has potential for bogging detection.

To sum up, methods based on the standard deviation of pressure or high-frequency component of a pressure signal can indicate the bogging phenomena. However, these methods are not only sensitive to the fluidization quality, but also to changes in the fluidization velocity (Van Ommen, 1999). This drawbackposes a problem for robust implementation of these methods in industrial fluidized beds where fluctuations in the fluidization velocity are common.

2.1.b.2. Non-linear methods

Many non-linear analysis methods have been developed based on the so-called state-space projection. In general, at a certain time, the state of a dynamical system such as a fluidized bed can be determined by projecting all state variables of the system into a multi-dimensional space. A set of successive states of the system during its evolution in time is called the "attractor". The attractor is often considered as the characteristic measure for a dynamical system. Takens showed that time series of just one characteristic

variable can, theoretically, reconstruct the dynamic state of the system (Takens, 1981). Using time-delay coordinates, it is possible to convert the time series of local pressure in the fluidized bed to delay vectors that can be seen as characteristic measure of the hydrodynamics of the fluidized bed (Takens, 1981). The “bin method” (Fuller, 1993), “symbol statistics method” (Daw, 1998), “attractor properties method” (van der Stappen, 1993) and “attractor comparison method” (van Ommen, 2000) are nonlinear pressure analysis methods that have been proposed to detect bogging based on space state projection. The “attractor comparison method” was shown to be insensitive towards effects other than bogging within specific limits.

Some studies have proposed statistical methods that are based on the statistical distance between the probability distribution of a reference pressure signal and the pressure signal at the current state of the fluidized bed. The Kullback-Leibler distribution distance (Gheorghiu, 2004) and the Kolmogorov–Smirnov statistic (Bartels, 2010) were proposed based on this analysis method to detect early bogging in a fluidized bed. Both methods were able to detect early agglomeration in the fluidized bed. While the sensitivity of the Kullback-Leibler method to fluidization velocity was not discussed in the publication, a comparison of the probability distribution of pressure signal based on Kolmogorov-Smirnov test was shown not to be sensitive to changes in the fluidization velocity. The reference probability distribution of pressure fluctuations need to be measured during the normal, desired operating condition of a fluidized bed, which is unfortunately not a constant condition in industrial fluidized beds.

The W-statistic method proposed by McDougall et al. is based on high frequency pressure fluctuation measurements in the fluidized bed to detect early bogging (McDougall, 2005). The underlying rationale is that in the poor fluidity condition, the fluidized bed transmit pressure fluctuations less well than a well-fluidized bed. Small pressure fluctuations can be considered the result of pressure waves transmitted from events far from the pressure tap, while large fluctuations are assumed to result primarily from local events. The small pressure fluctuations are calculated by subtracting from the raw signal, a signal smoothed using a wavelet transform of the raw signal. The method could detect early bogging with different liquid sprayed into a fluidized bed of coke powder. The W-statistic method was also successfully applied to a pilot-plant fluidized

bed where coke particles were fluidized with steam and heavy oil was the liquid sprayed into the bed. The effect of changes in fluidization velocity was not investigated.

In summary, non-linear analysis methods of pressure measurements received great attention in the reviewed publications. Attractor comparison and Kolmogorov–Smirnov test were shown to be insensitive to effects other than agglomeration.

2.1.c. Acoustic emission

Acoustic emissions refer to pressure waves with a specific frequency range that are emitted from a fluidized bed. They can therefore be considered as shift of pressure measurements to a higher frequency range and relevant to bogging in the fluidized bed.

Fluidized rigid particles emit sound when they collide with each other. For single size spherical particles, the generated fundamental frequencies and their harmonics can be calculated using equation of motion for isotropic elastic spheres. When two spheres with different diameters collide, the low frequency component of so-called "beat frequencies" results from the interference of their two fundamental frequency signals. Collision of particles with a Gaussian size distribution results in a distribution of frequency differences that causes characteristic beat frequency patterns. Leach et al. showed that beat patterns are linearly correlated with particle size and the mean frequency can be used to detect changes in particle size distribution and agglomeration (Leach, 1978).

Zukowski directly evaluated the amplitude of the acoustic emission signal during the combustion of gaseous fuels in a bubbling fluidized bed of inert particles. Sound waves with frequencies within the audible range were measured by a microphone placed outside the fluidized bed (Zukowski, 1999). The mean intensity of the acoustic signal was found to correlate with bed temperature. A low amplitude signal was observed when the process was relatively smooth at higher temperature in the range of 950 ^{o}C. The amplitude of the signal was higher at lower temperature when exploding bubbles were the dominant acoustic source. The work isn't directly related to bogging detection but made it is clear that acoustic signals contain valuable information about the bubbling behaviour in the fluidized bed.

Book et al. used two microphones and an accelerometer to determine the fluidization quality of a large scale gas–solid fluidized bed of particles, using multi-linear and power law regressions of traditional (Fourier analysis) and advanced (wavelet decomposition) signal analysis. The measurements were well correlated to physical measurements of fluidization quality in the bed (Book, 2011).

Principal component analysis (PCA) has also been used to analyseacoustic measurements in fluidized beds (Halstensen, 2006). High-temperature accelerometers were installed at different locations of a urea granulator to measure the sound waves. The process was monitored using the score-plot for the first two principal components of the measured signal. The method was capable of detecting unwanted lump-formation in the bed about 30 minutes in advance.

Wang et al. used chaos analysis to detect bogging in a fluidized bed (Wang, 2009). The signal measured by acoustic emission sensors was first divided into micro-, meso-, and macroscales by wavelet transform. A coefficient of malfunction was then defined based on Kolmogorov entropy and correlation dimension, which are measures of unpredictability of the signal. The proposed coefficient of malfunction was found tobe sensitive to bogging. However, the method could detect bogging in the fluidized bed only after formation of cohesive particles.

To sum up, acoustic emissions from fluidized bed processes have been used to determine the fluidization state and bogging. However, it is still not clear if this method can detect early bogging. Since other acoustic sources can affect the signal, one has to carefully select the measuring equipment and location to avoid irrelevant sound emissions (Chen, 2005).

2.1.d. Temperature measurement

Temperatures are often measured in fluidized beds (Werther, 1999). In some fluidized bed processes, temperature signals carry information on the level of mixing of the bed, i.e. how quickly differences among local measured temperatures disappear. Temperature measurements are generally more localized with smaller temporal resolution compared to pressure measurements.

Lau and Whalley developed a method to detect bogging based on the temperature difference between two radial locations in a batch fluidized bed of caking coals (Lau and Whalley, 1981). Since sticky bed material slowed down bed circulation, the thermal boundary surface shifted away from the wall toward the center of the fluidized bed. The temperature difference between two radially separated points was measured with a differential thermocouple (DT). One thermocouple mounted at the center of the bed and the other one was close to the wall. The temperature difference as well as the variance of local temperature was higher at lower bed fluidity so the method was able to detect bogging. However, the temperature difference was also sensitive to fluidization velocity.

Scala et al. proposed a method based on the variance of the measured temperature as well as the vertical temperature difference in a fluidized bed (Scala, 2006). Both of these parameters are influenced by the extent of mixing of particles in the fluidized bed. A laboratory-scale bubbling fluidized bed of silica sand equipped with electrical heaters was used for their experiments. During the experiments, operating conditions of the bed were held constant until defluidization occurred. The variance of the temperature signal measured by the upper probe decreased as it approached the initial point of defluidization while the normalized relative temperature difference increased at the same time. The results looked promising in terms of detection of bogging. However, the influence of fluidization velocity was not investigated.

In summary, the temperature uniformity is closely related to the fluidization quality. A decrease in the bed fluidity causes the temperature difference between different locations of the bed to increases while the variance in local temperatures decreases at the same time. The methods seem promising for detecting early bogging but variations in the fluidization velocity can make those methods problematic in industrial applications.

3. Research Objectives

This research work aimed at developing robust methods for detecting early bogging in industrial fluidized beds. In addition the work investigate the effect of bogging on gas and gas-liquid jet lengths and fluctuations. The work was broken down into six studies.

The objective of the first study was provide basic measurement tools that could be used in the rest of the thesis. A noiseless capacitance sensor was developed for void and liquid measurements in a fluidized bed.

The objective of the second study was to develop a non-invasive technique to detect early bogging in a fluidized bed based on capacitance measurements. Early bogging condition is defined from its impact on the breakage of wet agglomerates which is an inherent characteristic of the solid and liquid interaction. To provide basic information for the rest of the thesis, the impact of bogging on bubble properties was also studied.

The objective of the third study was to develop a method based on pressure fluctuations to detect early bogging. The objective of the fourth study was to investigate and model the impact of bogging on the speed of sound in the fluidized bed, and relate it to observed changes in bubble properties.

The objective of the fifth study was to measure the fluctuations of the penetration depth of supersonic jets in fluidized beds. A jet length correlation was also be developed.

The objective of the sixth study was to investigate the effect of bogging on the fluctuation of gas and gas liquid jets at different gas to liquid ratios and fluidization velocities.

4. References

Bartels, M. Nijenhuis, J. Kapteijn, F. Van Ommen, .J.R. “Case studies for selective agglomeration detection in fluidized beds: Application of a new screening methodology” Powder Technology 2010, 203(2):148-166.

Book G, Albion K, Briens L, Briens C, Berruti F, “On-line detection of bed fluidity in gas–solid fluidized beds with liquid injection by passive acoustic and vibrometric methods”, Powder Technology. 2011, 205: 126–113.

Bridgwater J, Forrest S, Parker DJ. “PEPT for agglomeration?” Powder Technology, 2004, 140(3):187 – 93.

Briens C, McDougall S, Chan E. "On-line detection of bed fluidity in a fluidized bed coker" Powder Technology. 2003, 138(23): 160-168.

Chaplin G, Pugsley T, van der Lee L, Kantzas A, Winters C, “The dynamic calibration of an electrical capacitance tomography sensor applied to the fluidized bed drying of pharmaceutical granule”, Meas. Sci. Technol. 2005,16:1281–1290.

Chen G, Parsa V, Briens L, Briens C, Smith R, “Application of Adaptive Noise Cancellation to Acoustic Emissions of A Rotary Dryer”, “Acoustics Week in Canada”, London, Canada, October 12 - 14, 2005.

Chirone R, Miccio F, Scala F. “Mechanism and prediction of bed agglomeration during fluidized bed combustion of a biomass fuel: effect of the reactor scale”, Chem Eng J. 2006, 123(3):71 – 80.

Daw CS, Finney CEA, Nguyen K, Halow JS. “Symbol statistics: a new tool for understanding multiphase flow phenomena”, In: Nelson Jr RA, Chopin T, Thynell ST, editors. Proceedings of the ASME heat transfer division, vol. 5. New York: ASME; 1998. p. 221 – 9.

Daw CS, Hawk JA; US Deptartment Energy (USAT). “Fluidisation quality analyser for fluidised beds” Patent US5435972A, 1995.

Du B, Fan L.S, “Characteristics of choking behavior in circulating fluidized beds for group B particles”, Ind. Eng. Chem. Res. 2004, 43:5507–5520.

Du B, Warsito W, Fan L.S, “ECT studies of the choking phenomenon in a gas–solid circulating fluidized bed”, AIChE J. 2004, 50:1386–1406.

Fuller TA, Flynn TJ, Daw CS, Halow JS. “Interpretation of pilot-scale, fluidizedbed behavior using chaotic time series analysis”, In: Rubow LN, editor, Proceedings of the 12th international FBC conference, vol. 1, 1993, p. 141 – 55.

Gheorghiu S, van Ommen JR, Coppens MO. “Monitoring fluidized bed hydrodynamics using power law statistics of pressure fluctuations”, In: Arena U, Chirone R, Miccio M, Salatino P, editors. Fluidization XI. Engineering conferences international; 2004. p. 403 – 10.

Halstensen M, de Bakker P, Esbensen KH. “Acoustic chemometric monitoring of an industrial granulation production process—a PAT feasibility study”, Chemometr Intell Lab Systems 2006, 84(1 – 2):88 – 97.

House, P., “Interaction of gas-liquid jets with gas-solid fluidized beds: Effect on liquid solid contact and impact on fluid coker operation”, Ph.D. dissertation. The University of Western Ontario, London, Canada, 2007.

Kai T, Furusaki S. “Methanation of carbon dioxide and fluidization quality in a fluid bed reactor—the influence of a decrease in gas volume”, Chem Eng Sci. 1987, 42(2):335 – 9.

Lau IT, Whalley BJP. “A differential thermal probe for anticipation of defluidization of caking coals”, Fuel Process Technol 1981, 4(2 – 3):101 – 15.

Leach MF, Rubin GA, Williams JC. “Analysis of Gaussian size distribution of rigid particles from their acoustic emission”, Powder Technology 1978, 19(2):189 – 95.

McDougall S, Saberian M, Briens C, Berruti F, Chan E. “Using dynamic pressure signals to assess the effects of injected liquid on fluidized bed properties” Chem Eng Process 2005, 44(7):701 – 8.

Pfeiffer, R. W.; Borey, D. S.; Jahnig, C. E. Fluid coking of heavy hydrocarbons US2881130, 1959.

Scala F, Chirone R. “Characterization and early detection of bed agglomeration during the fluidized bed combustion of olive husk”, Energy Fuels 2006, 20(1):120 – 32.

Syncrude Canada Ltd., <<http://www.syncrude.ca/users/folder.asp>>, 2011

Takens F. “Detecting strange attractors in turbulence. Lecture notes in mathematics. In: Rand DA, Young L-S, editors. Dynamical systems and turbulence”, Berlin, Germany: Springer; 1981. p. 366.

Van der Stappen MLM, Schouten JC, van den Bleek CM. “Deterministic chaos analysis of the dynamical behaviour of slugging and bubbling fluidized beds”, In: Rubow L, Commonwealth G, editors. Proceedings of the 12th international conference on fluidized bed combustion, vol. 1. New York, USA: ASME; 1993. p. 129 – 40.

Van Ommen JR, Coppens MO, van den Bleek CM, Schouten JC. “Early warning of agglomeration in fluidized beds by attractor comparison”, AIChE J 2000; 46:2183 – 97.

Van Ommen JR, Schouten JC, van den Bleek CM. “An early-warning-method for detecting bed agglomeration in fluidized bed combustors”, In: Reuther RB, editor. Proceedings of the 15th international conference on fluidized bed combustion, Paper no. FBC99-0150. New York: ASME; 1999

Wang H.G, Senior P.R, Mann R, Yang W.Q., “Online measurement and control of solids moisture in fluidised bed dryers”, Chem. Eng. Sci. 2009, 64:2893–2902.

Wang J, Cao Y, Jiang X, Yang Y. “Agglomeration detection by acoustic emission (AE) sensors in fluidized bed”, Ind. Eng. Chem. Res. 2009, 48:3466-3473

Werther J. “Measurement techniques in fluidized beds” Powder Technology, 1999, 102:15 – 36.

Yang W.Q, Hardware design of electrical capacitance tomography systems, Meas. Sci. Technol. 1996, 7, 225–232.H.G. Wang, W.Q. Yang, T. Dyakowski, S. Liu, Study of bubbling and slugging fluidized beds by simulation and ECT, AIChE J. 2006, 52:3078–3087

Zhao T, Takei M, “Discussion of the solids distribution behavior in a downer with new designed distributor based on concentration images obtained by electrical capacitance tomography”, Powder Technol. 2010, 198:120–130.

Zukowski W. “Acoustic effects during the combustion of gaseous fuels in a bubbling fluidized bed”, Combust Flame 1999, 117(3):629 – 35.

CHAPTER 2: A NOVEL AC-BASED IMPEDANCE METER TO REDUCE CAPACITIVE AND INDUCTIVE COUPLING NOISE

2.1. Introduction

Electrical impedance measurements have been used in material characterization and applied to several areas from biological tissue characterization (Geddes, 1989) to obtain information in fluidized beds (Du, 2006). Various methods have been described in literature, such as: network analysis method, FFT-based method, resonant method, RF I-V method and auto balancing bridge method (Yamazaki, 2010, Randus, 2011, Angrisani, 1996). The auto balancing bridge method has wide frequency coverage from LF to HF and high accuracy over a wide impedance measurement range while other methods are usually used for a specific frequency range (Angrisani, 1996). In industrial applications of the auto balancing bridge method, a capacitive and inductive coupling noise, can exist. This can affect the output signal, and cause errors in the amplitude and phase of the signal. Solutions have been proposed that included using analog filter, digital filter and lock-in amplifier in the output (Angrisani, 1996). Analog filter can't solve the problem completely because the signal phase will change due to phase response of the filter and the error is a function of frequency. In addition, instability of the filter decreases the amolitude measurement accuracy. If a lock-in amplifier is used, the output signal will be proportional to the product of the signal and reference frequency amplitudes, So the amplitude can be measured with high accuracy if the phase of the signal is known accurately and vice versa (Angrisani, 1996). Therefore an error in one of these parameters causes the error in measuring the other one. Using a digital filter can be a good solution to this problem but it in turn may increase the implementation complexity and costs. This paper presents a novel AC based impedance meter that uses differential measurement. The differential method for noise cancellation allows for a significant increase of the signal to noise ratio independent of the frequency of the noise. The effects of capacitive and inductive coupling noise on both the auto balancing bridge method and the new method are analysed. Experimental results are given to compare the performance of two methods.

2.2. Auto-balancing bridge method

In this method, the impedance is identified by measuring the voltage and current passes across the device under test (DUT). As shown in Figure 2.1 a sine-wave voltage is applied to the DUT and an AC input current is produced. The operational amplifier with a resistive feedback determines this current by converting it to an AC voltage. The DUT impedance can be calculated using the following expression:

$$Z_x = -\frac{V_S}{V_o} R_x$$

(2.1)

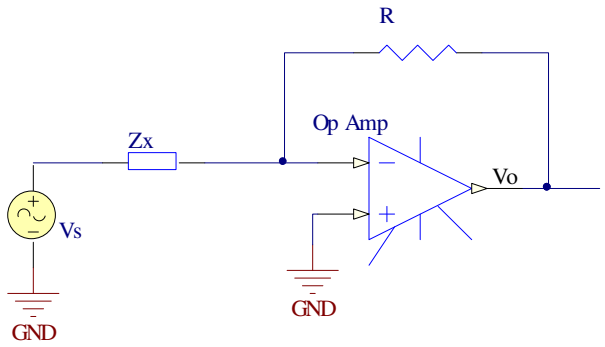

Figure 2.1: Auto balancing bridge circuit

To investigate the effect of capacitive and inductive coupling it is assumed that (Ott, 1988):

1- Shields are from nonmagnetic materials with a thickness much less than skin depth corresponds to the frequency of interest.

2- Induced currents in the cables and shields are small enough not to distort the original field

3- Length of cables is short compared to the wavelength corresponds to the frequency of signal.

Figure 2.2 shows the capacitive coupling between an external conductor and the cable between DUT and operational amplifier in the auto balancing bridge.

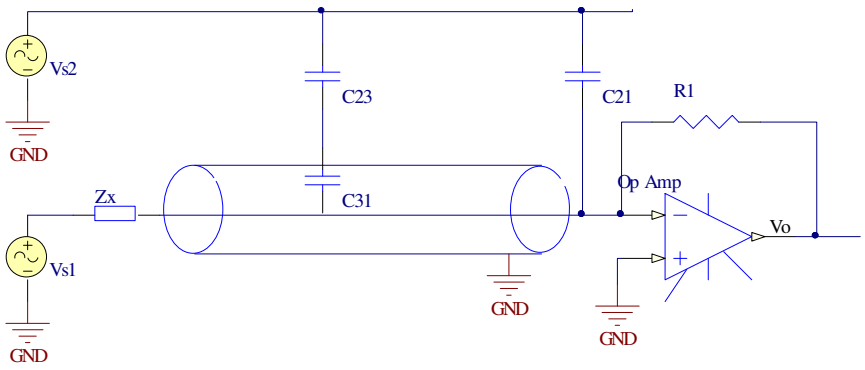

Figure 2.2: Capacitive coupling between a conductor and

The capacitor C_{31} is grounded on both sides and no current can pass through it. Therefore if the grounded shield covers all the interface cable between C_x and the operational amplifier, the noise current which passes through the cable is reduced to zero. However, in practice the cable usually does extend beyond the shield which results in forming a coupling capacitance C_{21}. Therefore a noise current exists in the cable and is amplified by the operational amplifier. The inductive coupling between an external conductor and the cable between DUT and operational amplifier in an auto balancing bridge is shows in Figure 2.3.

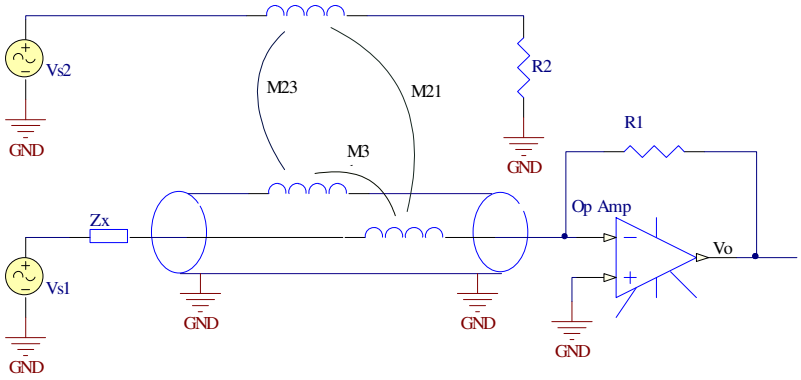

Figure 2.3: Inductive coupling between a conductor and auto balancing bridge circuit

When a current flows in an external conductor it produces a voltage in the cable as well as in the shield that is proportional to the mutual inductance. To reduce the noise the shield should be grounded at the both sides otherwise there is no benefit to use the shield (Ott, 1988). In addition, the noise voltage induced in shield generates a

circulating current and this in turn induces a noise voltage in the cable proportional to M_{31}. To evaluate the effect of this noise on the signal to noise ratio of the output signal, the equivalent circuit is presented in Figure 2.4.

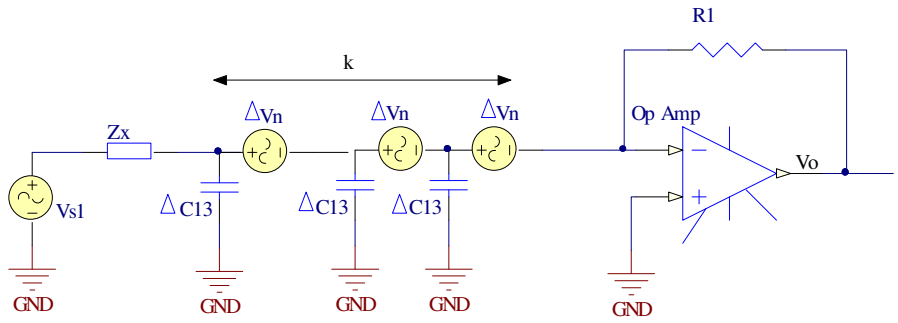

Figure 2.4: Equivalent circuit for the inductive coupling

To analyse the inductive coupling noise effect, the total noise voltage induced in the cable and the total stray capacitance between the cable and the shield are divided into k segments. The noise current passing through R_1 can be calculated as follow:

$$I_n = \Delta V_n \times j\Delta C_{13}\omega_n + 2\Delta V_n \times j\Delta C_{13}\omega_n + \cdots + k\Delta V_n \times j\Delta C_{13}\omega_n + \frac{\Delta V_n}{Z_x} \quad (2.2)$$

Where C_{13} represents the capacitance between the cable and shield, ω_n is the inductive coupling noise frequency. Assuming that:

$$V_n = k\Delta V_n \quad (2.3)$$

$$C_{13} = k\Delta C_{13} \quad (2.4)$$

The noise current can be rewritten as:

$$I_n = j\frac{k+1}{2k}C_{13}\omega_n V_n + \frac{\Delta V_n}{kZ_x} \quad (2.5)$$

And if k approaches infinity it will be:

$$\lim_{k\to\infty} I_n = j0.5C_{13}\omega_n V_n \quad (2.6)$$

The output signal to noise ratio can be written as:

$$SNR_{out} = \frac{P_s}{P_n} = \frac{(R_1 Z_x^{-1} V_{s1})^2}{(R_1 0.5 C_{13}\omega_n V_n)^2} = 4\left(\frac{Z_x^{-1}}{C_{13}\omega_n}\right)^2\left(\frac{V_{s1}}{V_n}\right)^2 \quad (2.7)$$

The supply voltage is always selected to be much greater than the induced noise voltage, therefore the output signal to noise ratio is low where:

$$Z_x \gg \frac{1}{C_{13}\omega_n} \tag{2.8}$$

This constraint limits the application of the Auto-balancing bridge method when the impedance of DUT is too large compared to the capacitive impedance between the cable and the ground or when the cable is too long and the frequency cannot be increased enough to compensate the effect of the length of the cable.

2.3. Proposed impedance meter

2.3.1. Circuit Design

Figure 2.5 shows the proposed circuit for measuring of impedance. The interface cable contains two wires inside a shield conductor. Each wire is connected to an operational amplifier with a resistive feedback like the auto-balancing bridge and the output of operational amplifiers are connected to an instrumentation amplifier.

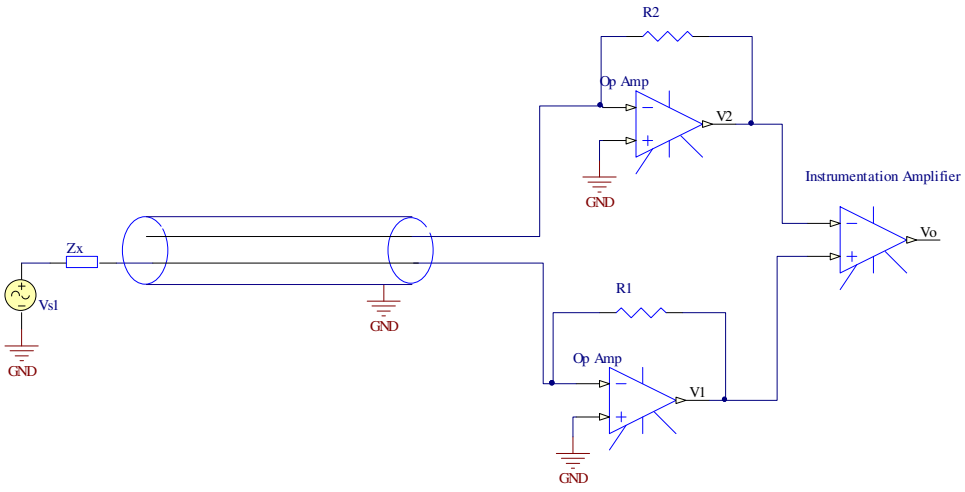

Figure 2.5: Proposed impedance meter

One operational amplifier amplifies the current that passes through DUT as well as the capacitive and inductive coupling noise while the other one just amplifies the same noise so that the noise is eliminated due to subtraction in the instrumentation amplifier.

2.3.2. Effect of capacitive coupling

Figure 2.6 shows the capacitive coupling between an external conductor and the cable between DUT and proposed impedance meter.

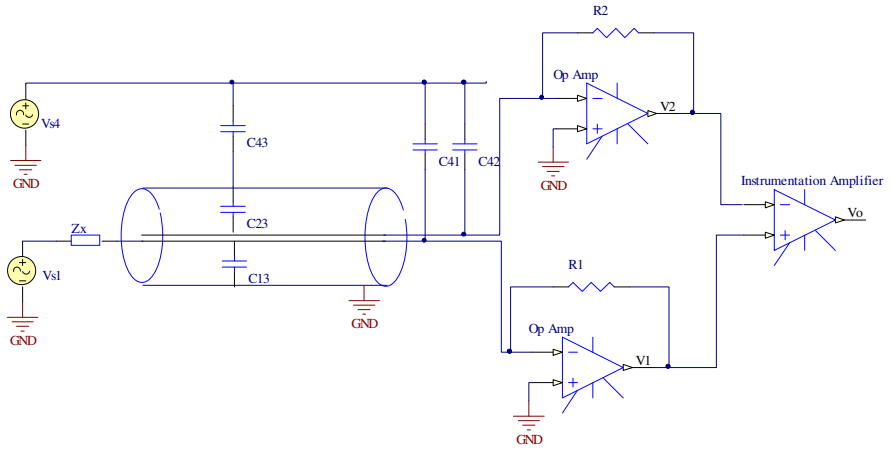

Figure 2.6: Capacitive coupling between a conductor and the proposed impedance meter

Using two twisted wires in the interface cable the value of the mutual capacitances C41 and C42 will be the same. Therefore an equal voltage will be induced in the wires and the noise will be cancelled in the final differential amplification.

2.4. Effect of inductive coupling

Figure 2.7 shows the inductive coupling between an external conductor and the cable between DUT and proposed impedance meter.

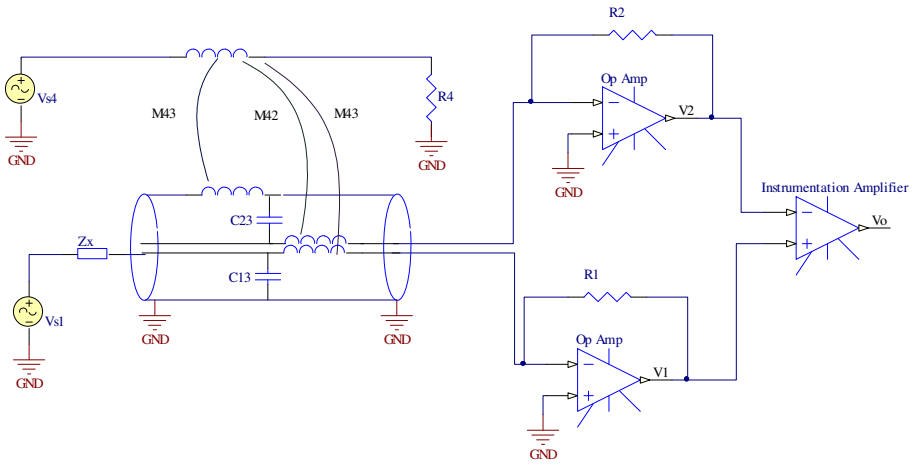

Figure 2.7: Inductive coupling between a conductor and the proposed impedance meter

Similar to the auto-balance bridge, noise voltages are induced to each conductor of the interface cable. Figure 2.8 shows the equivalent circuit for the inductive coupling. As in the section 2.2, the inductive noise currents in conductors are equal and can be expressed as:

$$I_n = j0.5C_{13}\omega_n V_n \tag{2.9}$$

And it is amplified in each operational amplifier with the same gain so we have:

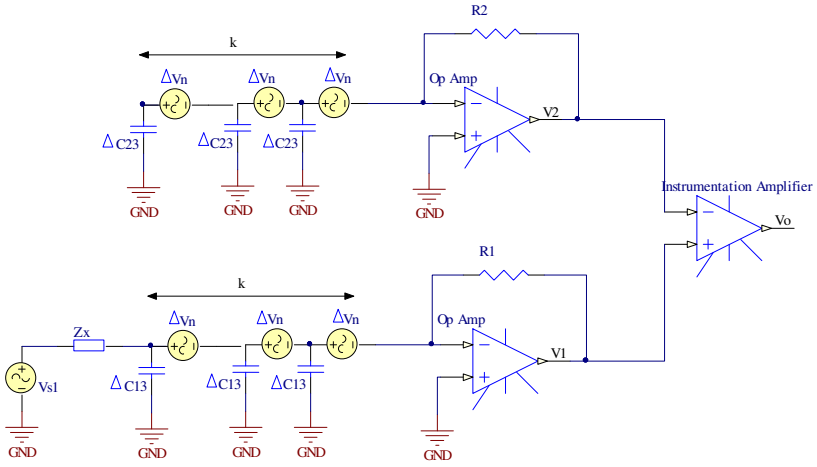

Figure 2.8: Equivalent circuit for Inductive coupling between a conductor and the proposed impedance meter

$$V_o = G\{R_1\left(\frac{V_{s1}}{Z_x} + j0.5C_{13}\omega_n V_n\right) - R_2(j0.5C_{23}\omega_n V_n)\} \quad (2.10)$$

Where G is the gain of instrumentation amplifier. With selecting similar resistors and cables for both amplifiers:

$$R_1 = R_2 \quad (2.11)$$

$$C_{13} = C_{23}$$

The output voltage becomes:

$$V_o = -\frac{V_S}{Z_x}R_1 \quad (2.12)$$

Therefore the circuit cancels the inductive coupling noise and the proposed circuit doesn't have limitations associated with the auto-balance bridge.

2.5. Disscussion and experimental results

To validate the novel impedance measurement method the output voltages of two impedance meters were recorded and the power spectrum of output signals were compared. Figure 2.9 shows the power spectrum of the output signal of the auto balancing bridge and the novel impedance meter when the signal generator's frequency is 7 KHz.

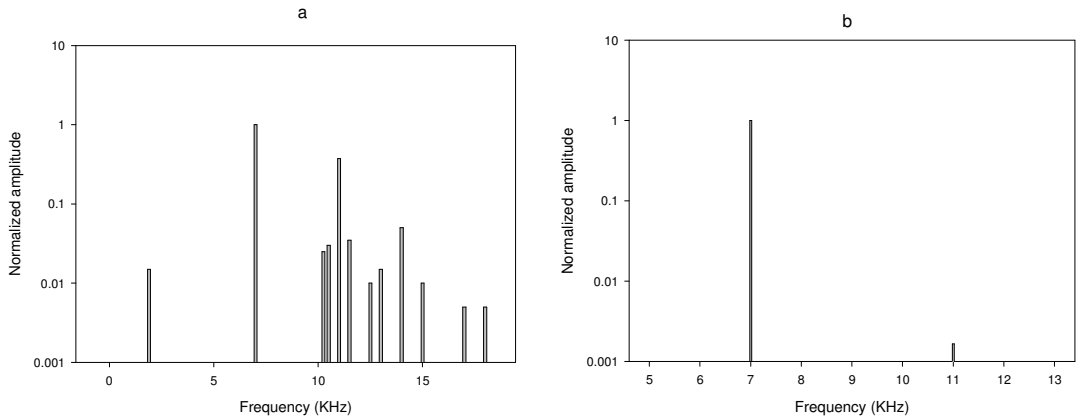

Figure 2.9: Power spectrum of output signal of a- auto balancing bridge b- novel impedance meter

As expected there is considerable noise in the output signal of the auto balancing bridge because all induced voltages in the interface cable are amplified by the operational amplifier. In contrast the noise has been cancelled in the output signal of the novel impedance meter because of the differential amplification of the current. To validate the accuracy of the novel method in measuring the impedance, a 100 KΩ resistor in parallel with a 5nF capacitor were used as DUT. Figure 2.10 illustrates the difference between theoretical and experimental values of amplitude and phase of the impedance versus frequency. For all the values the error is less than 5%. It is seen that with increasing the frequency the error increases gradually because of the limited bandwidth of the instrumentation amplifier. To reduce the error, the bandwidth can be selected according to the needed frequency for DUT.

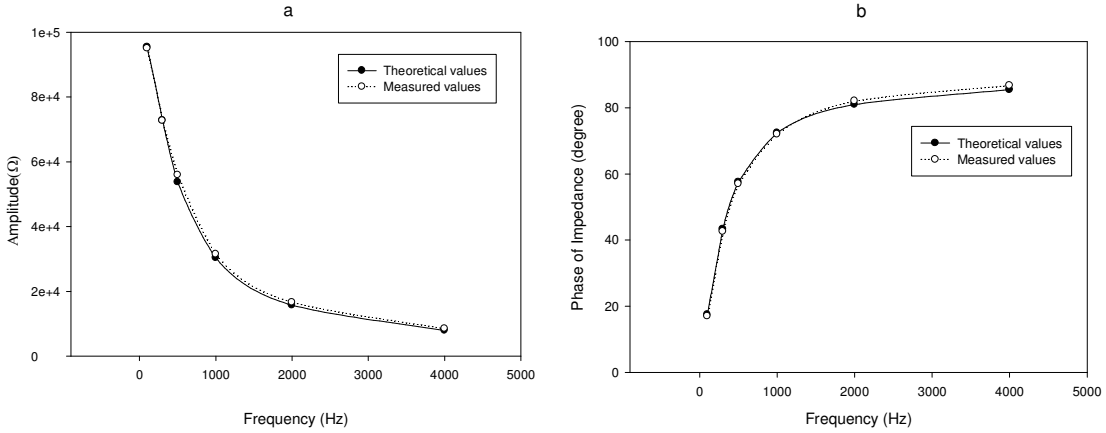

Figure 2.10: Theoretical and experimental values for a) amplitude of the impedance versus frequency b)phase of the impedance versus frequency

2.6. Conclusions

A novel AC based impedance meter has been designed and implemented and its performance in cancelling capacitive and inductive coupling noise has been analysed. The novel impedance meter then compared with a conventional AC-based impedance meter. The performance of the circuit has been proved independent of the frequency and tested experimentally. Using this impedance meter the amplitude and phase of impedance in a noisy environment can be measured with high accuracy. Since the filter has been

removed, the output signal is more stable compared to conventional AC- based methods which in turn adds to the measurement accuracy.

2.7. References

Angrisani L, Baccigalupi A, Pietrosanto A, “A digital signal processing instrument for impedance measurement”, IEEE transactions, 45(6) 930-934,1996.

Du B, Warsito W., and Fan L. S., “Imaging the choking transition in gas-solid

Geddes L.A, ”Electrodes in principles of applied biomedical instrumentation”, 3rd, ed. New York: Wiley, 1989, ch. 9.

Ott H. W, “Noise reduction techniques in electronic systems”, 2rd, ed. Wiley, 1988, ch. 2.

Randus M, Hoffmann K, “A method for direct impedance measurement in microwave and millimeter-wave bands”, IEEE Transactions, 59(8) 2129-1966,2011.

“Signal recovery technical note”
http://www.signalrecovery.com/_AppsNotes/TN1000.pdf

Yamazaki K, Ishikawa K, Haga A, Muramatsu K, “ Impedance measurement using a resonance circuit for detecting steel bars and cables inside pliable plastic conduit tubes buried in concrete walls and slabs”, IEEE transactions, 46(6) 1963-1966,2010.

CHAPTER3: EFFECT OF FLUIDIZED BED BOGGING ON THE DISTRIBUTION OF SPRAYED LIQUID ON FLUIDIZED PARTICLES

3.1. Introduction

In gas-fluidized bed processes such as Fluid Coking™ and Fluid Catalytic Cracking, a liquid feed stream is contacted with fluidized particles in the bed. In Fluid Coking, heavy oil is injected into a fluidized bed of hot coke particles, where it undergoes thermal cracking. A high local concentration of liquid in the fluidized bed may result in particles coated with liquid that stick together, which in turn causes defluidization, a condition called "bogging". There is no published study of the impact of this bogging on the distribution of the sprayed liquid on the fluidized particles.

Several methods have been developed to detect local defluidized zones in fluidized beds. Ropchan measured local heat transfer coefficients of fluidized particles and used their fluctuations to detect defluidized zones of a fluidized bed (Ropchan, 1981). Their results were confirmed by Marzocchella and Salatino (Marzocchella, 1995). Yutani found that auto correlation of local capacitance signals could be used to find defluidized zones between neighboring gas jets in the grid zone of a fluidized bed (Yutani, 1983). Triboelectric sensors can also be used to detect defluidized zones in the fluidized bed (Briens, 1999).

Other methods have been developed to detect bogging of the whole bed. Pressure fluctuations have been used with methods such as the W statistic to characterize the fluidized bed fluidity and detect bogging (Briens, 2003, Chong, 1987). Chaos analysis of pressure fluctuations was also used to identify the fluidization degradation caused by agglomeration of the fluidized particles (Van Ommen, 2000). However, chaos analysis is slow and requires several minutes of data. Bartels et al. compared fourteen different methods of pressure fluctuations analysis for their ability to detect process changes in a fluidized bed (Bartels, 2010). The Kolmogorov–Smirnov Test based on the mean crossing data with a 15 Hz low-pass filter performed best (Bartels, 2010).

Previous studies have shown that bubble behavior is greatly affected by the bed cohesivity (Briens, 2003, Chong, 1987). Reductions in bubble size and frequency as the fluidized bed approaches bogging has been attributed to an increase in minimum fluidization velocity (McLaughlin, 2001).

This paper has three objectives. First, it determines the effect of bogging on the distribution of sprayed liquid on fluidized particles. Second, it investigates how bogging affects the bubble properties. Third, it develops a simple bogging detection method based on capacitance measurements.

3.2. Experimental Set up

3.2.1. Equipment and Materials

Experiments were conducted in a 1.97 m high fluidized bed with a trapezoidal cross sectional area, shown in Figure 3.1.

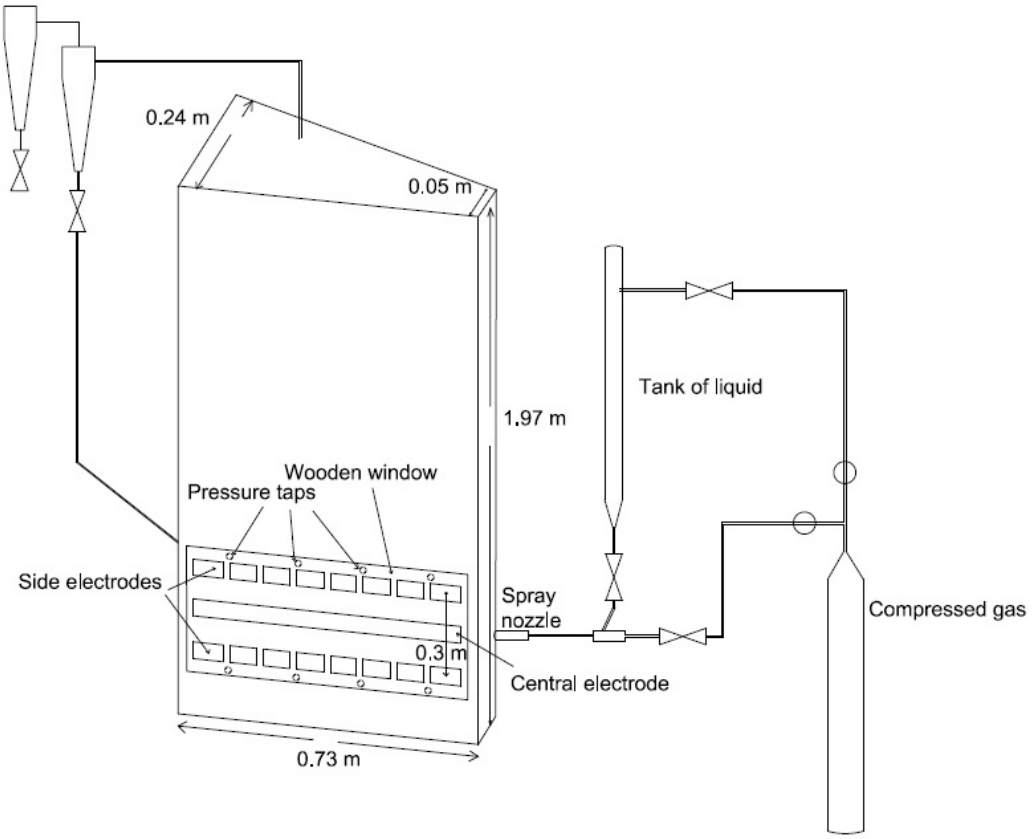

Figure 3.1: Schematic of experimental set up

Two rectangular wooden windows were mounted on two sides of the wall of the fluidized bed to enable capacitance measurement with electrodes on the outside of the bed wall. Coke particles with a Sauter mean diameter of 144 μm, density of 1450 kg/m^3 and a total mass of 42 kg were used for most experiments. For some experiments on the effect of liquid concentration on bubble properties, glycerol and sand particles Sauter mean diameter of 400 μm and mass of 40 kg were also used. Both types of solid particles belong to Geldart's type B particles. For all experiments, the bed was fluidized with air at a superficial velocity ranging from 0.1 to 0.2 m/s.

In typical applications, the liquid sprayed into a fluidized bed is also the liquid causing bogging. In this study, however, the method used to measure the quality of the liquid distribution on the fluidized particles requires a vaporizable liquid. Using the same liquid to induce bogging would have meant that the liquid concentration in the bed would have varied greatly with both time and location. This study, therefore, used two separate liquids: a non-vaporizable liquid to induce bogging and a vaporizable liquid to measure the quality of the liquid distribution on fluidized particles.

Voltesso^{TM} oil was selected as non-vaporizable liquid, with coke particles in the bed. Voltesso oil simulates, at room temperature, the properties of bitumen in Fluid Coking^{TM} . Voltesso oil at room temperature has the viscosity of 7 CPS and density of 864 kg/m^3 while bitumen at 300 ^{o}C has the viscosity of 5 CPS and density of 922 kg/m^3. Voltesso has a negligible vapor pressure at room temperature and can be used to provide a constant liquid background during each experiment. Voltesso was mechanically mixed with particles to ensure uniform coating of all the particles and to prevent the formation of coke-Voltesso agglomerates. Some additional experiments were conducted with a bed of sand particles and glycerol as background liquid.

To determine the impact of the background liquid on the distribution of sprayed liquid on fluidized coke particles, Varsol was sprayed into the bed with a scaled-down version of an industrial spray nozzle as shown in Figure 3.1. The nozzle has a convergent-divergent geometry with a throat diameter of 2 mm. The flowrate of Varsol was 0.016 kg/s while the gas to liquid ratio was 2 wt% and the injection time was 10 s. A significant fraction of the liquid sprayed into the fluidized bed forms agglomerates with the bed particles, and

these agglomerates gradually break up in the fluidized bed, thanks to the turbulence resulting from the gas bubbles. Varsol has a significant vapor pressure at room temperature, which allows for accurate measurement of the evolution of the liquid trapped in agglomerates.

3.2.2. Origin of bogging

Preliminary experiments were performed to determine the general cause of bogging in the experimental system used in this study. Degradation of fluidization quality has been attributed to a variety of fluidized bed phenomena such as particle cohesivity, particle agglomeration, reduced bubbling, increase in minimum fluidization velocity and channeling (Van Ommen, 2000, McLaughlin, 2001). In general, defluidization is a result of changes in the surface properties of particles in the fluidized bed and their interactions at presence of liquid bridges or sintering mechanisms (McLaughlin, 2001).

Some observations of changes in fluidization behavior caused by liquids that have been reported in the literature (McLaughlin, 2001, Seville, 1984, Molerus, 1982), suggest that adding liquid to Geldart group B particles may cause a transition to group A and group C behavior that finally can result in bogging or defluidization. Molerus mentioned that the balance between interparticle forces and fluid drag force on the particles is the main reason behind of BA and AC boundaries in Geldart diagram (Molerus, 1982). According to Molerus, the ratio of interparticle forces to drag force should increase and reach 6 and 100 to enable the transition from Geldart group B to A and A to C respectively. It has also been reported that the increase in particle cohesivity caused by liquid bridges between particles decreases the effective bulk density of particles (Nokhodchi, 2005). In this case, a lower bed pressure gradient would be expected, as was confirmed by McLaughlin et al (McLaughlin, 2001).

The agglomeration of fluidized particles has been proposed as another mechanism that can lead to bogging and defluidization (Van Ommen, 2000, Bartels, 2010). In an agglomerating fluidized bed, the increase in effective particle size results in a higher minimum fluidization velocity that in turn degrades the fluidization. Agglomeration thus

increases the bed density (Lipsanen, 2008), which results in a higher bed pressure gradient.

To determine the general cause of bogging, this study performed experiments with two different experiments systems: Voltesso with coke particles and glycerol with sand. Since direct measurement of wet particle size wasn't possible with particle size analyzer, the fluidized bed pressure gradient was studied to find whether agglomeration or particle group transition causes bogging. In both cases, the fluidized bed pressure gradient was determined from the measured pressure drop between two taps (Figure 3.1) at different concentrations of liquid. Figure 3.2 shows that, in both cases, the bed pressure gradient gradually decreases with increasing liquid concentration. This indicates that, in this study, bogging was not caused primarily by particle agglomeration but, instead, by an increase in particle cohesivity. Therefore, transition of wet coke particles from group B to A to C resulted in bogging.

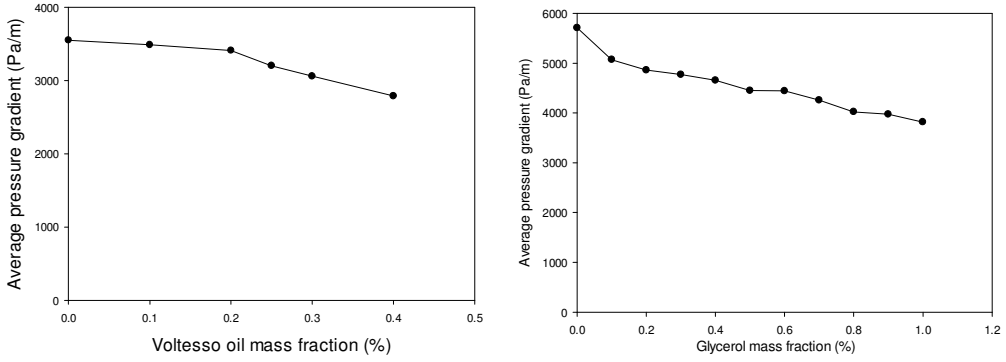

Figure 3.2: Average pressure gradient measured between two taps at heights 0.05 m and 0.45 m above the gas distributor versus mass fraction of Glycerol and Voltesso oil

3.2.3. Measuring Methods

Capacitance sensors have been applied for void and bubble measurements (Elkow, 1996), (Kobayashi, 2012). Capacitance sensors allows for measuring the distribution of materials with low dielectric constants like air and Varsol with dielectric constant of 1 and 3 inside materials with high dielectric constant like coke particles with dielectric

constant of 7 as measured for these experiments. Figure 3.1 shows the planar capacitance sensors that were used to measure the local bed capacitance between the central electrode and each side electrode on the wooden window of the bed. The capacitance meter was an AC based circuit with a differential noise cancelling system (Chapter 2). The local capacitance fluctuations were used to determine the local bubble properties while time-averaged local capacitance provided the local concentration of "free" Varsol liquid, i.e. Varsol that was not trapped in agglomerates. Taking the mixture of coke and Voltesso oil as the background material with a high dielectric permittivity allows the detection of the Varsol as the foreground material with a low dielectric permittivity. In experiments conducted to characterize bubble properties, the capacitance was measured with an acquisition frequency of 5 kHz during 15 seconds. Experiments conducted to investigate agglomerate breakage, used an acquisition frequency of 1 kHz.

Preliminary experiments showed that when Varsol is added to coke particles, Varsol trapped within agglomerates has no significant impact on the bed capacitance, which was affected only by the free liquid that is not trapped within agglomerates (Mohagheghi, 2013). Some calibration experiments were required to determine the relationship between bed capacitance and free liquid concentration, i.e. the mass fraction of the Varsol liquid in the fluidized bed that was not trapped within liquid-solid agglomerates. In these experiments, Varsol was injected into the bed with a special "ideal" spray nozzle operating with an atomization gas to liquid ratio of 50 wt% to prevent the formation of agglomerates. Figure 3.3 shows the calibration curve for average capacitance of all electrodes in which the average capacitance is a linear function of the free liquid concentration in the bed.

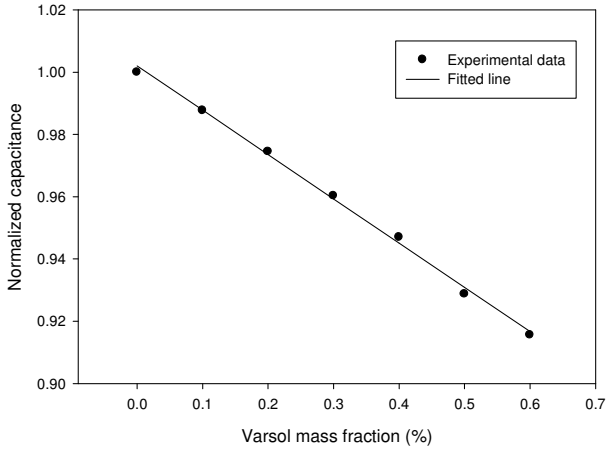

Figure 3.3: Calibration curve

Normal experiments were performed with a more common atomization gas to liquid ratio of 2 wt%, using a scaled-down version of an industrial spray nozzle. The free Varsol mass fraction was calculated with capacitance sensors, using the calibration relationship. After each injection, free Varsol is continuously generated from agglomerate breakage and gradually disappears from the bed through evaporation:

$$\frac{d(M_l)}{dt} = \left[\frac{d(M_l)}{dt}\right]_{br} + \left[\frac{d(M_l)}{dt}\right]_{e} \tag{3.1}$$

Since both the fluidization velocity (U_f) and mass of solid (M_S) were kept constant after injection in all experiments, the evaporation rate was only a function of the mass of free Varsol liquid. Therefore, the results of calibration experiments could be used to determine the relationship between the free Varsol concentration X and the evaporation rate at a given superficial gas velocity, since there were then no agglomerates. Substituting the calibration results for the evaporation rate in Equation 3.1, we obtain:

$$M_S\left[\frac{dX}{dt}\right]_{br} = M_S\left[\frac{dX}{dt}\right] - M_S\left[\frac{dX}{dt}\right]_{cal} \tag{3.2}$$

Where $(dX/dt)_{cal}$ is calculated for the instantaneous value of X. The free Varsol content X at any time can be calculated as the sum of the free Varsol during injection and the cumulative Varsol freed from agglomerates after injection. The ratio of the total free Varsol to the total mass of injected Varsol (M_L) can be obtained from:

$$g(t) = \frac{f(t)}{M_L} = \frac{M_S}{M_L}\left[X|_{t=0} + \int_0^t \left[\left(\frac{dX}{dt}\right) - \left(\frac{dX}{dt}\right)_{cal}\right] dt\right] \quad (3.3)$$

$g(t)$ has been plotted as a function of time after injection for different Voltesso mass fractions and for several fluidization velocities. For instance, Figure 3.4 shows $g(t)$ as a function of time after injection for a 0.3% Voltesso mass fraction and fluidization velocities of 0.1 m/s during injection.

The data was fitted with an exponential curve that can be expressed as:

$$g(t) = 1 + (g(0) - 1)e^{-\alpha t} \quad (3.4)$$

Where $g(0)$ is the value of $g(t)$ at the end of injection and α is the natural frequency of agglomerate breakage. Bogging was determined from its impact on the distribution of sprayed liquid, by measuring α at different oil mass fractions and fluidization velocities.

Figure 3.4 shows that most of the Varsol injected into the bed was initially trapped within agglomerates while the background Voltesso oil was not trapped within agglomerates. As a result, during the Varsol injection, practically all the free liquid, which affects the bed bogging, is in the form of Voltesso oil and the impact of Varsol on bogging is then negligible.

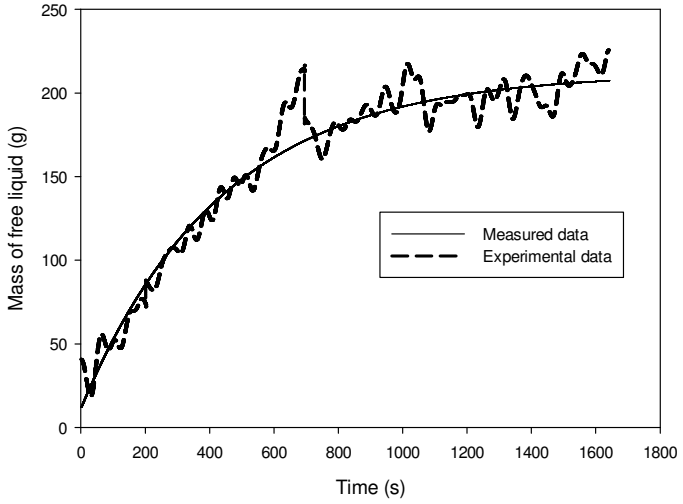

Figure 3.4: The mass of total Varsol freed from agglomerate versus time

3.3. Results And Discussion

3.3.1. Bogging Condition in the Fluidized Bed

The increase of particle cohesivity that is caused by increasing liquid concentration in a fluidized bed, and can lead to bogging, is a gradual phenomenon. In a wet bed, the minimum liquid concentration above which the bed becomes bogged depends on each practical application. The focus of this study is the impact of the liquid background on the distribution of sprayed liquid on fluidized particles. Bogging in the fluidized bed has, therefore, been characterized by directly investigating the impact of the background liquid concentration on the breakage kinetics of the wet agglomerates of coke and Varsol formed when Varsol was injected in a bed previously wetted with Voltesso oil.

Figure 3.5 illustrates the effects of the Voltesso oil concentration in the bed on the natural frequency of agglomerate breakage, for various fluidization velocities during liquid injection. The natural frequency of agglomerate breakage increases with increasing fluidization velocity during Varsol injection.

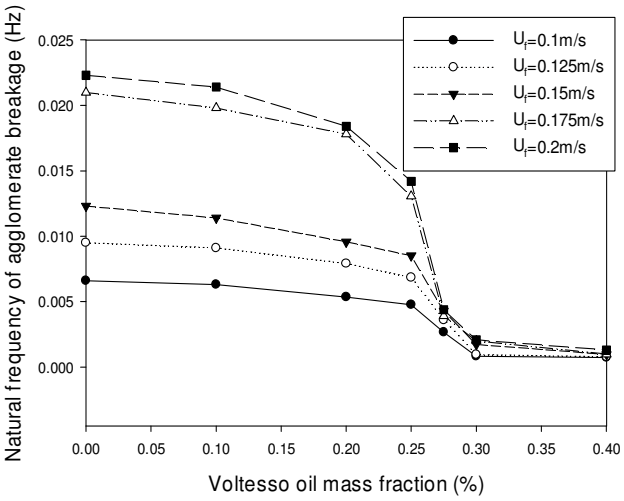

Figure 3.5: Effects of Voltesso oil mass fraction on natural frequency of agglomerate breakage for various fluidization velocities during liquid injection

Figure 3.5 also shows that increasing the concentration of background Voltesso oil has a detrimental impact on the distribution of the sprayed Varsol, since the natural frequency of agglomerate breakage is reduced. A sharp drop occurs when the Voltesso oil fraction is

increased from 0.25 to 0.275 wt%. These experiments, thus, indicate that bogging occurs when the oil mass fraction is increased from 0.25 to 0.275 wt%. There are two possible causes: wetter beds may not distribute injected Varsol as well as dry beds, and wet beds, by affecting bubble properties, may hinder agglomerate breakage. The following section, therefore, studies the impact of background oil concentration on bubble properties.

3.3.2. Effect of Bogging on Bubble Properties

The objective of this section is to determine how bubble properties, measured with capacitance sensors, are related to the onset of bogging detected from the distribution of liquid sprayed into the fluidized bed. This might also provide a method to detect conditions under which sprayed liquid could no longer be distributed properly and stronger agglomerates would be formed (Figure 3.5).

Previous studies confirmed that bogging has a considerable effect on bubble rise velocity, which can be measured directly with planar capacitance sensors (Briens, 2003, Chong, 1987). In this study, measured capacitance signal was smoothed using a low pass filter with a cut off frequency of 25 Hz to remove the effect of small bubbles. Then, the rise velocity was determined for each bubble from the ratio of the vertical distance between two electrodes (D in Figure 3.6a) to the measured bubble rise time. Figure 3.6 shows how the bubble rise time was calculated from the time lag (t_r in Figure 3.6b) between the drops in the capacitance signal caused by the passage of a gas bubble presence past each electrode.

(a)

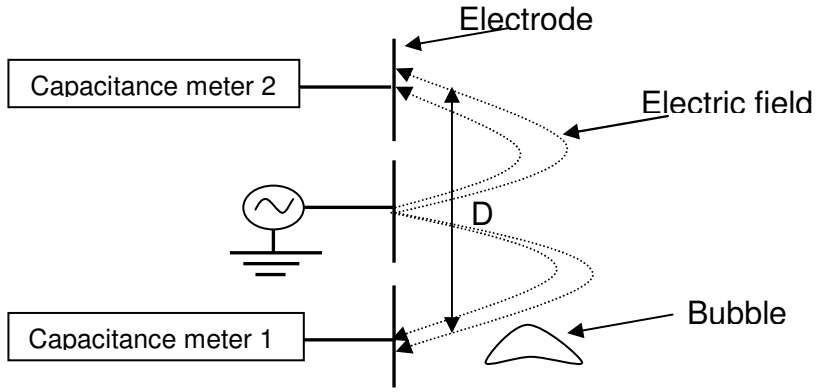

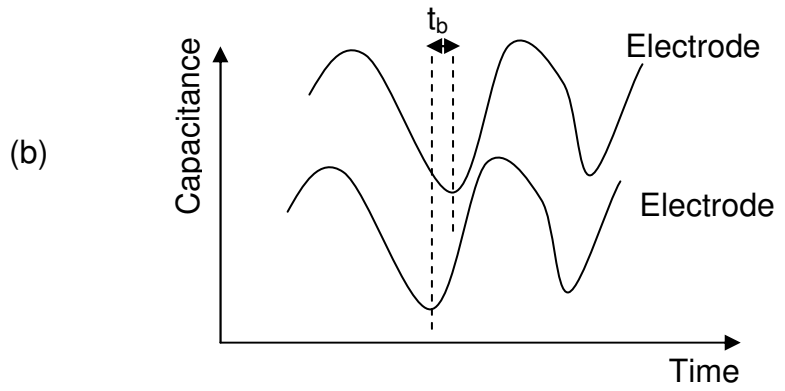

Figure 3.6: a) bubble crosses the electric field of three electrodes b) The effect of crossing on capacitance signals – calculation of bubble rise time

Simulation of the effect of a moving bubble on capacitance signal (section 5.3.3) with COMSOL electrostatic toolbox also confirms the curve shown in Figure 3.6b. Using planar capacitance sensors, one can measure bubble frequency as well as bubble rise velocity. When bogging occurs, poorly fluidized zones form at some fluidized bed locations which can cause a strong variation in bubble frequency with location within the bed. Therefore, the standard deviation of the bubble frequencies obtained from eight pairs of electrodes across the bed can be used to detect the changes in bubble properties caused by bogging.

This paper uses the bubble rise velocity and the standard deviation of bubble frequency to detect bogging and to investigate the effect of liquid concentration and fluidization velocity on bogging. The fluidized bed was operated with a constant fluidization velocity and Voltesso oil was added to coke particles in several steps until bogging was observed. For each step, the bubble rise velocity and the standard deviation of bubble frequency as well as the bed pressure drop were measured. The same experiments were performed for different fluidization velocities between 0.1 and 0.2 m/s. Another set of similar experiments were performed in the same column with sand particles and glycerol.

3.3.3. Results of Experiments with Coke Particles

In our fluidized bed, the bubble rise velocity was found to be log-normally distributed, as in other studies (McLaughlin, 2001, Seville, 1984). Figure 3.7 shows the effect of bogging and fluidization velocity on the average bubble velocity. Figure 3.7 indicates that bubble velocity increases with fluidization velocity, as expected (McLaughlin, 2001). As displayed in Figure 3.7, the bubble velocity first decreases slightly with increasing Voltesso oil content: if bed particles become cohesive, their effective diameter increases resulting in an increase in the minimum fluidization velocity, which explains the decrease in bubble velocity (McLaughlin, 2001).

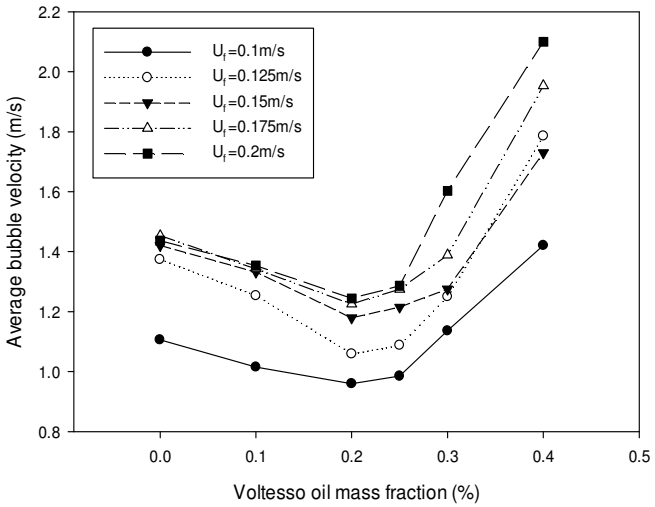

Figure 3.7: Effects of fluidization velocity and oil mass fraction on average bubble velocity

When the Voltesso oil fraction increases past 0.2 wt%, the bubble velocity starts increasing sharply with increasing oil fraction: this is likely caused by the appearance of channeling. When the channeling begins at some locations of the fluidized bed, the bubble rise velocity increases due to limited routes for the fluidization gas.

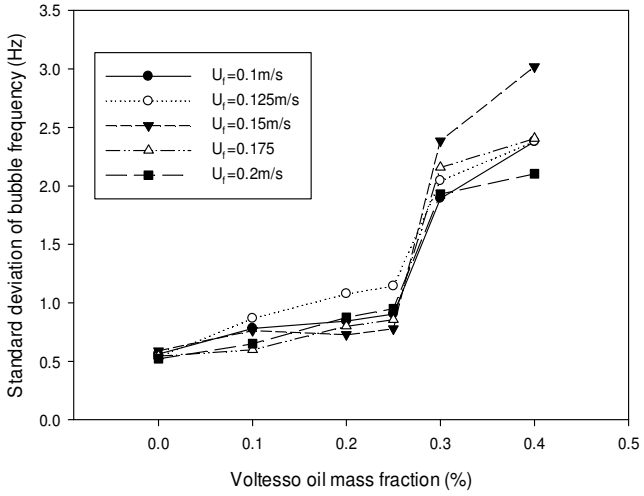

Figure 3.8: Effects of fluidization velocity and oil mass fraction on standard deviation of bubble frequency

Figure 3.8 illustrates the effect of fluidization velocity and Voltesso oil mass fraction on the standard deviation of the bubble frequency, which characterizes the variation of the bubble frequency over the bed width. At first, the standard deviation of the bubble frequency increases gradually with increasing Voltesso oil fraction. When the Voltesso oil fraction goes past 0.2 wt% and channeling starts at some locations, the standard deviation of bubble frequency starts increasing much more quickly with increasing Voltesso oil fraction.

A comparison of Figures 3.5, 3.7 and 3.8 shows that the bogging transitions observed from abrupt changes in sprayed Varsol distribution, bubble velocity and standard deviation of bubble frequency all occur at about the same Voltesso oil concentration. Partial channeling caused by the increase in particle cohesiveness due to the increase in background Voltesso oil concentration is, therefore, likely to cause the observed major degradation in sprayed Varsol distribution.

3.3.4. Results of Experiments with Sand Particles

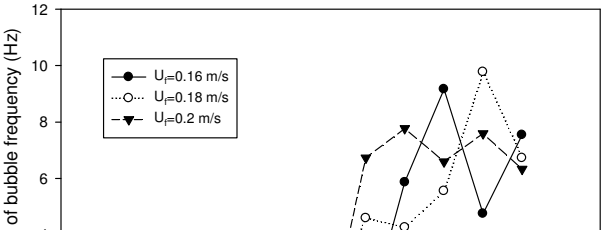

Figure 3.9: Effects of fluidization velocity and glycerol mass fraction on standard deviation of bubble frequency

Figure 3.9 illustrates the effect of fluidization velocity and glycerol mass fraction on the standard deviation of the bubble frequency. A sharp increase happens at a glycerol mass fraction of 0.5% which shows the initial point of channeling at some locations of the fluidized bed. The results are similar to the results obtained with Voltesso oil and coke (Figure 3.8). This suggests that the standard deviation of the bubble frequency is a better way to detect the onset of bogging than the average bubble velocity.

3.4. Conclusions

When the Voltesso oil concentration in a fluidized bed increases past a critical value, the breakage rate of wet agglomerates slows down, which results in a poorer distribution on the fluidized particles of the Varsol sprayed into the bed.

Bubble properties in a wet fluidized bed of coke particles were measured with planar capacitance sensors at different levels of bed moisture and fluidization velocity. Major changes in bubble properties and changes in the kinetics of wet agglomeration breakage occur at the same Voltesso oil mass fractions. Results indicate that the standard deviation of the bubble frequency can be used as a bogging index, since it increases sharply when the agglomerate breakage drops. This index provides effective detection of bed bogging in a few seconds.

3.5. References

Andreux R, Chaouki J, (2008) "Behaviors of the Bubble, Cloud, and Emulsion Phases in a Fluidized Bed" AIChE 54(2): 406-414.

Bartels M, Nijenhuis J, Kapteijn F, Van Ommen J.R. (2010). "Case studies for selective agglomeration detection in fluidized beds: Application of a new screening methodology" Powder Technology 203(2) 148-146.

Briens C, McDougall S, Chan E. (2003) "On-line detection of bed fluidity in a fluidized bed coker" Powder Technology 138(23): 160-168.

Briens C.L, Briens L.A, Barthel E, Le Blevec J.M, Tedoldi A, Margaritis A. (1999). "Detection of local fluidization characteristics using the V statistic" Powder Technology 102(1): 95-103.

Chong Y.O , O'Dea D.P , White E.T , Lee P.L , Leung L.S, (1987). "Control of the quality of fluidization in a tall bed using the variance of pressure fluctuations" Powder Technology 53(3): 237-246.

Elkow K.J, Rezkallah K.S (1996) “Void fraction measurements in gas-liquid flows using capacitance sensors” Measurement science and technology 7(8):1153:1160

Hamidi M, Berruti F, Briens C, McMillan J, (2014) “A Novel AC-based Impedance Meter to Reduce Capacitive and Inductive Coupling Noise”

Kobayashi A, Hiraoka H, Yamaguchi M, (2012) “Capacitive gas-bubble sensor for solid oxide fuel cell” IMCS Conference

Lipsanen T, (2008) " Process analytical technology approach on fluid bed granulation and drying" MESc thesis, University of Helsinki, Finland

Marzocchella A, Salatino P, (1995) National AIChE Meeting.

McLaughlin L.J, Rhodes M.J, (2001) "Prediction of fluidized bed behaviour in the presence of liquid bridges" Powder Technology 114 (1-3): 213–223

Mohagheghi M, Hamidi M, Berruti F, Briens C and McMillan J, (2013) “Study of the effect of local hydrodynamics on liquid distribution in a gas-solid fluidized bed using a capacitance method”. Fuel Journal, 107 236-45.

Molerus O, (1982) "Interpretation of Geldart’s type A, B, C, and D powders by taking into account interparticle cohesion forces" Powder Technology 33(1): 81–87.

Nokhodchi A, (2005) " An overview of the effect of moisture on compaction and compression" Pharmaceutical Technology

Ropchan W.T, (1981). Heat transfer and grid jets, Stanford University. PhD.

Seville J.P.K, Clift R, (1984) "The effect of thin liquid layers on fluidisation characteristics" Powder Technology 37 (1): 117–129

Werther J, Morelus O, (1973). "The local structure of gas fluidized beds—I. A statistically based measuring system" Multiphase Flow 1(1): 103–122.

Yutani N, Ho T.C, Fan L.T , Walawender W.P , Song J.C , (1983). "Statistical study of the grid zone behavior in a shallow gas solid fluidized bed using a mini-capacitance probe" Chemical Engineering Science 38(4): 575-582.

CHAPTER4: EARLY DETECTION OF DEFLUIDIZATION USING WAVELET ANALYSIS OF PRESSURE FLUCTUATIONS

4.1. Introduction

Bogging degrades fluidized bed processes. It usually occurs when particles stick together or become too cohesive due to an excess of liquid or too high a temperature. Bogging generally occurs due to changes in the surface properties of the bed particles and particles adhesion resulting from sintering or the presence of liquid bridges (Molerus, 1982).

Two main interpretations of the bogging phenomena have been proposed:

1) It can result from increasing particle cohesivity. It has been reported that adding an excess amount of liquid to Geldart group B particles may cause a transition to group A and group C behaviour that can eventually result in defluidization (Molerus, 1982, McLaughlin, 2001, Seville, 1984). Molerus et al found that the

balance between interparticle forces and fluid drag force on the particles is the underlying reason for BA and AC boundaries in Geldart diagram (Molerus, 1982). They observed that the transition from Geldart group B to A and A to C occurs when the ratio of interparticle force to drag force increases and reaches 6 and 100, respectively.

2) It can result from more permanent particle agglomeration (Fuller, 1993, Briens, 2003). Due to agglomeration, the effective particle size increases, which increases the minimum fluidization velocity and may eventually result in bogging.

In chapter 3, it is shown in the system used in the present study, which is intended to simulate Fluid Coking conditions at room temperature, bogging results from increasing particle cohesivity.

Early detection of bogging in the fluidized bed would provide opportunities for timely, corrective action. Several published methods detect early bogging in the fluidized bed. Methods based on pressure fluctuations are more attractive since other methods are still facing practical limitations in their potential application to industrial fluidized beds (Werther, 1999). Furthermore, pressure fluctuations result from different phenomena affected by bogging such as bubble frequency, bubble coalescence and bubble size and shape (Van der Schaaf, 1998).

Pressure fluctuations are obtained from the instantaneous, local bed pressure gradient, measured from the pressure drop per unit height between two locations within the dense fluidized bed. The simplest criteria use the time-averaged pressure gradient or its standard deviation to detect changes in fluidization quality but are not effective for bogging detection (Schouten, 1998). The normalized standard deviation of high frequency components of the pressure fluctuations has been applied to bogging detection (Weinstein, 2000). Principal component analysis (PCA) has also been implemented on pressure signals to identify bogging (Schouten, 1998). However, both methods are sensitive to fluidization velocity, which makes them difficult to implement in industrial fluidized beds. A W-statistic was proposed based on to detect bogging in the fluidized bed: it uses filters to differentiate between pressure fluctuations from local bubbles and

pressure fluctuations from bubbles further away in the fluidized bed, whose transmission is affected by particle cohesivity (Briens, 2003). Van Ommen et al. detected early bogging using Chaos analysis of pressure fluctuations in a fluidized bed, but this method is slow when compared to methods based on the frequency analysis of pressure fluctuations (Van Ommen, 2000). Bartels et al. compared different bogging detection methods and concluded that the Kolmogorov-Smirnov Test based on the mean crossing data with a 15 Hz low-pass filter is the most suitable one (Bartels, 2010).

All previous methods for bogging detection can find an initial point of bogging that is not unique and depends on the implemented method. Since bogging affects liquid distribution and consequently the yield of reaction in the fluidized beds with chemical reactions, detection of initial bogging based on liquid distribution properties is of importance. The effect of bogging on liquid distribution can be investigated with from the breakup kinetics of the agglomerates formed during liquid injection, as well as from the bubble properties in the fluidized bed, both of which can be obtained from sophisticated local bed capacitance measurements (chapter 3). However, such capacitance measurements would be difficult to perform in industrial units.

The objective of this study is to develop a new bogging detection method based on pressure fluctuations, which could be performed in industrial units, to detect early bogging as defined from the breakup kinetics of agglomerates formed during liquid injection (chapter 3). The proposed bogging index should be insensitive to moderate changes in fluidization velocity. It should also be compared with other bogging detection methods using defined performance indices.

4.2. Experimental

4.2.1. Experimental Setup

All the measurements were performed in a 1.97 m high Pie-shape fluidized bed, as shown in Figure 4.1.

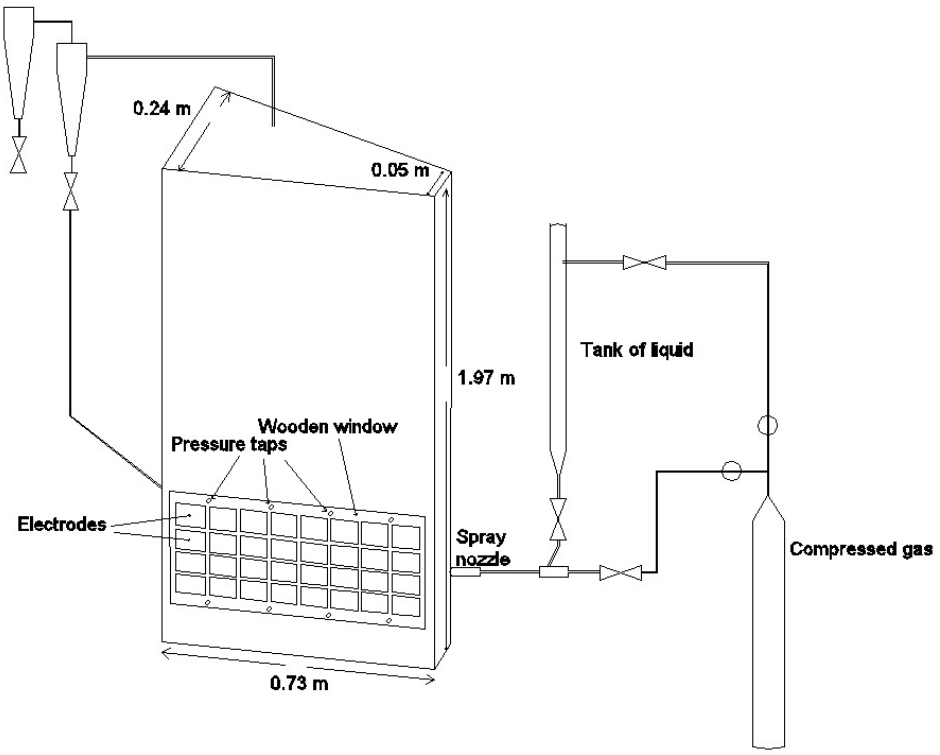

Figure 4.1: Schematic diagram of experimental set up

Coke particles with a Sauter mean diameter of 144 μm and a mass of 42 kg were used for experiments. Air at room temperature was the fluidization gas for all experiments with its superficial velocity ranging from 0.1 to 0.2 m/s. The bed height was approximately 0.4 m when the fluidization superficial velocity was 0.2 m/s.

Measurements were performed with different concentrations of Voltesso oil in the fluidized bed of coke particles. Since Voltesso oil has a negligible vapor pressure at room temperature, it could provide a constant liquid background during each experiment. Voltesso oil at room temperature simulates the properties of heavy oil at high coker temperatures, making the results of this study relevant to processes such as Fluid Coking^{TM}. Voltesso was mechanically mixed with particles to ensure that the liquid coated individual particles and that no coke-Voltesso agglomerates were formed.

The impact of the background liquid on the distribution of sprayed liquid on fluidized coke particles was determined by spraying Varsol into the bed with a scaled-down version of an industrial spray nozzle (chapter 3). The fluidization velocity was kept constant during injection and after injection. Agglomerates are formed by a significant

fraction of the liquid sprayed into the bed particles, and these agglomerates gradually break up in the fluidized bed, due to the shear forces resulting from the gas bubbles (chapter 3).

The differential pressure was measured between each two vertically separated pressure taps (Figure 4.1) with acquisition frequency of 1 kHz. The taps were located 5 cm and 42 cm m above the gas distributor. The pressure fluctuation data during 6 minutes was acquired with pressure transducers at different oil mass fractions ranging from 0 to 0.4 wt% in the bed of coke particles and different fluidization velocities ranging from 0.1 to 0.2 m/s.

4.2.2. Measuring methods

Figure 4.1 shows the planar capacitance sensors; each sensor was used to measure the local bed capacitance between a small electrode and a large electrode on the opposite side of the bed. The capacitance meter was an AC based circuit with a differential noise cancelling system (chapter 2). The time-averaged local capacitance provided the local concentration of "free" Varsol liquid, i.e. Varsol that was not trapped in agglomerates. Taking the mixture of coke and Voltesso oil as the background material with a high dielectric allows the detection of the Varsol as the sprayed material with a low dielectric (chapter 3).

Calibration experiments determined the relationship between local bed capacitance and free liquid concentration, i.e. the mass fraction of the Varsol liquid in the fluidized bed that was not trapped within liquid-solid agglomerates (preliminary experiments indicated that Varsol trapped within agglomerates has a negligible impact on the bed capacitance (Mohagheghi, 2013). In the calibration experiments, Varsol was injected into the bed with a special "ideal" spray nozzle operating with an atomization gas to liquid ratio of 50 wt% to prevent the formation of agglomerates as discussed in chapter 3.

4.3. Kinetics of agglomerate breakage

Experiments were performed with a more common atomization gas to liquid ratio of 2 wt%, using a scaled-down version of an industrial spray nozzle. VoltEsso oil was selected

as non-evaporating background liquid to generate the bogging condition, while Varsol was the sprayed liquid. The detail of these experiments can be found in a previous publication (chapter 3).

Bogging has been determined by measuring the natural frequency of agglomerate breakage (α) at different oil mass fractions and fluidization velocities. Figure 3.5 illustrates the effects of oil mass fraction and fluidization velocity during and after liquid injection on the natural frequency of agglomerate breakage. The natural frequency of agglomerate breakage increases with increasing fluidization velocity and decreases at higher Voltesso oil concentration and increased particle cohesiveness but when the Voltesso oil concentration passes 0.275%, the effect of fluidization velocity becomes negligible. The Voltesso oil concentration of 0.25% therefore can be considered as initial point of bogging.

4.4. Results of previous methods

Figure 4.2 shows that the pressure data at normal operating conditions and at initial point of bogging exhibit different patterns.

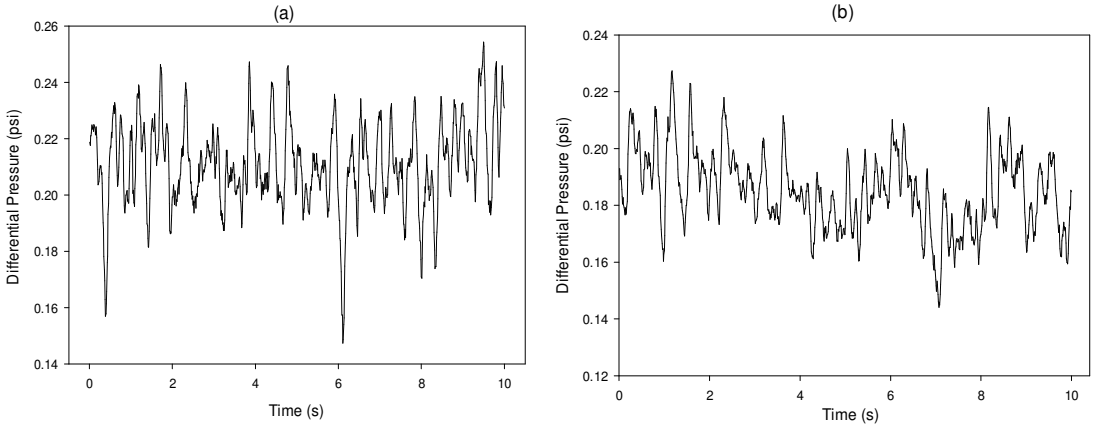

Figure 4.2: Differential pressure data measured between two vertically separated pressure tapes at a) Normal operation b) Initial point of bogging

The question is, therefore, which method can best extract a single number from pressure data that can be used to determine whether the bed is bogged or not. Ideally, such a number:

- Would clearly distinguish between bogged and non-bogged beds
- Could be calculated quickly
- Would not be very sensitive to small changes in fluidization velocity, since it may vary significantly with location in commercial units.

Average and standard deviation of pressure fluctuations have been used to detect defluidization (Schouten, 1998). As shown in Figure 4.3, both of those change with increasing the concentration of Voltesso oil in coke particles. However, those are not sensitive enough at initial point of bogging. For standard deviation of pressure fluctuation, the high sensitivity to fluidization velocity is also make it difficult to recognize the initial bogging. In this section, results of implementation of three previous methods, Kolmogorov-Smirnov test, Wstat and attractors difference index is provided using 6 minutes of pressure data.

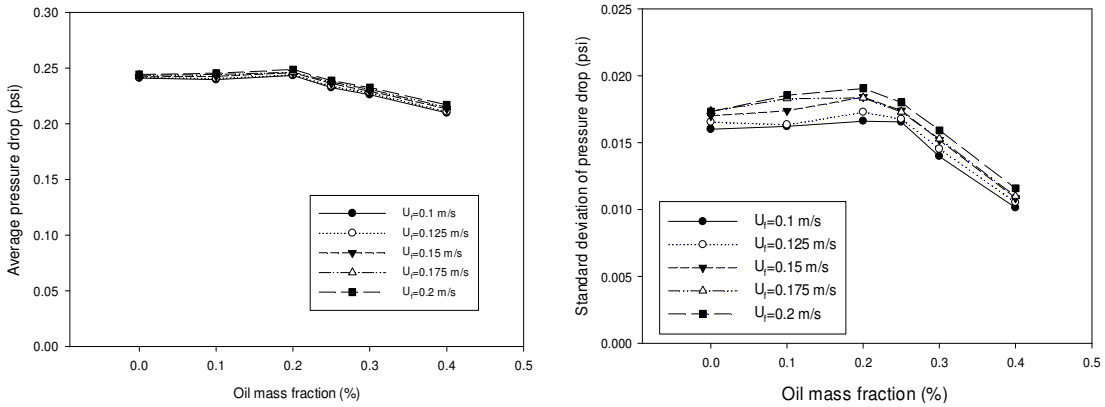

Figure 4.3: Average and standard deviation of measured pressure versus oil mass fraction and fluidization velocity

Kolmogorov-Smirnov test of mean crossing data extracted from low pass filtered pressure fluctuation has been found in previous studies to be the best method to detect particle agglomeration when compared to all proposed pressure based methods until 2010 (Bartels, 2010). In this method, the data is first filtered with a low pass filter with a cut-off frequency of 15 Hz. The cumulative distribution of distances between mean crossing points at filtered time series is then compared with a reference cumulative distribution by implementing the Kolmogorov-Smirnov test.

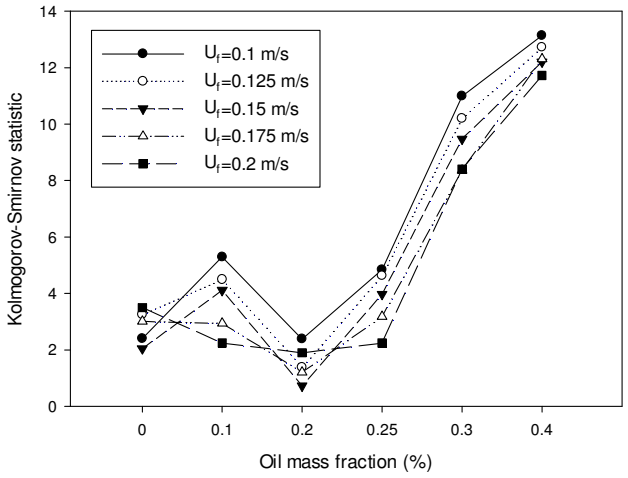

Figure 4.4: Kolmogorov-Smirnov statistic (Bartels, 2010) of measured pressure versus oil mass fraction and fluidization velocity after injection

Here, data extracted from pressure fluctuations with dry particles has been used as the reference. Pressure data acquired while Voltesso oil was progressively added to coke particles. Figure 4.4 shows the Kolmogorov-Smirnov stat of pressure fluctuations at different oil mass fractions and fluidization velocities. As it is shown in Figure 4.4, the Kolmogorov-Smirnov statistic increases before oil mass fraction reaches 0.25% where natural frequency of agglomeration breakage changes

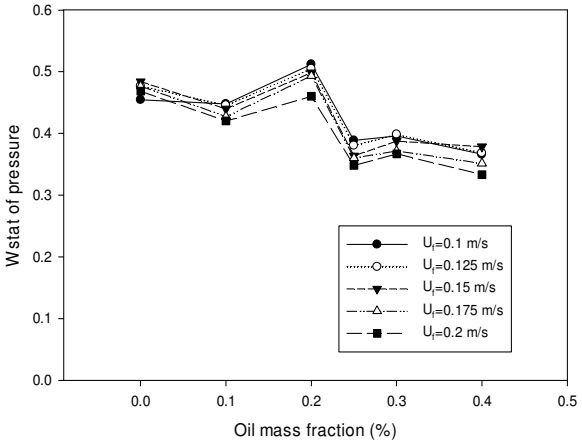

Figure 4.5: Wstat of measured pressure versus oil mass fraction and fluidization velocity

However, due to fluctuations in the index at low oil fractions, bogging cannot be detected for individual gas velocities until the oil mass fraction reaches about 0.275 %: it cannot provide early detection. This index is also sensitive to fluidization velocity and may give false alarm due to change in local fluidization velocity in the fluidized bed.

Figure 4.5 and Figure 4.6 show the Wstat with 95% compression, using the Daubechies 4 wavelet (Briens, 2003), and the attractors difference index at different Voltesso oil mass fractions and fluidization velocities respectively (Schouten, 1998, Briens, 2003).

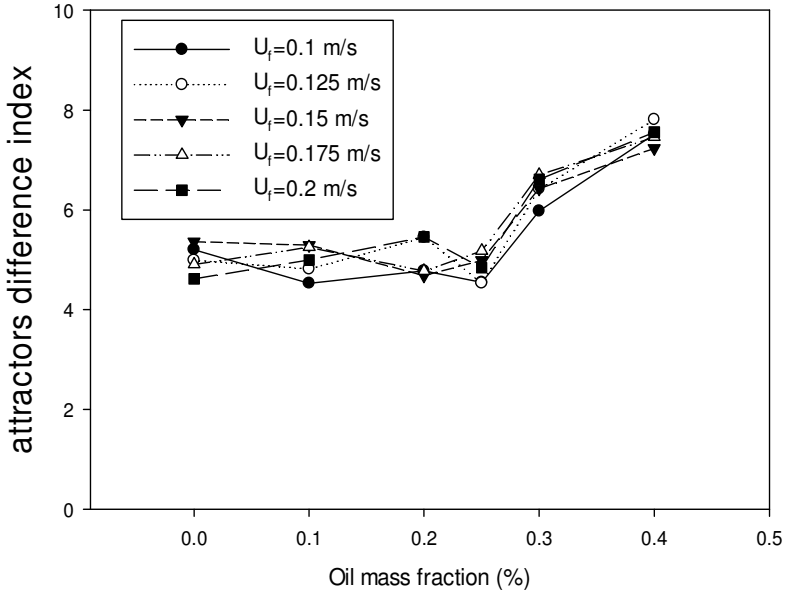

Figure 4.6: Attractors difference index versus oil mass fraction and fluidization velocity (measured pressure at dry bed is the reference)

As it is shown in the Figure 4.5, Wstat can predict the bogging earlier since it drops at Voltesso oil mass fraction of 0.2%; however, due to fluctuations in the index at low oil fractions, bogging cannot be detected for individual gas velocities until the oil mass fraction reaches about 0.225 %. Because the initial point of bogging according to Figure 3.5 corresponds to an oil fraction of about 0.25%, the Wstat would provide early detection. The attractors difference index starts increasing at an oil fraction of 0.25%; however, due to fluctuations in the index at low oil fractions, bogging cannot be detected for individual gas velocities until the oil mass fraction reaches about 0.275 %.

A problem with both the Wstat and attractors difference indices is their sensitivity to fluidization velocity. For example, with the Wstat, if one takes a Wstat value of 0.4 to prevent any risk of erroneous bogging detection at low oil fractions, bogging will be detected at an oil fraction ranging from 0.225 to 0.25 %, depending on the fluidization velocity. Therefore, if the exact fluidization velocity is not known, the Wstat can only reliability detect bogging at its initial point, for an oil fraction of 0.25 %, and cannot always provide early detection. The attractors difference index is significantly worse, since, if the exact fluidization velocity is not known, it can only reliably detect bogging for an oil fraction of 0.29 %, well past initial bogging.

4.5. Wavelet analysis of pressure fluctuations

4.5.1. Wavelet transform

Wavelet transform is a mathematical tool for representing a signal in time and frequency simultaneously. Wavelets transform can be used in two general forms: a continuous and a discrete Wavelets transform. The continuous wavelet transform of a signal y at time t of scale a is defined as:

$$W_a y(t) = \frac{1}{\sqrt{a}} \int y(t) \Psi \left(\frac{t-\tau}{a} \right) d\tau$$

(4.1)

Continuous wavelet transform is a convolution of the signal with the scaled version of the function Ψ called “mother wavelet”. The function Ψ must be localized well in time and frequency to satisfy the admissibility criterion.

Discrete wavelet transform implements a pair of digital filters to decompose the signal into a low frequency component A1 called the approximation and a high frequency component D1 called the detail. Decomposition is then repeated at the next level using A1 as the input signal. With repeating the decomposition at nw levels, a hierarchical multi-resolution representation of the signal x will be obtained:

$$y = D_1 + D_2 + \cdots + D_{nw} + A_{nw}$$

(4.2)

Each detail component Di contains information at frequencies between fs/2i to fs/2i+1 where fs is the sampling frequency and i is called the octave number.

Since there was no need to obtain all the wavelet coefficients of the continuous wavelet transform of pressure signals, this study uses the discrete wavelet transform to analyze the data. The discrete wavelet transform calculation is also much faster, which is major advantage for on-line bogging detection.

4.5.2. Optimized bogging index based on wavelet coefficients

Bogging in a fluidized bed deteriorates the fluidization quality which affects bubble properties and consequently pressure fluctuations in the fluidized bed. Since the change in fluidization velocity also affects bubble properties and pressure fluctuations, an optimized bogging index should be defined as a function of pressure fluctuations that detects the particle cohesion or agglomeration exactly at the time of deterioration of fluidization quality in the fluidized bed without sensitivity to fluidization velocity. The liquid concentration at initial point of deterioration of fluidization can be detected through the measurements of natural frequency of agglomerate breakage in the fluidized bed and can be used to calibrate the pressure fluctuation based bogging index.

Attenuation of pressure fluctuations at different frequency bands is a function of particle-particle interactions (Seville, 1984). Bogging in a fluidized bed changes the interactions between particles that in turn affects the source of pressure fluctuations and its attenuation at different frequencies. So it is possible to detect early bogging in the fluidized bed through fitting a function on wavelet coefficients of pressure fluctuations. Since pressure fluctuation is a non-stationary time series, a function based on statistical test is a better option for detection of early bogging. Here, Kolmogorov-Smirnov test (Cohn, 2012) as a function of cycle rms of wavelet coefficients has been used to compare the pressure fluctuations measured in wet particles with the pressure fluctuation measured in less wet particles as reference data. Kolmogorov-Smirnov test is a statistical test for the equality of probability distributions of two samples and is sensitive to difference in both shape and location of cumulative distribution of two samples. When the frequency

characteristics of pressure fluctuation changes due to agglomeration, the Kolmogorov-Smirnov statistic increases.

The bogging index can be expressed as Kolmogorov-Smirnov statistic of product of cycle rms of wavelet coefficients with unknown exponents:

$$B = KS(\prod_{i=1}^{nw} d_i^{\gamma_i}) \tag{4.3}$$

Where nw is the number of octaves of wavelet coefficients and d represents the cycle rms of wavelet coefficients at each octave. Unknown exponents in Equation 4.1 can be determined through optimization of the proposed index based on the information from kinetic of agglomeration breakage. Assuming that initial point of early agglomeration occurs at the oil mass fraction equal to 0.25%, , the proposed index at Equation 4.1 should be optimized to change sharply at this point.

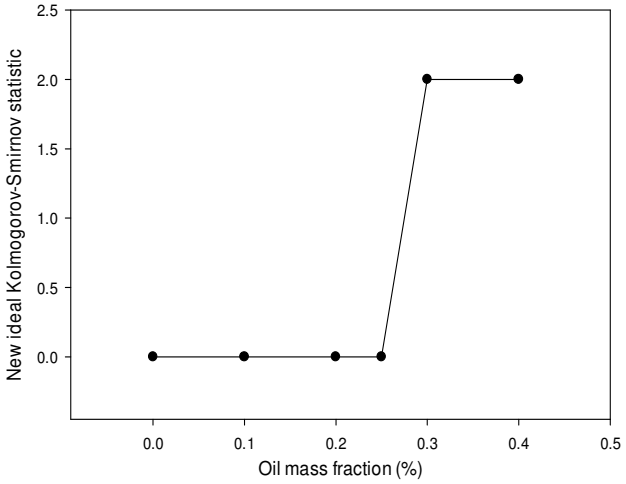

Figure 4.7: New ideal bogging index

The proposed index at Equation 4.1 should increase to a high value at initial point of bogging and should not change at other oil mass fractions and be independent of fluidization velocity as it is shown in the Figure 4.7. Therefore the optimization problem can be expressed as:

$$Max\left\{\frac{mean\{B|_{3<n\leq 6,m}\ \}}{mean\{B|_{0<n\leq 4}\ \}+\frac{1}{n}\sum\frac{\partial(B)}{\partial U_f}}\right\} \tag{4.4}$$

Where n represents oil mass fraction level ranges between 0 and 6 (corresponds to 0% and 4% oil mass fraction) and U_f represents fluidization velocity.

4.6. Results and discussion

The measured pressure data for all Voltesso oil mass fractions and fluidization velocities was decomposed to 16 octaves. The cycle rms of each octave at every second was calculated. A genetic algorithm was used to optimize the objective function shown in Equation 4.8 with an initial population size of 1000 and 2500 iterations. Table 4.1 shows the initial result for exponent of octaves at Equation 4.7:

Table 4.1: Exponents of wavelet coefficients at each octave calculated with Genetic algorithm

Octaves	1	2	3	4	5	6	7	8	9	10	11	12	13	14	15	16
Highest frequency (Hz)	166	83	41	21	10	5.2	2.6	1.3	0.65	0.32	0.16	0.08	0.04	0.02	0.01	0.005
Lowest frequency (Hz)	83	41	21	10	5.2	2.6	1.3	0.65	0.32	0.16	0.08	0.04	0.02	0.01	0.005	0.002
Exponents	0.01	0.07	-2.18	0.62	0.217	0.017	0.015	0.020	0.023	0.025	0.027	0.020	0.019	0.015	0.018	0.017

Since octaves 3, 4 and 5 were dominant due to higher exponents, the optimization was done again considering just octaves 3, 4 and 5 and the result is given in Table 4.2.

Table 4.2: Exponents of wavelet coefficients at dominant octaves calculated with Genetic algorithm

Octaves	3	4	5
Exponents	-2.66	0.76	0.061

Figure 4.8 shows the new Kolmogorov-Smirnov statistic from Equation 4.1 with the exponents of Table 4.2 versus the oil mass fraction at various fluidization velocities for 6 minutes of data when the reference is pressure data measured in dry coke. According to Figure 4.8 the proposed index increases sharply at 0.25% oil mass fraction while its sensitivity to fluidization velocity is small. A threshold value β was defined to determine

whether the fluidized bed is normal or failure. When the bogging index was larger than β, it can be judged that the fluidized bed is in malfunction. The red line in Figure 4.8 represents β with the selected value of 4. For a value of β of 4, the new Kolmogorov-Smirnov statistic can reliably detect bogging for oil fractions greater than 0.275 %, independently of the fluidization velocity.

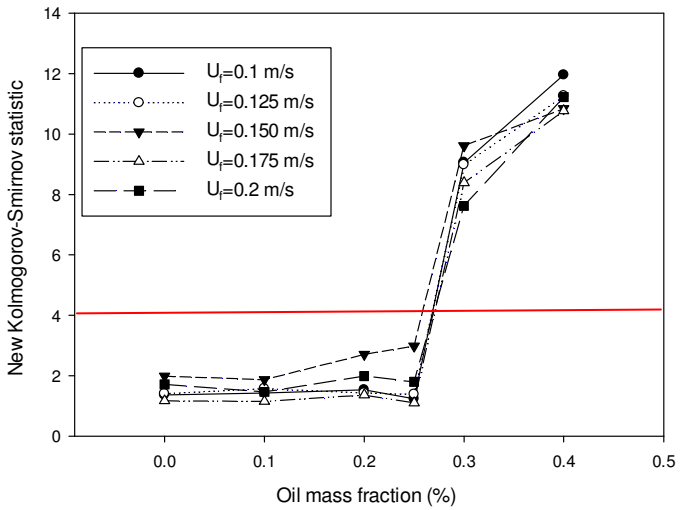

Figure 4.8: New Kolmogorov-Smirnov statistic versus oil mass fraction and fluidization velocity

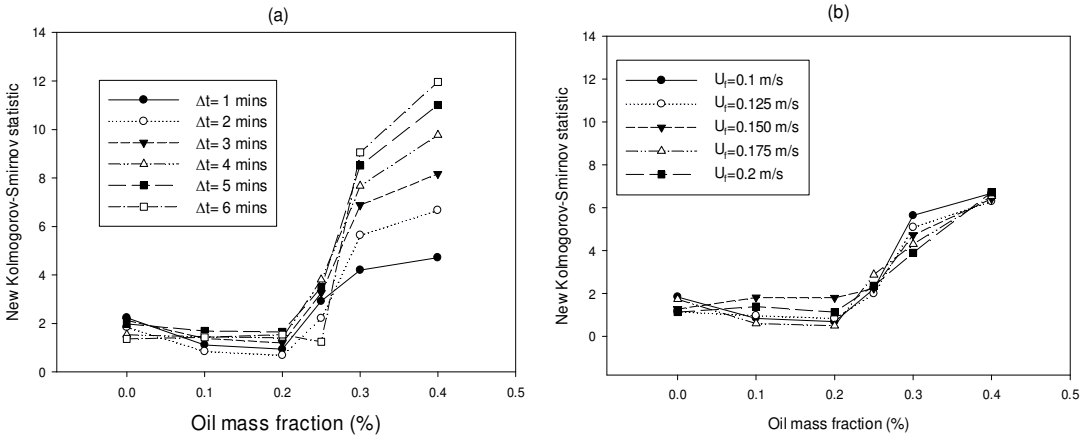

Figure 4.9: New Kolmogorov-Smirnov statistic versus oil mass fraction a) at different length of data (U_f=0.1 m/s) b) at different fluidization velocities for 2 minutes of pressure data

For β of 3, bogging could be detected for oil fractions greater than 0.25 %.

Figure 4.9-a shows the new Kolmogrov-Smirnov statistic for different lengths of pressure data. It can be seen that the new Kolmogrov-Smirnov statistic performs better with longer data as the sensitivity to bogging increases. Figure 4.9-b shows the new Kolmogrov-Smirnov statistic at different fluidization velocities for two minutes of data. According to this Figure the sensitivity to fluidization velocity is still low enough and with the same value for β, 2 minutes of data can be used to detect bogging.

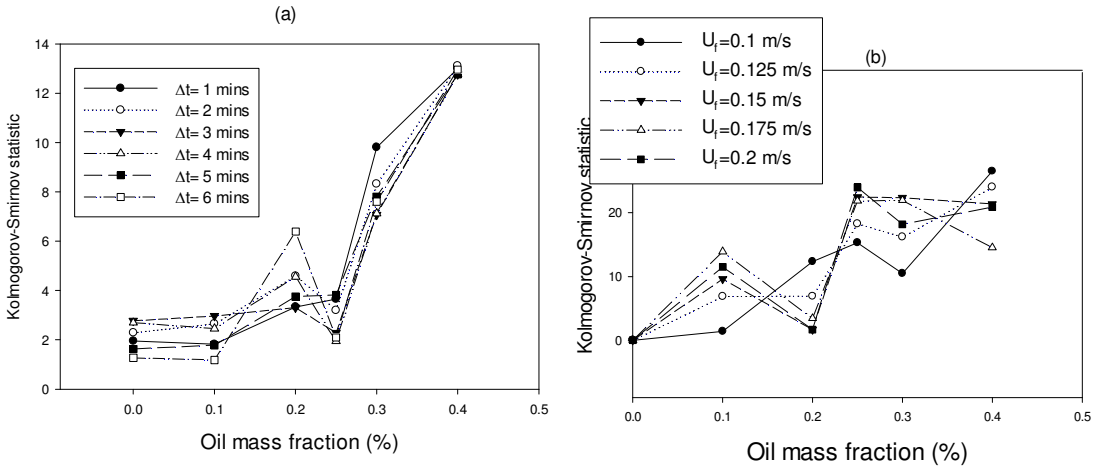

Figure 4.10: Kolmogorov-Smirnov statistic (Bartels, 2010) of measured pressure versus oil mass fraction a) at different length of data (U_f=0.1 m/s) b) at different fluidization velocities for 2 minutes of pressure data

Figure 4.10, 4.11 and 4.12 show the Kolmogrov-Smirnov statistic (Bartels, 2010), Wstat and attractors difference index for different length of pressure data. For all three indices, when the length of pressure data is reduced, the sensitivity to fluidization velocity increases that makes the detection of bogging more difficult. If just 2 minutes of pressure data be available, the new Kolmogrov-Smirnov statistic can perform better since it is less sensitive to fluidization velocity when compared to other presented methods.

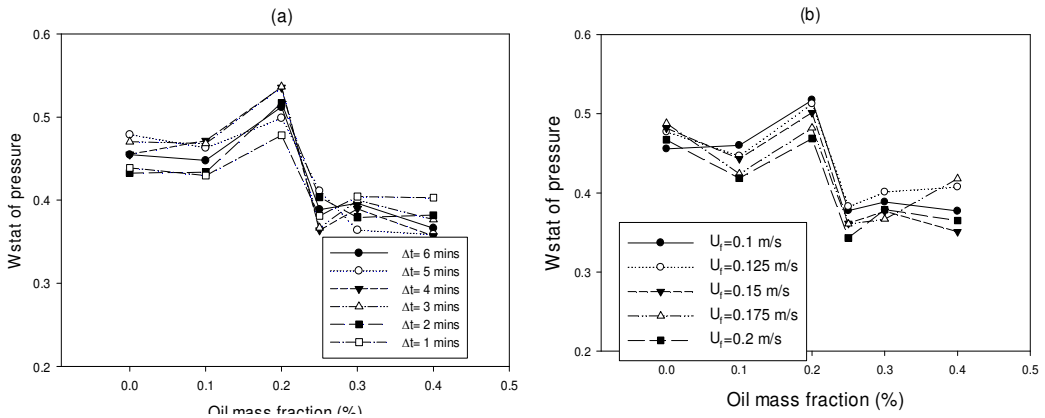

Figure 4.11: Wstat of measured pressure versus oil mass fraction a) at different length of data (U_f=0.1 m/s) b) at different fluidization velocities for 2 minutes of pressure data

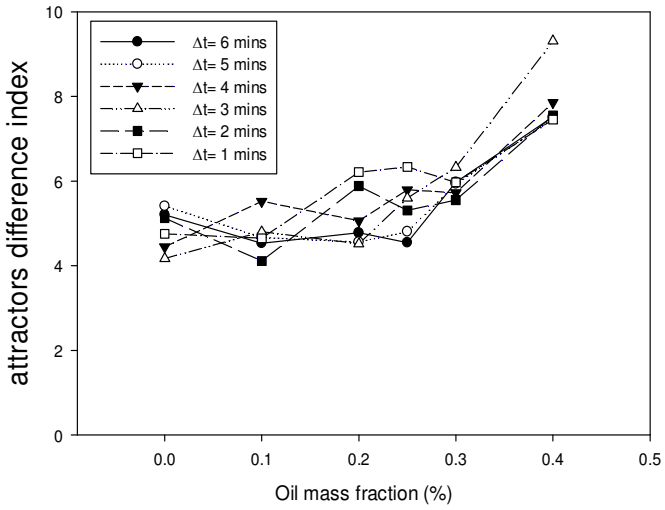

Figure 4.12: Attractors difference index versus oil mass fraction at different length of data (U_f=0.1 m/s)

In practice, pressure data of fluidized dry particles with the same fluidization condition as the reference data is not available since the fluidization is usually a continuous process. The evaluation of new Kolmogrov-Smirnov statistic with pressure data of different oil concentration as the reference is therefore necessary. Figures 4.13-a and 4.13-b show the new Kolmogrov-Smirnov statistic while the reference pressure data measured at 0.1% and 0.2% of Voltesso oil mass fraction instead of dry coke. According to these Figures, if

the reference data is measured in wet fluidized particles, the new Kolmogrov-Smirnov statistic increases sharply at 0.25% oil mass fraction while its sensitivity to fluidization velocity is still negligible since the highest index at oil mass fraction of 0.2% is still much lower than the lowest index at oil mass fraction of 0.3% and can't cause false detection of bogging. The new Kolmogrov-Smirnov statistic therefore can be used to detect bogging if the reference data is measured in wet fluidized particles. Comparison of all bogging detection methods is provided in Table 4.3.

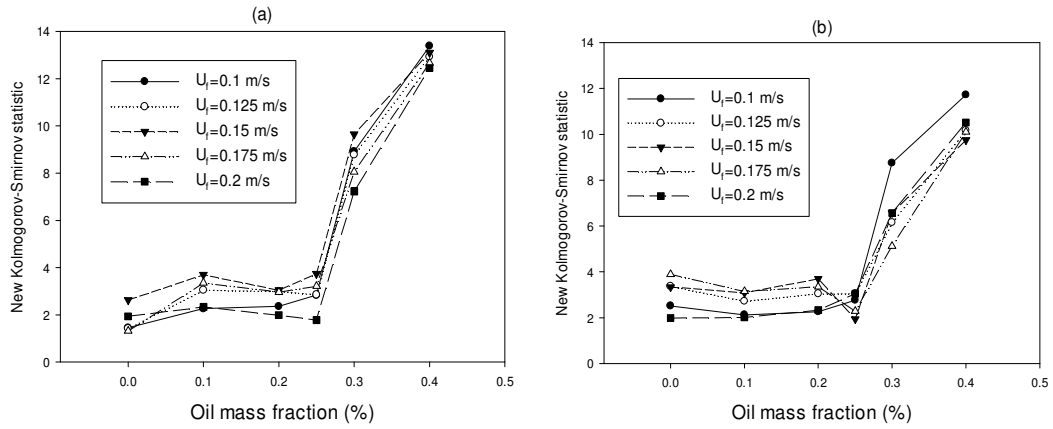

Figure 4.13: New Kolmogorov-Smirnov statistic versus oil mass fraction and fluidization velocity a) The reference data measured at 0.1% oil fraction b) The reference data measured at 0.2% oil fraction

4.7. Comparison of new KS test with other bogging detection methods

To compare different bogging detection methods, first, all bogging index values calculated at different oil mass fractions and fluidization velocities were normalized:

$$I_{nm} = \frac{B_{nm} - B_{0,m}}{B_{6,m} - B_{0,m}} \quad (4.5)$$

Where n represents oil mass fraction and m represents fluidization velocities. $B_{0,m}$ and $B_{6,m}$ are therefore calculated bogging index values at dry bed and bogged bed respectively. Four indices defined using normalized values:

a) As it is shown in the Figure 4.7 the ideal bogging index should be constant before initial bogging at oil mass fraction of 0.25% regardless of length of pressure data.

To evaluate methods based on this criteria, 6 minutes of measured pressure data was divided in 3 sections, each with a length of 2 minutes, then the standard deviation between the 3 values of I_{nm} calculated for each of the 2 minutes sections ($std(I_{nm})$) was averaged over the three oil mass fractions at which the bed was normally operated, 0%, 0.1% and 0.2% for all 5 fluidization velocities to obtain the first performance index:

$$PI_1 = \frac{1}{15}\sum_{m=1}^{5}\sum_{n=0}^{2} std(I_{nm}) \tag{4.6}$$

b) The ideal bogging index should not be sensitive to fluidization velocity. The high sensitivity to fluidization velocity prevents distinction between normal operation and initial bogging. This criteria therefore can be formulated as:

$$PI_2 = \frac{0.5*(std(I_{0m})+std(I_{5m}))}{\frac{1}{5}(\sum_{m=1}^{5} I_{5m}-\sum_{m=1}^{5} I_{0m})} \tag{4.7}$$

c) Some bogging detection methods can detect bogging using few minutes of pressure data while others may require more than 10 minutes of pressure data. So, the minimum length of pressure data needed for bogging detection is another important criteria. In general, with reducing the length of pressure data for a given bogging detection method, the sensitivity of calculated values to fluidization velocity increases. This criteria therefore can be formulated by implementing the PI_2 for 2 minutes of pressure data, giving the criterion PI_3.

d) The time that is needed for calculation of the bogging index also should be low enough to enable immediate remedial actions. The processor used here for calculations is a 4 core, 2.2 GHz Intel i7, and the software is Matlab. The calculation time of each bogging index is the fourth performance index.

Results of all three performance indices are given in table 4.3. All three performance indices should be minimum at ideal condition. According to this table the new Ks test outperforms other bogging detection methods at PI_2 and is close to best index at PI1 and PI_3. Surprisingly, the time-averaged pressure gradient performs relatively well, which means that bogging detection could be performed even if only the time-averaged pressure gradient was available. With the exception of the chaos analysis method, all methods require less than 1 s of calculation time, which is much smaller than the time required to acquire the data.

Table 4.3: Comparison of bogging detection methods

	PI_1 (%)	PI_2	PI_3	PI_4
Average of pressure data	3.61	5.95	7.3	<1s
Standard deviation of pressure data	6.37	6.32	8.62	<1s
Kolmogorov-Smirnov test (Bartels, 2010)	5.47	5.75	6.61	<1s
Wstat	8.79	6.42	11.41	<1s
New Kolmogorov-Smirnov test	4.15	3.8	7.12	<1s
Chaos analysis	12.184	13.3	28.31	<10 min

Although the results obtained for PI_3 suggest that bogging detection could be achieved with as little as 40 s of pressure fluctuations data, table 3 shows that much better results are obtained with PI_2, indicating that using 2 minutes of data would give much better results. With 2 minutes of data, the new Kolmogorov-Smirnov index was clearly superior to the other bogging indices.

4.8. Effect of bogging on the frequency spectrum of pressure fluctuations

It has been reported that measured pressure fluctuations originate from bubble formation, bubble velocity, bubble frequency and changes in bed voidage (Schouten, 1998). The change in frequency spectrum of pressure fluctuations due to bogging can be a result of the change in source or medium of pressure waves in fluidized bed since any medium can attenuate or magnifies each mechanical traveling wave with a specific frequency at different levels. According to the measurements, the average bubble velocity first

decreases with increasing Voltesso oil mass fraction but increases after passing the initial point of bogging (Figure 4.14).

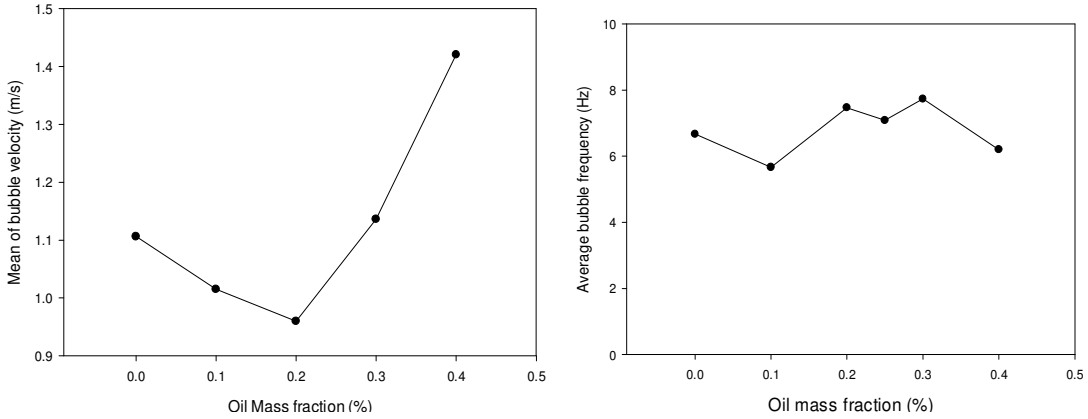

Figure 4.14: Average bubble velocity and frequency at different Voltesso oil mass fractions (U_f=0.1 m/s)

The change in bubble frequency is negligible with increasing oil mass fraction as shown in Figure 4.14. Therefore, regardless of changes in the source of pressure fluctuations, the effect of bogging on the medium was studied here using a speaker as the source that is independent of bed hydrodynamics.

In order to study the effect of particle wetness on attenuation of pressure fluctuations, the attenuation of sound waves with different frequencies was measured in the fluidized bed. A subwoofer speaker generated the sound with frequencies ranging from 5 to 110 Hz at constant amplitude. A microphone was used to measure the intensity of the sound that passed the fluidized particles at minimum fluidization velocity. Experiments were performed using air, dry particles and wet particles with different liquid mass fractions as the propagating medium.

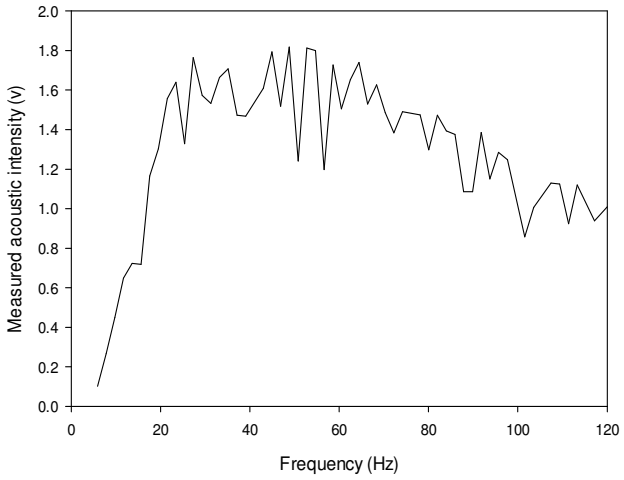

Figure 4.15: Measured acoustic intensity generated by subwoofer in air

Figure 4.15 shows the measured sound intensity in the empty bed when the medium was air. This Figure actually shows the frequency response of the subwoofer speaker. Figure 4.16 shows the measured sound intensity at different oil mass fraction in coke particles.

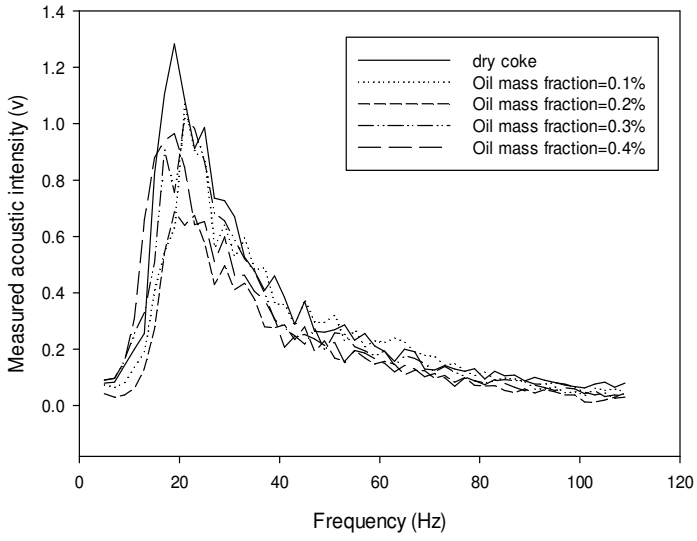

Figure 4.16: Measured acoustic intensity generated by subwoofer in a fluidized bed of dry or wet coke particles

According to this Figure, the sound intensity decreased much more sharply with increasing frequency than in air due to loss of acoustic energy caused by particles vibration and friction. Figure 4.17 shows the acoustic intensity measured at different oil

mass fraction in coke particles that was smoothed using a low pass filter with normalized cut-off frequency of 0.1 (normalized by Nyquist frequency).

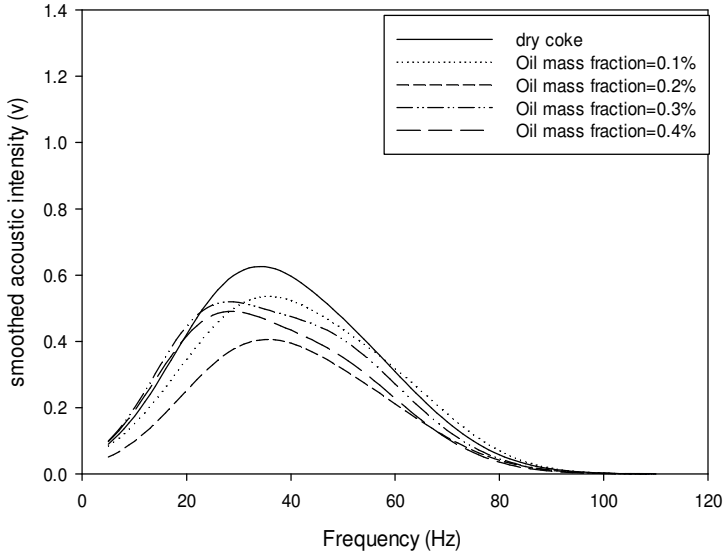

Figure 4.17: Smoothed acoustic intensity generated by subwoofer in a fluidized bed of dry or wet coke particles

The sound intensity associated with wet coke particles normalized by the sound intensity measured with dry coke has been shown in Figure 4.18. As it can be seen in the Figure 4.18, the sound attenuation in wet particles is stronger at higher frequencies; this stems from the higher loss of acoustic energy due to more friction loss between cohesive, wet particles. At higher oil mass fractions, particles act like a low pass filter with a cut off frequency close to 20 Hz and this is the main clue for the negative exponent for octave 3 with frequency above 20 Hz and positive exponent for octave 4 and 5 with frequencies below 20 Hz, as shown in Table 4.2.

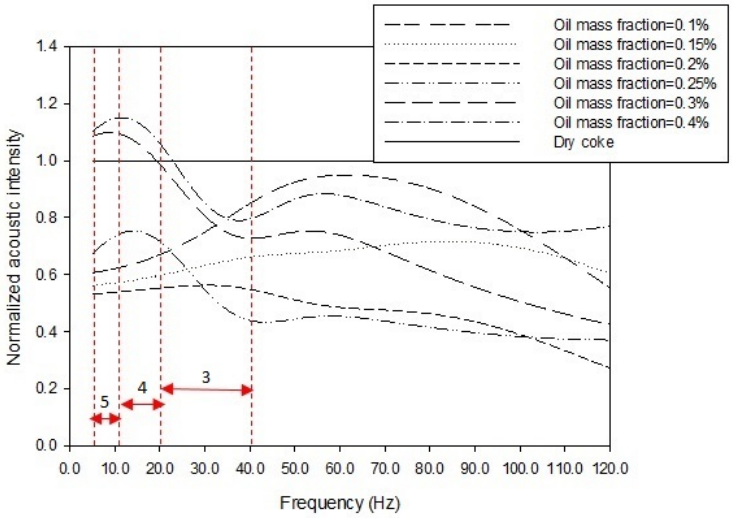

Figure 4.18: Normalized acoustic intensity generated by subwoofer in a fluidized bed of dry or wet coke particles (Octaves 3,4 and 5 are labeled)

4.9. Conclusion

Various methods for the detection of bogging in a fluidized bed from pressure fluctuations were tested. The best results were obtained with a new index based on wavelet decomposition of pressure fluctuations. Results shows that the proposed method detects the early bogging caused by the injection of liquid into the fluidized bed. This method is not affected by fluidization velocity and its success has been explained based on the variation with bogging of the transmission of sound at different frequencies in the fluidized bed.

4.10. References

Bartels, M. Nijenhuis, J. Kapteijn, F. Van Ommen, .J.R. “Case studies for selective agglomeration detection in fluidized beds: Application of a new screening methodology” Powder Technology 203(2) 148-166 (2010).

Briens, C. McDougall, S. Chan, E. "On-line detection of bed fluidity in a fluidized bed coker" Powder Technology 138(23) 160-168 (2003).

Cohn, R. Russel, J. “Kolmogorov-Smirnov test”, VSD (2012)

Fuller, TA. Flynn, TJ. Daw, CS. Halow, JS. “Interpretation of pilot-scale, fluidized bed behaviour using chaotic time series analysis”, Proceedings of the 12th international FBC conference, (1) 141–55 (1993)

Hamidi, M. Berruti, F. Briens, C. McMillan, J. “A Novel AC-based Impedance Meter to Reduce Capacitive and Inductive Coupling Noise” (2014)

Hamidi, M. Berruti, F. Briens, C. McMillan, J. “Bogging Detection in a Fluidized Bed Using Plannar Capacitance Sensors” The 14th International Conference on Fluidization – From Fundamentals to Products (2013)

McLaughlin, L.J., Rhodes, M.J. "Prediction of fluidized bed behaviour in the presence of liquid bridges" Powder Technology 114 (1-3): 213–223 (2001)

Mohagheghi, M. Hamidi, M. Berruti, F. Briens, C. McMillan, J. “Study of the effect of local hydrodynamics on liquid distribution in a gas–solid fluidized bed using a capacitance method” Fuel, 107 236-245 (2013)

Molerus, O. "Interpretation of Geldart’s type A, B, C, and D powders by taking into account interparticle cohesion forces" Powder Technology 33(1): 81–87 (1982)

Schouten, J. C. Van den Bleek, C. M. “Monitoring the Quality of fluidization using the short –term predictability of pressure fluctuations”, AICh,E J.,44(1) 48-60(1998)

Seville, J.P.K. Clift, R. "The effect of thin liquid layers on fluidisation characteristics" Powder Technology 37 (1): 117–129 (1984)

Van der Schaaf, J. Schouten, J.C. Van den Bleek C.M. “Origin, propagation and attenuation of pressure waves in gas—solid fluidized beds”, Powder Tech. 95(3) 220-233(1998)

Van Ommen, J.R. Coppens, M.O. Van Den Bleek, C.M. Schouten, J.C. "Early warning of agglomeration in fluidized beds by attractor comparison" AIChE 46(11) 2183-2197 (2000).

Weinstein, H. Shabaker, RH. Tiller, ML. Taylor, JH. Pitzer, DR." Exxonmobil Res & Eng CO (ESSO). Process for detecting, monitoring changes in property of particulate to produce synthesis gas involves sensing pressure in fluidized bed, processing collected pressure fluctuation data and comparing it over time" Patent WO 00/43118-A.,(2000)

Werther, J. "Measurement techniques in fluidized beds" ", Powder Tech. 102(15) (1999)

CHAPTER 5: EARLY DETECTION OF DEFLUIDIZATION FROM THE MEASURED SPEED OF SOUND

5.1. Introduction

Bogging is an important problem in some fluidized beds, which degrades the process. In a fluidized bed, bogging usually happens when particles stick together due to excess liquid or too high a temperature. This results in uneven distribution of the gas, poor solids mixing and defluidized zones. Early detection of bogging in fluidized beds is attractive as it provides time for remedial action.

Several methods were published to detect defluidization in fluidized beds. Among them, pressure fluctuations (Briens, 2003, Chong, 1987,Van Ommen,2000), electrostatic(Briens, 1999), heat transfer (Ropchan, 1981) and acoustic emission (Tsujimonto, 2000) are popular. Analysis of pressure fluctuations is widely used to detect early defluidization through the associated changes in bubble properties, which in turn affect the pressure fluctuations; however the shortcoming of this method is that the cohesive particles can easily block the pressure probe and hinder the required measurements.

Propagation of pressure waves in fluidized bed has been studied to find proper explanation for pressure fluctuations behavior and diagnostics of local hydrodynamics (Grace, 1995, Roy, 1990). Roy et al. (Roy, 1990) studied the speed of sound in a gas-fluidized bed by cross-correlating pressure fluctuations induced by a disturbance measured at two different locations in the fluidized bed. Roy et al. (Roy, 1990) derived an expression for the speed of sound in a homogenous two-phase medium that was verified later by Khawaja et al (Khawaja, 2011) using CFD-DEM numerical simulation. Grace et al. (Grace, 1995) found that the speed of pressure wave in a fluidized bed is in the order of 10 m/s while it tends to be higher when the bed is defluidized. Grace et al. (Grace, 1995) observed that the propagation velocity of pressure waves in gas-solids fluidized beds can be well predicted by the pseudo-homogeneous compressible wave theory and the separated flow compressible wave theory for group A and B particles. However, both

theories fail to predict the tremendous increase in propagation velocity of pressure wave that occurs below the minimum fluidization velocity.

Based on the above mentioned works, it might be possible to use the speed of sound to detect early bogging in the fluidized bed since its value varies greatly between fluidized and defluidized conditions. However, no research has been conducted in this area so far.

The main objective of this study is to develop a new bogging detection method developed based on measured speed of sound in the fluidized bed of cohesive particles, where the bogging is defined from the kinetics of wet agglomerate breakage in the fluidized bed. This study has three goals:

1) Show that the measured speed of sound in a fluidized bed is greatly affected by bogging and not greatly affected by fluidization velocity. This would mean the speed of sound could be used to detect bogging in commercial beds where the local velocity may not be exactly known.
2) Measure the bubble properties with an independent method and show which bubble properties are affected by bogging and not greatly affected by the fluidization velocity.
3) Use simulation to verify that the impacts of bogging and fluidization velocity on bubble properties explain why changes in speed of sound are mostly affected by bogging.

5.2. Speed of sound in the fluidized bed

The speed of sound in continuous compressible medium can be expressed as (Lamb, 1963):

$$u_s = \sqrt{\frac{dp}{d\rho}} \tag{5.1}$$

Where u_s represents the speed of sound, p is the pressure and ρ is the density of the medium. Roy et al. (Roy, 1990) made a number of assumptions to apply Equation 5.1 to a two-phase mixture of gas and particles:

1. The gas and particles move together

2. The interstitial gas is compressible and obeys the ideal gas law
3. The gas and particles are isothermal
4. Particles are incompressible

The speed of sound in the two phase mixture is then:

$$u_s = \sqrt{\frac{\rho_g RT}{\varepsilon(\rho_p(1-\varepsilon)+\rho_g\varepsilon)}} \tag{5.2}$$

The speed of sound in an ideal gas is $u_{s0} = \sqrt{\gamma RT}$, where γ is the ratio of specific heat constants. Therefore the speed of sound in the two phase medium can be related to the speed of sound in pure gas by

$$u_s = u_{s0}\sqrt{\frac{\rho_g}{\gamma\varepsilon[\rho_p(1-\varepsilon)+\rho_g\varepsilon]}} \tag{5.3}$$

Two other approaches also were published in the literature for the calculation of speed of sound: the isentropic flow (Grace, 1995), and the separated phase flow (Weir, 2001). Table 5.1 summarizes the calculated speed of sound according to different assumptions where the frequency of sound is 250 Hz, ρ_p = 1480 kg m^{-3}, ρg = 1.25 kg m^{-3}, ε =0.4, γ = 1.4 and uso = 340 ms^{-1}

Table 5.1: Speed of sound calculated with different assumptions

250 Hz, ρ_p = 1480 kg m^{-3}, ρ_g = 1.25 kg m^{-3}, ε =0.4, γ = 1.4 and u_{so} = 340 ms^{-1}

One phase isothermal flow (Roy, 1990)	One phase isentropic flow (Grace, 1995)	Separated phase flow (Weir, 2001)
17.04 m/s	20.99 m/s	22.53 m/s

5.3. Experimental

5.3.1 Experimental set up

Experiments were conducted in a 1.97 m high fluidized bed with a trapezoidal cross sectional area, as shown in Figure 5.1. Coke particles with a Sauter mean diameter of 144 μm and a total mass of 42 kg were used for all the experiments. The bed was fluidized with air at a superficial velocity ranging from 0.1 to 0.2 m/s.

Two rectangular wooden windows were mounted on two sides of the wall of the fluidized bed to enable capacitance measurement with electrodes on the outside of the bed wall. The capacitance between the central electrode and each side electrode at the bottom of wooden window was measured with a capacitance meter with an acquisition frequency of 5 kHz during 15 seconds.

A speaker was mounted above the freeboard and eight microphones installed on the wooden window to enable measurement of speed of sound in the fluidized bed. The outputs of microphones amplified and measured with an acquisition frequency of 100 kHz.

Measurements have been performed as Voltesso oil was progressively added to the fluidized bed. Voltesso oil simulates, at room temperature, the properties of heavy oil at high coker temperatures. Voltesso oil, which has a negligible vapor pressure at room temperature, was used to provide a constant liquid background during each experiment and was mechanically mixed with particles to ensure that all the liquid coated individual particles and that no coke-Voltesso agglomerates were formed.

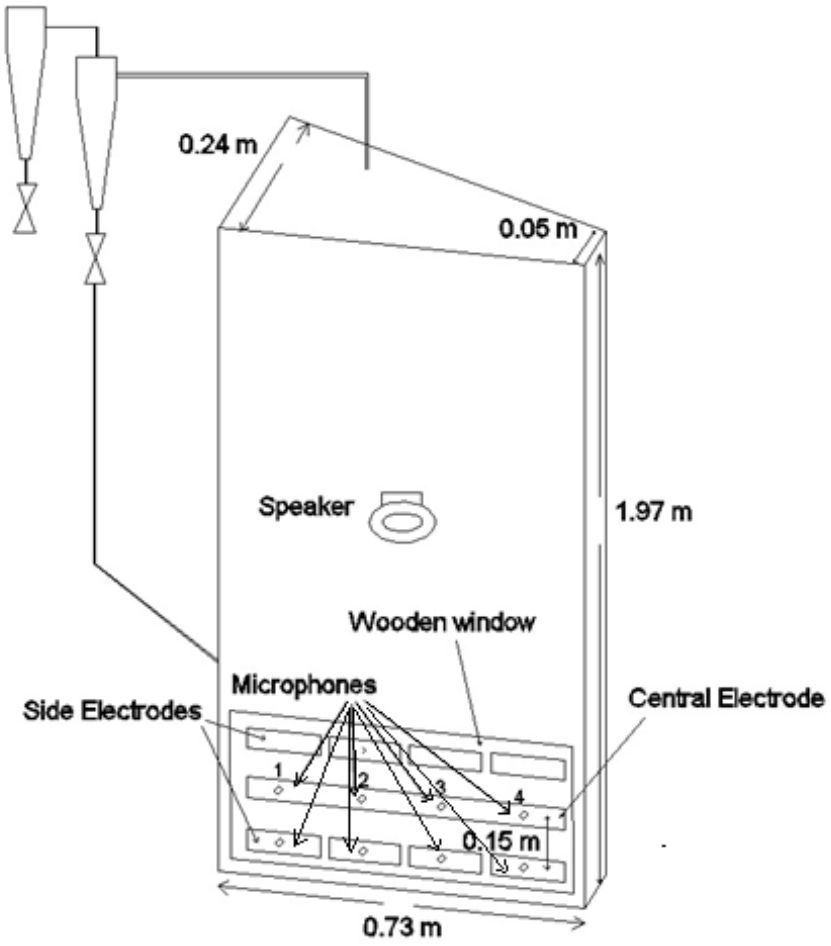

Figure 5.1: Schematic diagram of experimental set up

5.3.2. Measuring the speed of sound

To measure the speed of the sound, a speaker mounted at top of the bed to generate the sound as it is shown in the Figure 5.1. Train pulses with the frequency of 250 Hz were generated with a microcontroller to drive the speaker as shown in the Figure 5.2. This frequency eliminated any risk of resonance of height of the bed or the column.

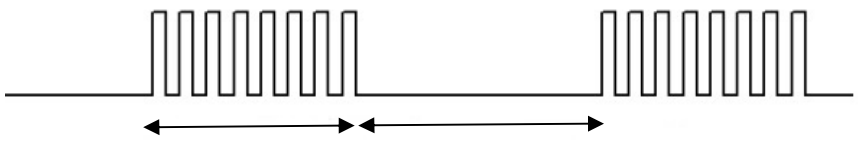

Eight microphones were installed along two rows and 4 columns.. The first row of microphones was 5 cm above the gas distributor while the second row of microphones was 45 cm above the gas distributor and actual height of the bed was 60 cm at minimum

fluidization velocity. All microphones where flash mounted to the inside wall of the bed. The speed of sound between two vertically separated microphones in a column was calculated by dividing the distance between the microphones with the associated time delay, which was obtained from cross correlation between the microphones signals. The large difference in speed of sound between fluidized and defluidized beds means that the time delay between pulses measured by two microphones varied over a wide range. Using a pulse train to generate sound with adequate delay between two subsequent trains of pulses instead of using low frequency sound, enables the measurement of the time delay between microphones outputs over a wide range.

5.3.3. Measuring the bubble geometry and bubble distance from the wall

Planar capacitance sensors were used to determine the bubble geometries in the fluidized bed. This was done by comparing simulated capacitance variations due to the passage of gas bubbles of various characteristics, and then finding which of these simulated capacitance variations fitted best the observed capacitance variations. These calculations would have been slow, so neural networks were used to greatly speed this determination of the bubble geometries.

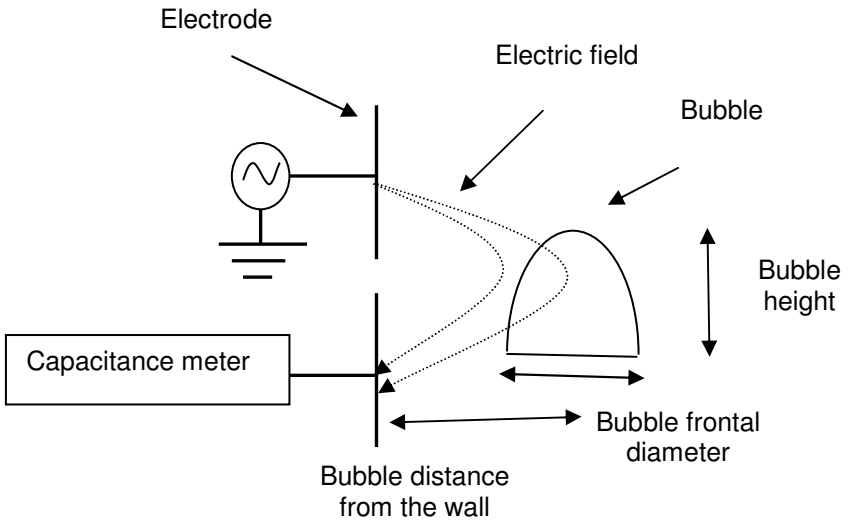

Figure 5.3: A bubble crosses the electric field

The capacitance time series due to passing bubbles with a certain height, frontal diameter and distance from the wall was generated with simulation using Comsol Electrostatic toolbox as shown in Figures 5.3 and 5.4. The simulation results were, then, used to train three neural networks to enable the prediction of the vertical bubble height, frontal diameter and distance from the wall from measured capacitance time series. First, the capacitance time series was normalized in amplitude by dividing the measured capacitance with the measured background capacitance (i.e. the capacitance of the defluidized bed). It also was normalized in time, for each bubble, by dividing the time with the total time of passage of the bubble, as determined from the resulting capacitance disruption; the normalized time series was, then, independent of bubble velocity. Using 16 values of normalized capacitance for each bubble (Figure 5.5), neural networks were trained to predict the bubble geometries.

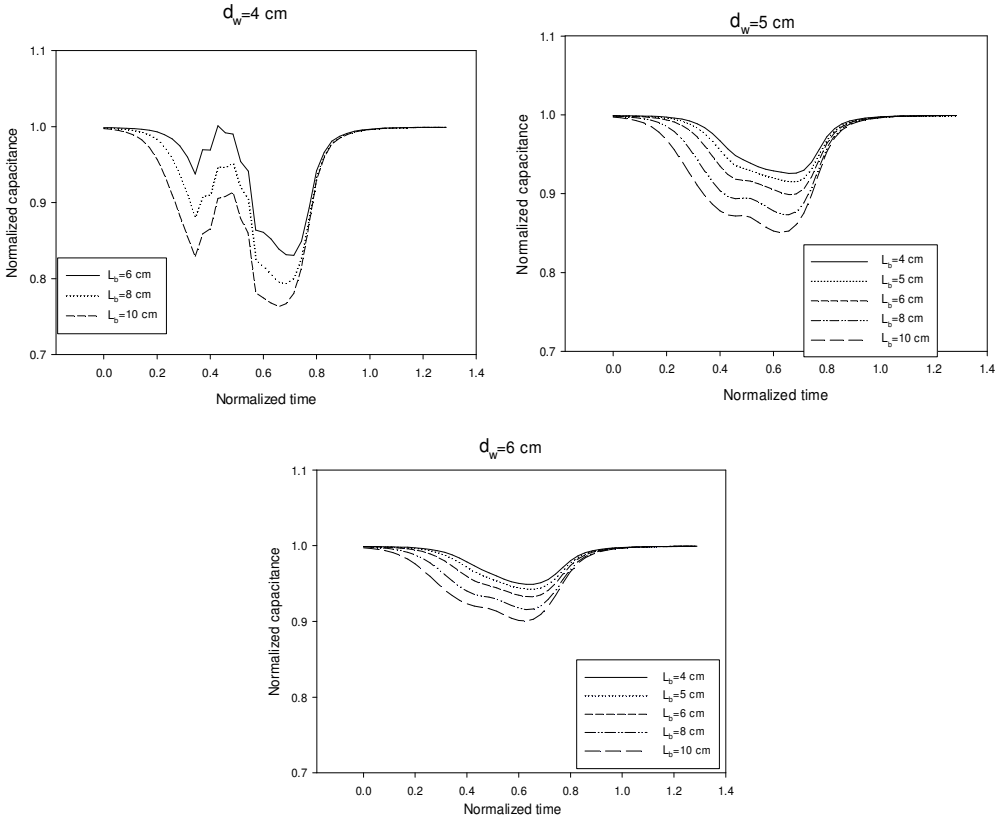

Figure 5.4: Time series of simulated normalized capacitance at different bubble height when the bubble frontal diameter is 8 cm and the bubble distance from the wall ranges from 4 cm to 6 cm

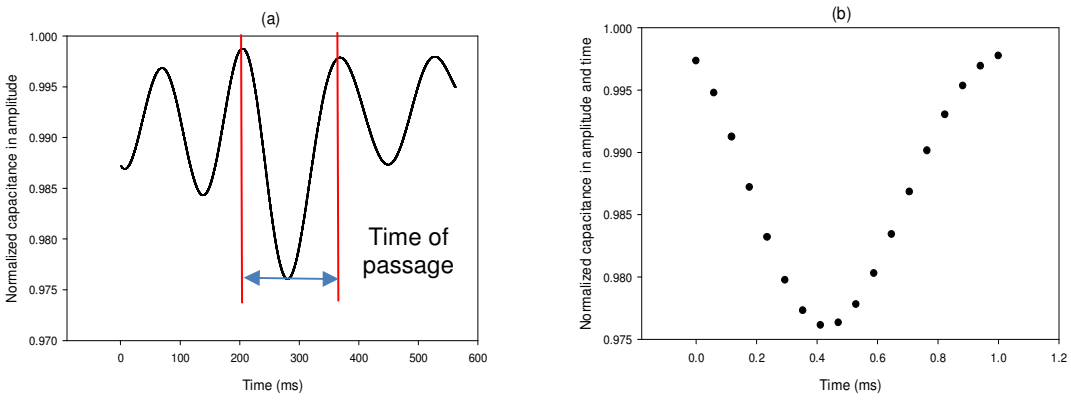

Figure 5.5: a) Normalized capacitance in amplitude b) Normalized capacitance in amplitude and time, showing the 18 points used as input to the neural network

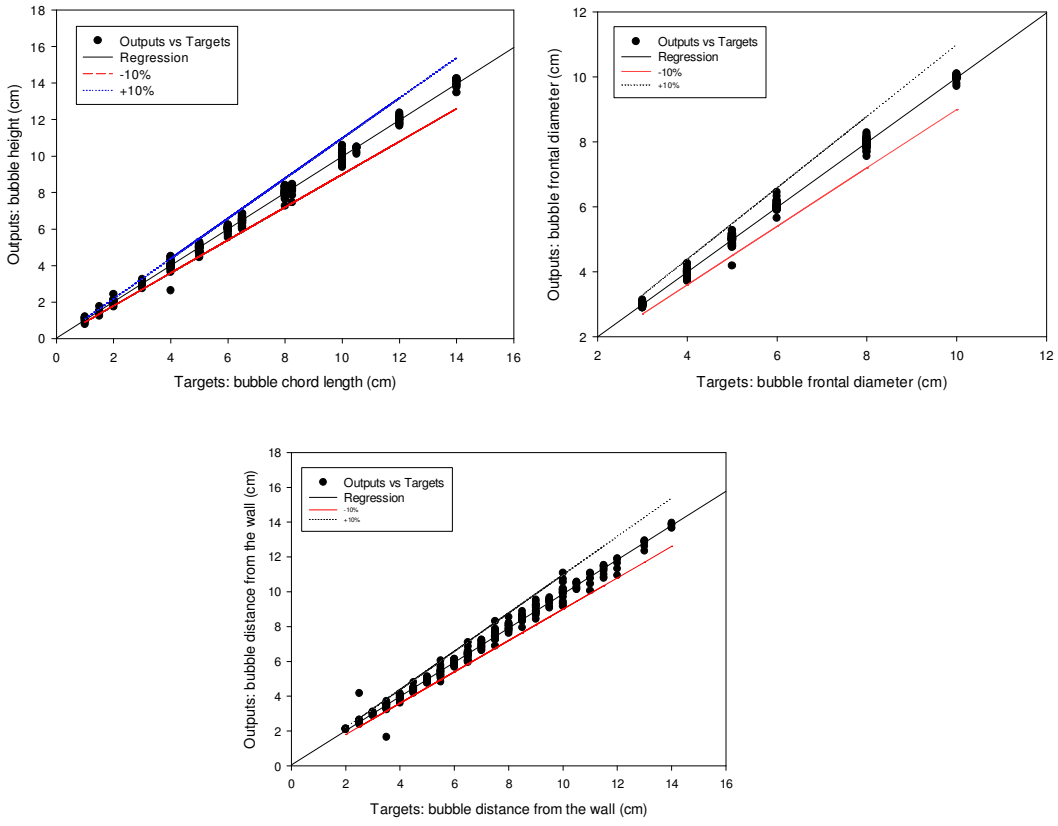

Figure 5.6: Outputs of neural networks versus targets for all the simulated data

Show dashed lines e.g. + 10 % and – 10%

Each neural network was implemented with three layers, 18 inputs in the first layer, 13 neurons in the hidden layer and one output in the third layer. 280 time series of capacitance were generated by simulation for different bubble geometries and bubble distances from the wall. 90% of the data was used for training while 5% of the data was used for testing and 5% of data for validation. Figure 5.6 shows the outputs of neural networks versus targets for all the data.

5.4. Results: Measured Speed of Sound

The speed of sound in the fluidized bed is much lower than the speed of sound in the defluidized bed. Figure 5.7 shows the speed of sound at different superficial gas velocities. The speed of sound measured in the fluidized bed is 26 m/s which is more close to the separate phase flow assumptions (Weir, 2001).

To investigate the effect of bogging and fluidization velocity on the speed of sound, the fluidized bed was operated with a constant fluidization velocity and Voltesso oil was added to coke particles in several steps until channeling occurred in the bed. At each step, the speed of sound as well as capacitance were measured.

Figure 5.8 shows the speed of sound measured at four locations in the bed for different concentrations of Voltesso oil and fluidization velocities. According to Figure 5.8, the speed of sound is almost constant before the concentration of Voltesso oil reaches 0.25 wt%, which was identified as the initial point of bogging for a fluidized bed of coke and Voltesso oil in chapter 3. The sudden increase in the speed of sound at this point for all fluidization velocities shows that this method can detect initial bogging even if the fluidization velocity is unknown. Furthermore, it can be used with two vertically separated microphones within the fluidized bed without any concerns that cohesive particles may plug the microphones.

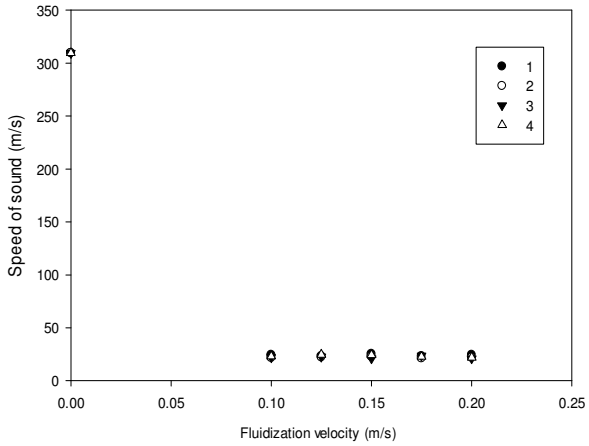

Figure 5.7: Measured speed of sound at different superficial gas velocities measured at four horizontally separated locations

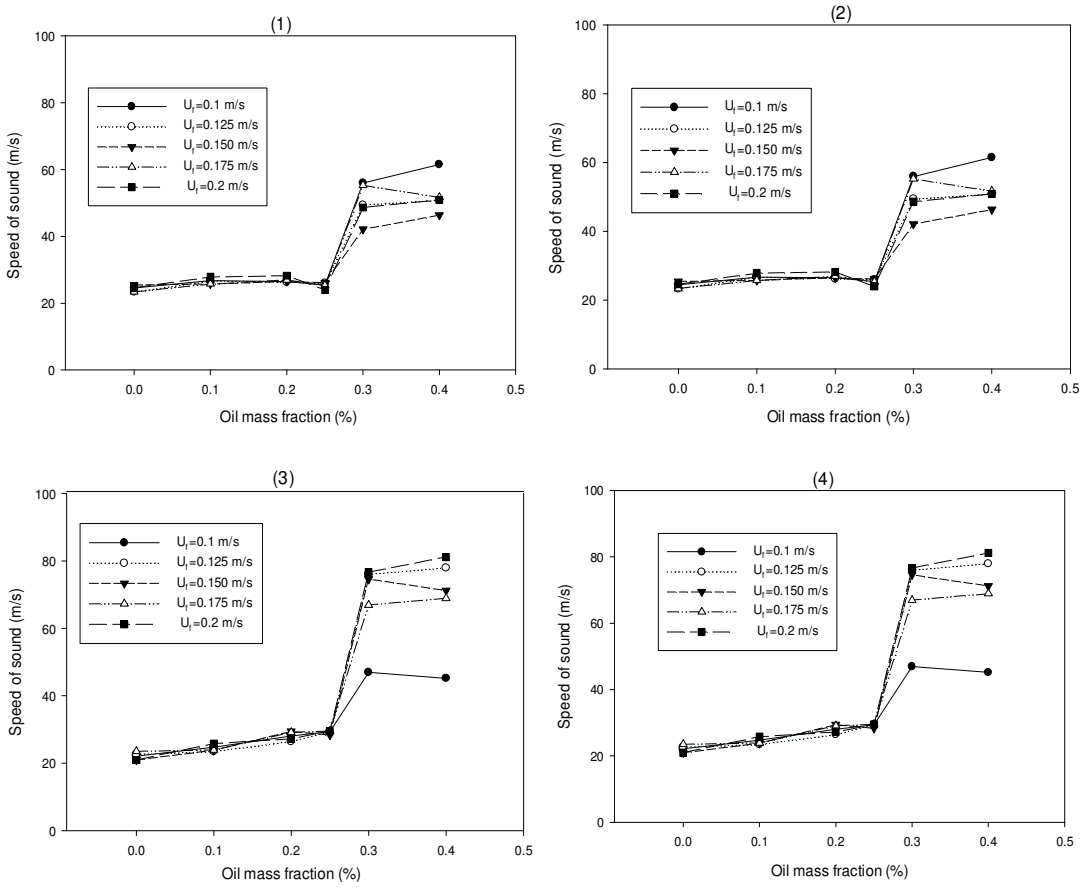

Figure 5.8: Measured speed of sound at different oil mass fractions and fluidization velocities measured at four horizontally separated locations

Interpretation of Results

5.3.1. The Simulation Approach

Since the speed of sound changes with the fluidization velocity after initial point of bogging in the well mixed bed, the effect of bubbles geometry on speed of sound can be significant. The inter-particle friction as another parameter that may change with bogging can also affect the speed of sound (Weir, 2001). Weir included the inter-particle friction in the equations of speed of sound and mentioned that the friction between particles increases the speed of sound (Weir, 2001).

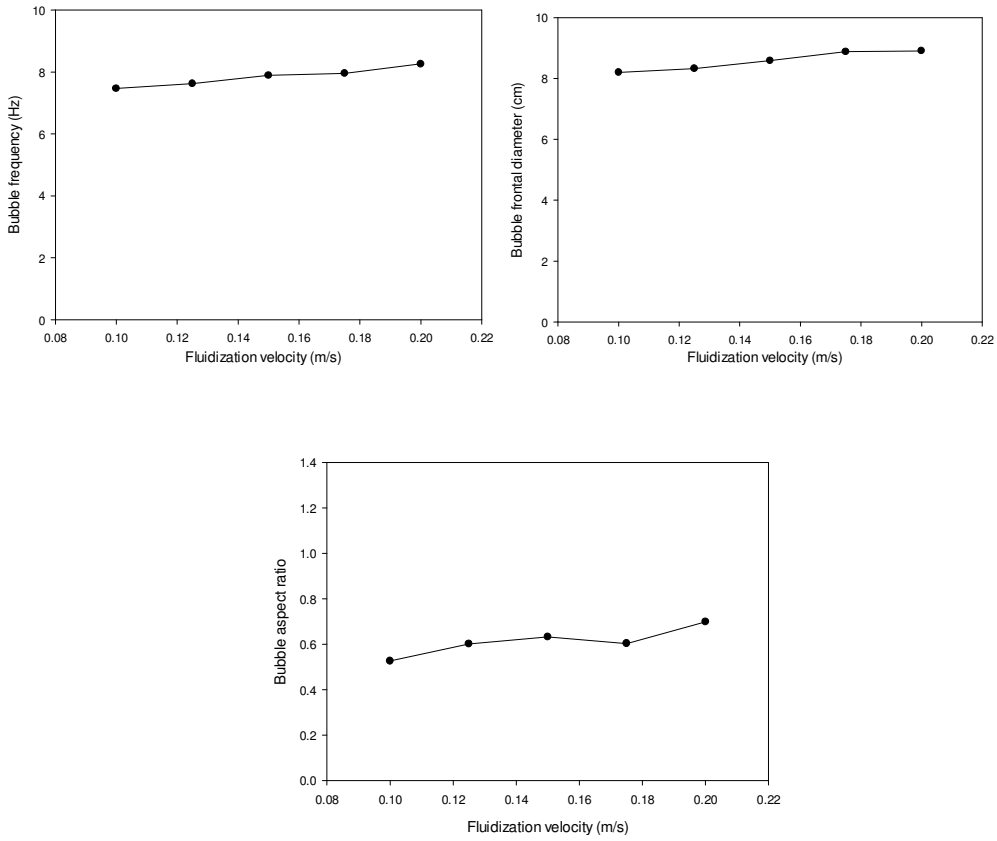

Figure 5.9: a) Effect of fluidization velocity on the bubble frequency b) Effect of fluidization velocity on the bubble frontal diameter c) Effect of fluidization velocity on the bubble aspect ratio

However the inter-particle friction is difficult to measure in the fluidized bed and this approach is more qualitative. In a bubbling fluidized bed, it is much easier to accurately measure the impact of inter-particle friction on the geometry of the gas bubbles.

Figure 5.9 shows the impact, in a dry bed, of the fluidization velocity on the bubble frequency, bubble frontal diameter and bubble aspect ratio as characterized from the ratio of bubble height to frontal diameter. The bubble frequency, frontal diameter and bubble shape are not greatly affected by the fluidization velocity, as shown in Figure 5.9.

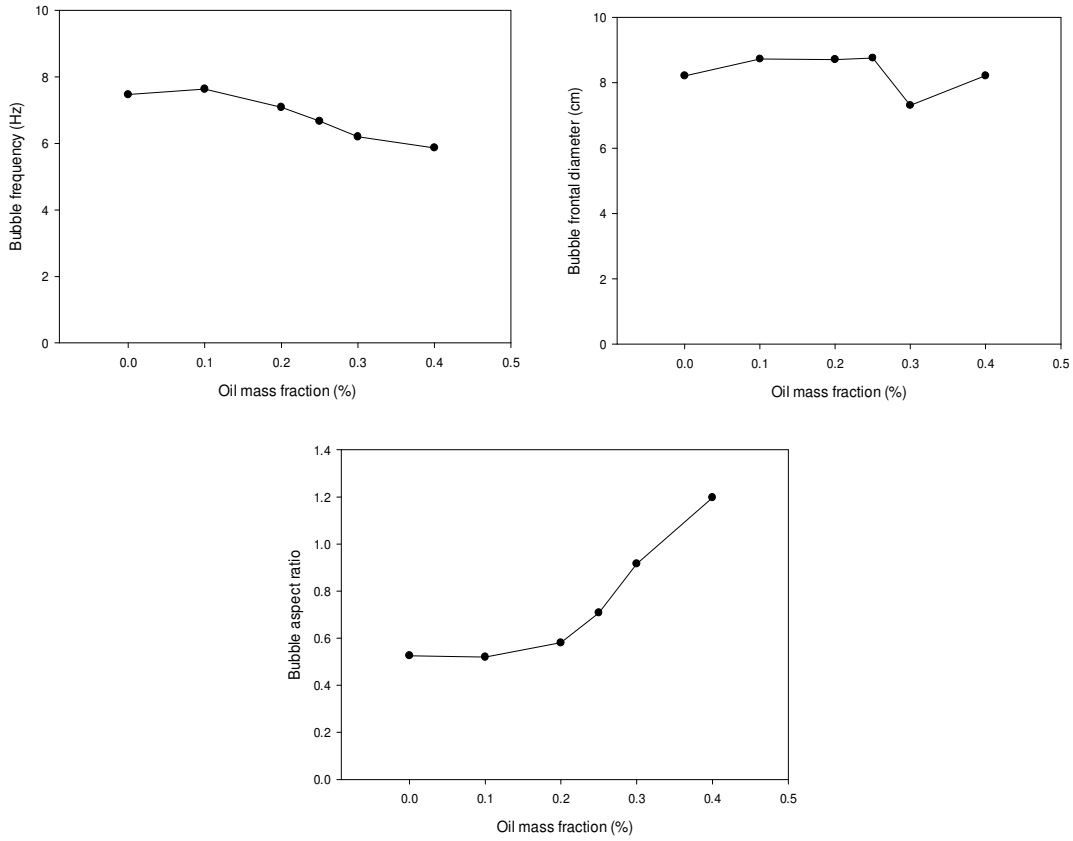

Figure 5.10: a) Effect of oil mass fraction on the bubble frequency b) Effect of oil mass fraction on the bubble frontal diameter c) Effect of oil mass fraction on the bubble aspect ratio

Figure 5.10 shows the impact of the oil fraction on the bubble frequency, bubble frontal diameter and bubble aspect ratio. The bubble frequency decreases with increasing oil fraction, as shown in Figures 5.10-a while the bubble frontal diameter does not change

much with oil mass fraction as shown in Figure 5.10-b. However, the bubble aspect ratio is greatly affected by the oil fraction, as shown in Figure 5.10-c, and it is much more affected by the oil fraction than by the fluidization velocity (Figure 5.9-c). When the bed approaches bogging, the particles are more sticky and bubbles elongate to decrease the drag force.

The main assumption of this study, to be verified with simulation in this section, is that, although the speed of sound is not greatly affected by the changes in bubble size and frequency associated with large variations in fluidization velocity in a dry bed (Figure 5.7), it is greatly affected by the changes in bubble shape associated with bogging.

5.3.2. The Wave-Equation For Sound Propagation

To investigate the effect of bubbles on speed of sound, the propagation of sound in the fluidized bed was modeled with Comsol. The equations that describe the sound propagation in fluidized particles are derived from the equations of fluid flow. The continuity equation or conservation of mass, the conservation of momentum that is often referred to as the Navier-Stokes equation, the equation of energy conservation, and an equation of state that describes the thermodynamic state of the matter. In the pressure acoustics model, the flow is assumed lossless, viscous effects are neglected, and a linearized isentropic equation of state is used. Under these assumptions the acoustic field can be described by the pressure p, and is governed by the wave equation.

$$\frac{1}{\rho c^2}\frac{\partial^2 p}{\partial t^2} + \nabla.\left(-\frac{1}{\rho}(\nabla p - q)\right) = Q \quad (5.4)$$

Where p is the pressure, q and Q are the dipole and monopole acoustic sources respectively. An acoustic monopole propagates the sound equally at all directions. An example of acoustic monopole is a small sphere whose radius alternately expands and contracts. An acoustic dipole forms when two monopoles of equal source strength, but opposite phase, are separated by a small distance d such that $kds \ll 1$ where k is the wave number and is equal to $2\pi/\lambda$ where λ is the wavelength. In general, any sound source with the dimensions much smaller than the wavelength of the generated sound can be

considered as a monopole source. This relationship between wavelength and dimension for a monopole is usually expressed as kas<<1, where k is the wave number and as is a characteristic dimension of the source and if the source is a speaker, as would be the diameter of the speaker (Russell, 1998).

When the sound is propagating in a media, particles assist the transmission of the sound wave but they return to their original state without net movement. Particle velocity is the velocity of a particle in a medium as it moves back and forth in the direction that the sound wave is traveling as it passes. The particle velocity v can be related to the particle displacement and acceleration for a single frequency sound wave:

$$v = \xi . \omega = \frac{a_p}{\omega} = \frac{p}{Z} \tag{5.5}$$

Where ξ represents the particle displacement, a_p is particle acceleration and Z is the specific acoustic impedance. The specific acoustic impedance is an inherent property of the medium and is equal to the product of density of medium and speed of sound in the medium. With solving the Equation 5.4 with the finite element method in a medium, one can calculate the pressure as well as particle acceleration and particle velocity everywhere in the medium.

5.3.3. Simulation Results

The simulation of sound propagation in the fluidized bed performed by solving Equation 5.4 with Comsol while a single bubble with different geometry and distance from the wall was placed between two microphones and the speed of sound was calculated for each case. The speaker that was used in the experimental setup was 10 cm in diameter and generated sound with a frequency of 250 Hz. So for this case, k= 2π/λ= 2πf/c=4.58 rad/m where c=343 m/s, the speed of sound in the air above the freeboard where the speaker is installed. Thus, for the speaker used in the experimental setup, kas=0.46 rad, which is close to monopole approximation. Therefore in Equation 5.4, the value for dipole source considered zero and the speaker was assumed as a monopole source.

After solving Equation 5.4, the particle acceleration at the location of each microphone was calculated as it is shown in Figure 5.11 for a typical bubble when it is located between two microphones. Each microphone measures a different signal versus time due

to its different height and corresponding sound attenuation. The time lag between two microphone curves, as shown in Figure 5.11, was obtained using cross-correlation. Then the speed of sound was calculated by dividing the distance between the two microphones with the obtained time lag. Figure 5.12 shows how the speed of sound in the presence of various bubbles varies with the bubble distance from the wall.

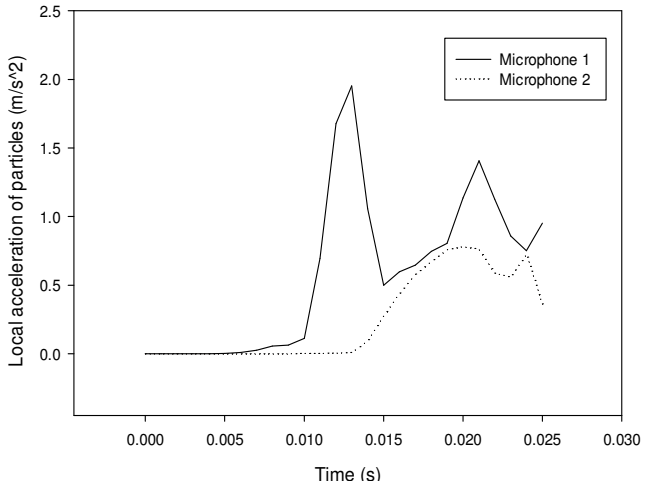

Figure 5.11: Local acceleration of particles at microphone location simulated with COMSOL using a bubble with a height of 8 cm and a frontal diameter of 6 cm, located 5 cm far from the wall

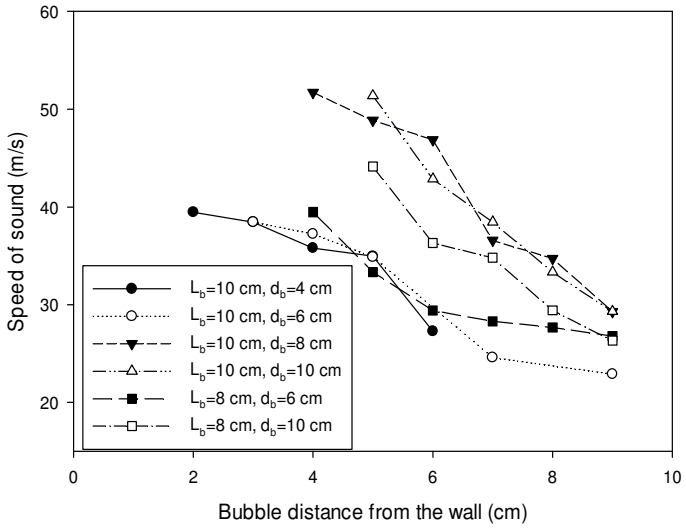

Figure 5.12: Simulated speed of sound versus bubble distance from the wall

According to Figure 5.12, there is a critical distance from the wall where the bubbles beyond which the smaller bubbles cannot affect the measured speed of sound. The critical distance according to Figure 5.12 is about 6 cm. The rest of the simulation was performed by considering only the bubbles close to the wall i.e. at a distance from the wall smaller than the critical distance.

Figure 5.13 shows the speed of sound for different bubble heights and frontal diameters. According to Figure 5.13, a single bubble can affect the measured speed of sound when its height and frontal diameter exceed threshold values. The speed of sound varied from 25 to 50 m/s over the range of bubble properties relevant to this study: it was therefore assumed that the threshold was located at the half-way point, between 35 and 40 m/s that is the region in the Figure 5.13 where the blue color turns to green color. The underlying reason can be explained as when the sound wave passes a bubble, first it comes from the dense phase to the dilute phase. At the boundary, part of the sound wave reflects and part of it comes inside the dilute phase.

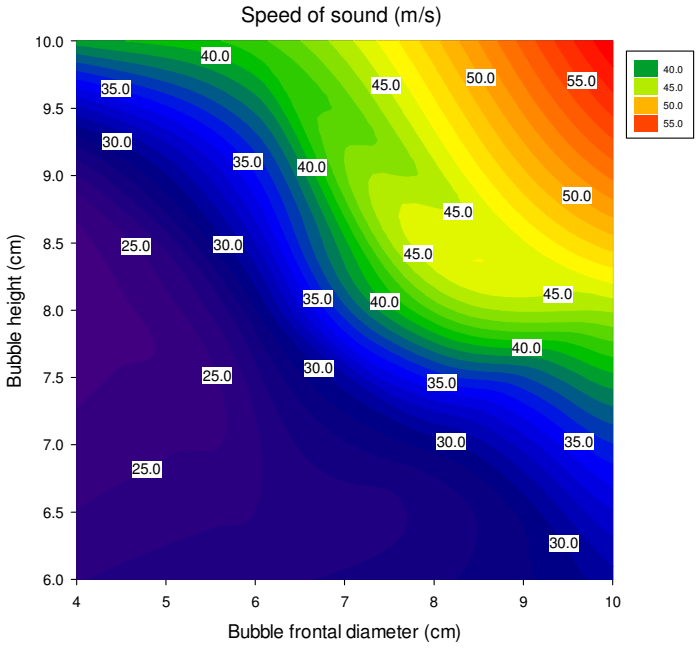

Figure 5.13: Simulated speed of sound versus bubble height and bubble frontal diameter

At the second boundary, when the sound wave comes from the dilute phase to dense phase, the same reflection and transmission happen again. The sound wave that passes through the bubble arrive earlier to the microphone location when compared to the sound wave comes directly through the rest of the bed to the microphone location from the speaker. However, the former is weaker than the later. The energy of the sound wave passes through the bubble depends on the bubble size because the sound intensity at a certain distance from a monopole source is constant and the energy of the wave that passes through the bubble is proportional to the surface of the bubble. So when the bubble has a bigger height or frontal diameter, the energy of the sound wave passes through the bubble is bigger so it can affect the measured time lag between outputs of two microphones and eventually affect the measured speed of sound while the similar effects associated with small bubbles are negligible.

Figure 5.14 compares the measured speed of sound with the values obtained by modeling using the data presented on bubble properties obtained from capacitance measurements. As shown in Figure 5.14, the values of the speed of sound predicted by the model are in fair agreement with the measured results. There is, however, a systematic error between experimental and simulation data: the measured speed of sound is always lower than the speed of sound obtained by simulation. The underlying reason can be explained as follows: when two small bubbles moving side by side cross the electric field at the same time, the capacitance signal is equivalent of signal of one big bubble (Figure 5.15) but the effect of two small bubbles on the speed of sound is smaller than the effect of one big bubble due to attenuation of sound which them crosses twice as many boundaries between dilute and dense phases. Figure 5.14 confirms that the speed of sound in a fluidized bed is greatly affected by bogging. It also shows that, in the dry bed, the speed of sound is not greatly affected by the fluidization velocity.

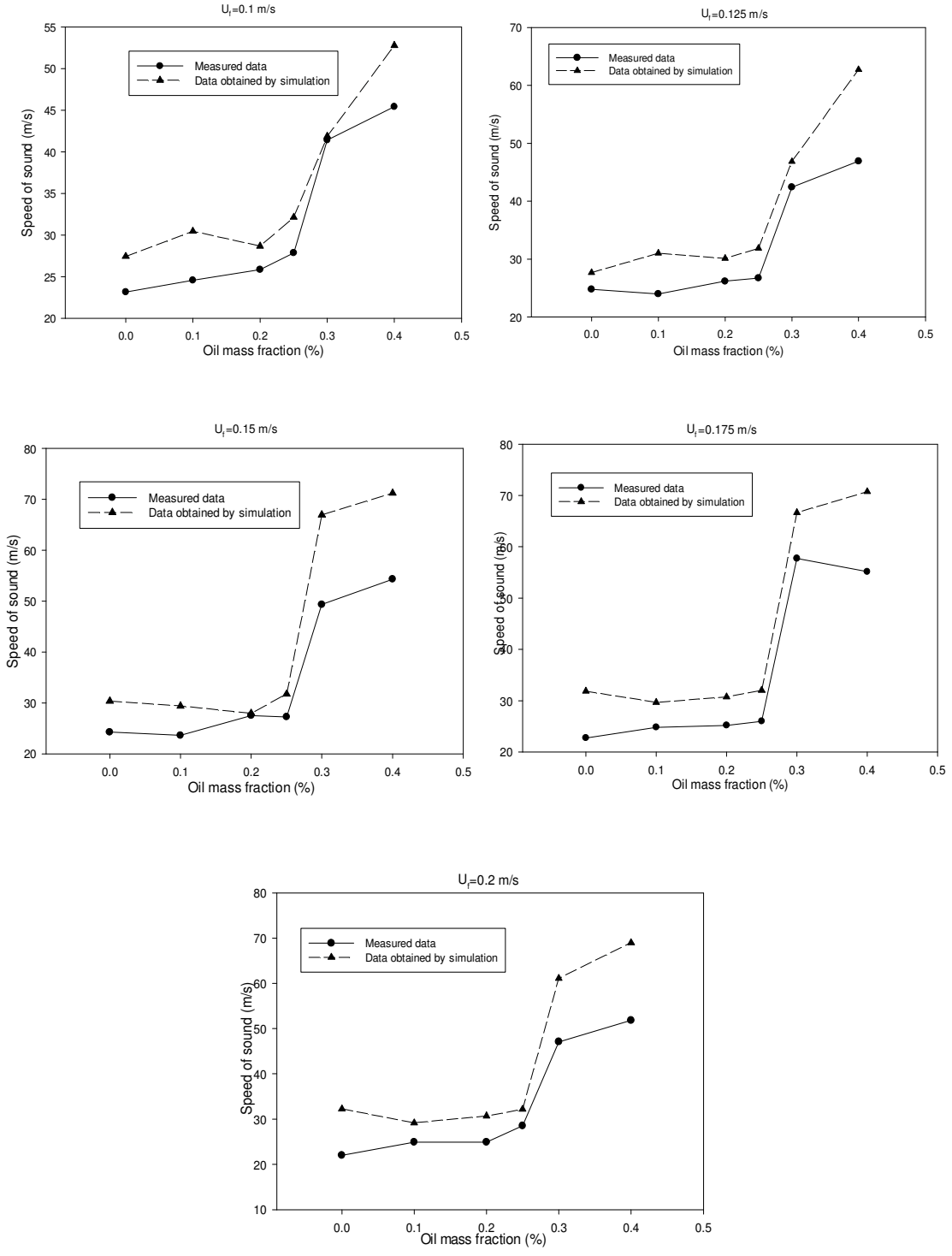

Figure 5.14: Measured speed of sound versus predicted speed of sound from the model Remove error bars, add dashed curve

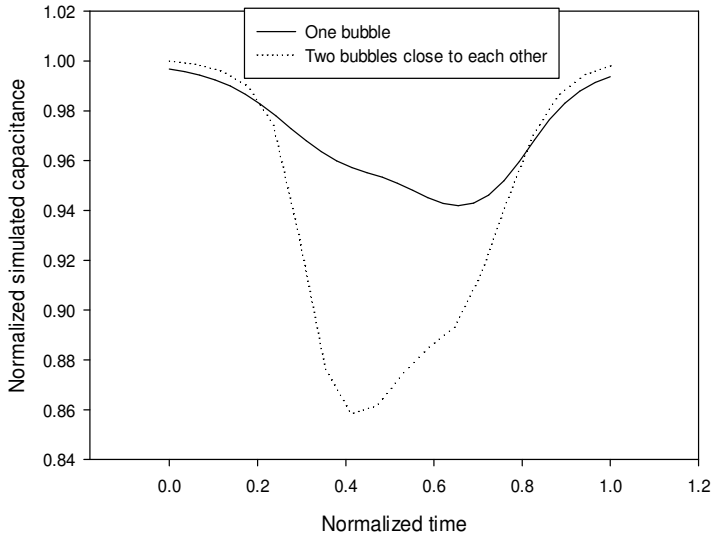

Figure 5.15: Normalized simulated capacitance versus normalized time- Dash line when a bubble with frontal diameter of 6 cm and height of 8 cm is passing- Continuous line when another bubble with frontal diameter of 6 cm and height of 4 cm is passing beside the first bubble

Conclusion

A novel method proposed that can detect initial bogging of a fluidized bed by measuring the speed of sound within the bed.

The geometry of the gas bubbles and their distance from the wall were measured with capacitance sensors to understand how bubble properties affect the transmission of sound through a fluidized bed. The propagation of sound in the presence of bubbles of various geometries was simulated with Comsol. Simulation results agreed with the experimental results.

The proposed method can detect initial bogging and its application in industrial fluidized beds is not subject to the limitations of pressure transducers.

References

Bi H.T, Grace J.R, Zhu J, (1995). “Propagation of pressure waves and forced oscillations in gas-solid fluidized beds and their influence on diagnostics of local hydrodynamics” Powder Technology 82(3): 239-253.

Briens C, McDougall S, Chan E. (2003). "On-line detection of bed fluidity in a fluidized bed coker" Powder Technology 138(23): 160-168.

Briens C.L, Briens L.A, Barthel E, Le Blevec J.M, Tedoldi A, Margaritis A. (1999). "Detection of local fluidization characteristics using the V statistic" Powder Technology 102(1): 95-103.

Chong Y.O, O'Dea D.P , White E.T, Lee P.L, Leung L.S, (1987). "Control of the quality of fluidization in a tall bed using the variance of pressure fluctuations" Powder Technology 53(3): 237-246.

Hamidi M, Berruti F, Briens C, McMillan J, (2013) “Bogging detection in a fluidized bed using plannar capacitance sensors” Fluidization XIV From Fundamentals to Products, May 25, 2013

Khawaja H.A, Scott S.A, (2011) “CFD-DEM Simulation of Propagation of Sound Waves in Fluid Particles Fluidised Medium” Journal of Multiphysics, 5(1), 47-59

Lamb H. (1963) Hydrodynamics, Cambridge University Press, Cambridge.

Ropchan W.T, (1981). Heat transfer and grid jets, Stanford University. PhD.

Roy R., Davidson J.F, Tuponogov V.G.. (1990) “The velocity of sound in fluidised beds”, Chemical Engineering Science, 45(11), 3233–3245.

Russell D.A, Titlow J.P, Bemmen Y.J, (1998) “Acoustic monopoles, dipoles, and quadrupoles: An experiment revisited” American Journal of Physics. 67(8):660-664

Tsujimoto H, Yokoyama T, Huang CC, Sekiguchi I. 2000 Monitoring particle fluidization in a fluidized bed granulator with an acoustic emission sensor.Powder Technology;113(1–2):88–96.

Van Ommen J.R, Coppens M.O, Van Den Bleek C.M., Schouten J.C. (2000). "Early warning of agglomeration in fluidized beds by attractor comparison" AIChE 46(11): 2183-2197.

Weir G. J, (2001) “Sound speed and attenuation in dense, non-cohesive air-granular systems”, Chemical Engineering Science, 56, 3699–3717.

CHAPTER 6: STUDY OF SUPERSONIC GAS JETS FLUCTUATIONS IN A GAS-SOLID FLUIDIZED BED WITH CAPACITANCE SENSORS

6.1. Introduction

High velocity horizontal gas jets are used for particle attrition in several industrial processes such as the Fluid Coking™ process. In the Fluid Coking™ process, heavy oil is injected into a fluidized bed of coke particles where it undergoes thermal cracking; a by-product of the thermal cracking reactions is solid coke that deposits on the bed particles, increasing their size. The particle size must be controlled to avoid poor fluidization and poor operation of the coke transport lines (Dunlop, 1958). The particle size is reduced by injecting high velocity steam into the fluidized bed through supersonic attrition nozzles. If jets issuing from the attrition nozzles hit fluidized bed internals, they would cause significant erosion, and, therefore, such interactions must be avoided.

Dawe et al. developed a correlation to predict the penetration of gas jets from supersonic nozzles (Dawe, 2007). Ariyapadi et al. proposed a model to predict the jet penetration of sonic horizontal gas-liquid jets by adapting a correlation from Benjelloun et al. (Ariyapadi, 2004, Benjelloun, 1995). Some published correlations for the jet penetration length in fluidized beds are provided in Table 6.1 (Gouhua, 1997, Hong, 1997, Hong, 2003, Zhong, 2005). Correlations provided by Cruz et al. (Cruz, 2011) and Dawe et al. (Dawe, 2007) are the only correlations that were developed for supersonic jets.

Jet penetration depends on parameters such as fluidization gas properties, solid density, particle diameter, bed height, fluidization velocity, void fraction, velocity of the injected gas, and injection nozzle diameter (Hong, 1997, Merry, 1971). Vaccaro et al. mentioned that the expansion angle is another important factor to be considered when describing jet behavior, as it may affect the prediction of gas and particle entrainment in the jet (Vaccaro, 1997). An increase in gas and solids entrainment into the jet reduces jet penetration because energy dissipation occurs faster. It is generally accepted that jet penetration increases with increasing nozzle diameter and increasing velocity of the injected gas (Dawe, 2007, Ariyapadi, 2004). Increasing the fluidization velocity also

increases the length of a horizontal jet (Wang, 2010).

Table 6.1: Some correlations for horizontal jet penetration length

$\frac{L_{jet}}{d_0} + 4.5 = 5.52 \left[\frac{\rho_e U_0^2}{(1-\epsilon)\rho_p g d_p}\right]^{0.4} \left[\frac{\rho_f}{\rho_p}\right]^{0.2} \left[\frac{d_p}{d_0}\right]^{0.2}$	Subsonic	Merry et al. (1971)
$\frac{L_{jet}}{d_0} = 5.52 \left[\frac{\rho_e U_0^2}{(\rho_p - \rho_f) g d_0}\right]^{0.27}$	Subsonic	Benjelloun et al. (1995)
$\frac{L_{jet}}{d_0} = 55.6 \left[\frac{\rho_e U_0^2}{(\rho_p - \rho_f) g d_0}\right]^{0.27} \left[\frac{(\rho_p - \rho_f) d_p^2 U_0}{\mu d_0}\right]^{-0.124}$	Subsonic	Luo et al. (1997)
$\frac{L_{jet}}{d_0} = C \left[\frac{\rho_e U_0^2}{(1-\epsilon)\rho_p g d_p}\right]^{a1} \left[\frac{\rho_f}{\rho_p}\right]^{a_2} \left[\frac{d_p}{d_0}\right]^{a_3} [\alpha + \frac{\pi}{2}]^{a_4} \left[\frac{d_p}{d_0}\right]^{a_3}$	Subsonic	Hong et al. (1997)
$\frac{L_{jet}}{d_0} = 26.47 \left[\frac{\rho_e U_0^2}{(\rho_p - \rho_f) g d_0}\right]^{0.293} \left[\frac{\rho_e U_0 d_p}{\mu}\right]^{-0.1138}$	Subsonic	Hong et al. (2003)
$\frac{L_{jet}}{d_0} = 10.86 \left[\frac{\rho_e U_0^2}{(\rho_p - \rho_f) g d_0}\right]^{0.39} \left[\frac{H_0}{D_c}\right]^{-0.17} \left[\frac{U_f}{U_{mf}}\right]^{-0.11} \left[\frac{\rho_e U_0 d_p}{\mu}\right]^{-0.1138}$	Subsonic	Zhong and Zhang (2005)
$\frac{L_{jet}}{d_0} = \alpha . U_{sound,eq}^{0.488} . \rho_{tip}^{0.329} + \frac{\beta}{d_0}$	Supersonic	Dawe et al. (2007)
$\frac{L_{jet}}{d_0} = 5.52 \left[\frac{\rho_e U_0^2}{(\rho_p - \rho_f) g d_0}\right]^{0.27} * (1.72 - 93.06 d_0)$	Supersonic	Cruz et al. (2011)

Considerable discrepancies have been reported between invasive and non-invasive measurements in fluidized beds. Liu et al (Liu, 2010) found that intrusive optical probes overestimates bubble chord lengths because they cannot detect small bubbles. Capacitance measurement is a non-invasive method that is not limited by the bubble size.

Supersonic jets in a fluidized bed fluctuate. To avoid erosion of internals, it is, therefore, essential to not only know the time-averaged jet penetration length but, also, its fluctuations. The first objective of the current study was, therefore, to measure the fluctuations of the penetration depth of supersonic jets in a fluidized bed. The second objective was to develop a correlation to predict the fluctuations of the penetration depth of supersonic jets.

6.2. Experimental

6.2.1. Experimental Setup

The experiments were performed in a small pie-shape fluidized bed column with a height of 1.9 m, and a width of 0.69 m, as shown in Figure 6.1. For all the experiments, coke particles with an initial Sauter mean diameter of 140 μm and a particle density of 1450 kg/m3 were attrited using nitrogen as the attrition gas. The tip of the horizontal attrition nozzle was located inside the bed at 0.245 m above the porous plate gas distributor, and penetrated 0.06 m from the wall. The bed height was approximately 0.29 m when defluidized, and around 0.35 m when the fluidization velocity was 0.2 m/s. The minimum fluidization velocity was 0.03 m/s for all experiments.

Two attrition nozzles were tested to determine the effect of nozzle scale on the jet penetration length. Both nozzles were convergent-divergent, Laval-type nozzles with a diameter at the nozzle throat of either 2.4 or 2.8 mm, as shown in Figures 6.2 and 6.3. For all experiments, nitrogen was injected into the bed except otherwise stated.

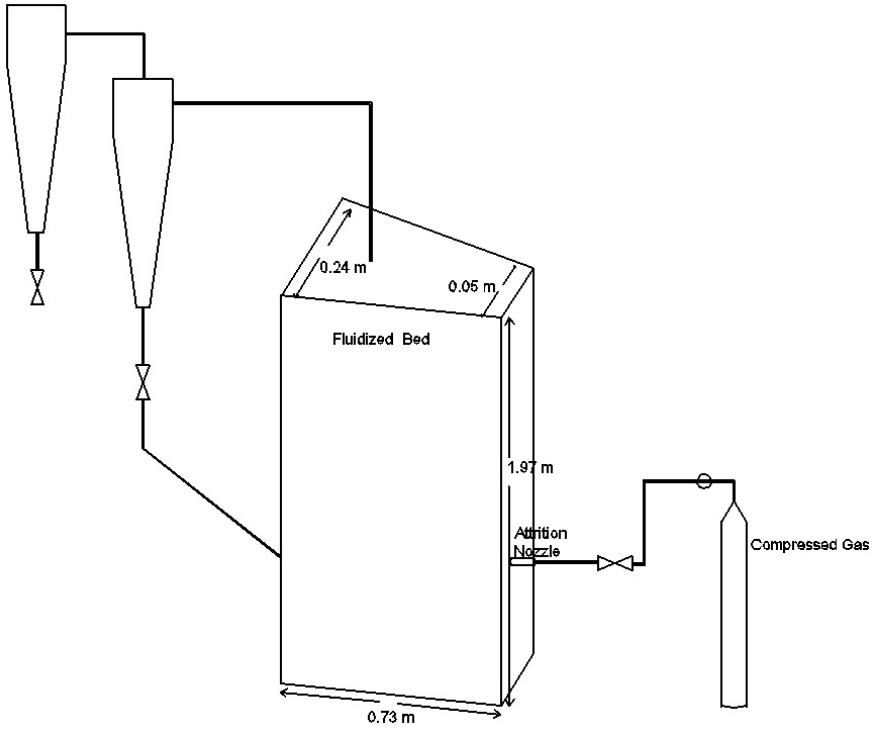

Figure 6.1: Experimental set up

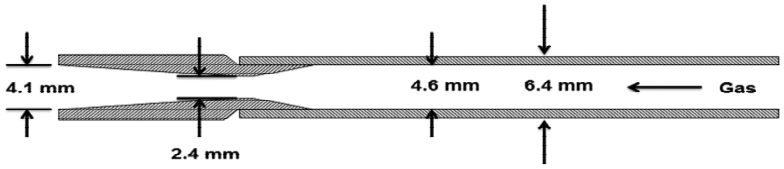

Figure 6.2: Laval type nozzle, d_{th} =2.4 mm

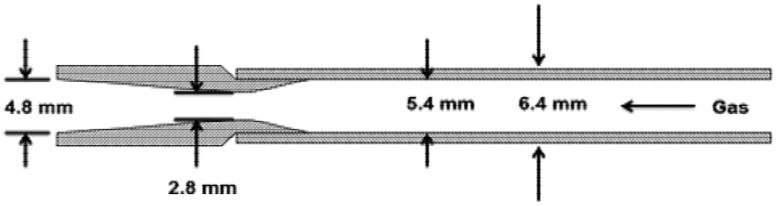

Figure 6.3: Laval type nozzle, d_{th} =2.8 mm

The capacitance meter used for this study was an AC based circuit with a differential noise cancelling system. Figure 6.4 shows the configuration of 30 electrodes mounted externally on one side of the fluidized bed, on the outside surface of a wooden window, while on the other side one single electrode covered the entire wall, and was also installed on the outside surface of a wooden window.

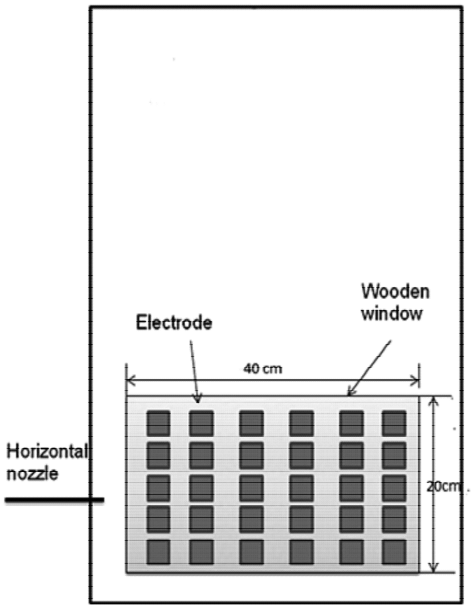

Figure 6.4: configuration of electrodes

This electrode was connected to the signal generator, acting as a transmitter, while the rest of electrodes were connected to the virtual ground of the amplifier, functioning as receivers. Samples were acquired with a frequency of 100 kHz using an analog to digital converter connected to the 30 electrodes through an amplifier and a multiplexer. The multiplexer connected each electrode for 200 μs and then switched to the next electrode. By taking the rms value of the measurements in each 200 μs time window, the capacitance of each electrode was measured at 6 ms intervals.

6.2.2. Measurement of Local Voidage

Coke particles in the fluidized bed have a considerable dielectric constant and can concentrate an electric field within themselves. Using capacitance measurement, the voidage distribution within the fluidized bed could be visualized based on the difference in dielectric constant between coke particles and the fluidization gas. The average voidage of the bed at different fluidization velocities was calculated from the bed pressure gradient obtained from pressure transducers at different heights within the bed using Equation 6.1.

$$\frac{\Delta p}{\Delta z} = \rho_p(1-\varepsilon)g \qquad (6.1)$$

The bed capacitance was measured at different fluidization velocities and was normalized with respect to the defluidized bed capacitance. Figure 6.5 shows that the average normalized bed capacitance is a linear function of the average bed voidage.

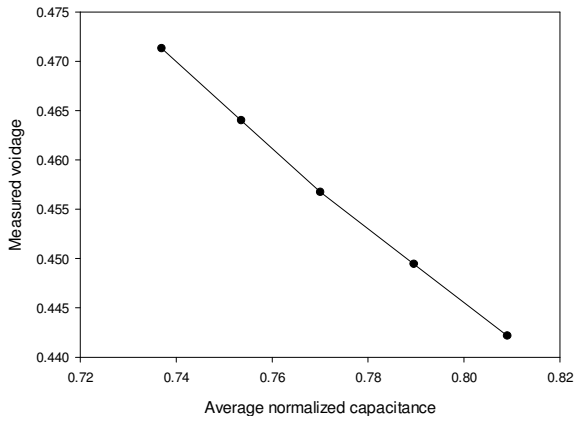

Figure 6.5: Average normalized capacitance of 30 electrodes versus the average bed voidage measured with pressure transducers

The local bed voidage can, thus, be obtained from the normalized capacitance of any electrode, using the linear relationship of Figure 6.5.

6.2.3. Pre-Test Imaging Experiments

To confirm the ability of this system to get a precise image of the jet, a preliminary experiment was carried out. A void tube with a diameter of 7 cm and a height of 13 cm was inserted horizontally in the minimally fluidized bed of coke particles and the measured capacitances were converted to voidage using the method described in section 6.2.2. Figure 6.6 shows the resulting image of the void tube, viewed from the top. Figure 6.6 indicates that the maximum measurement error was less than 1 cm.

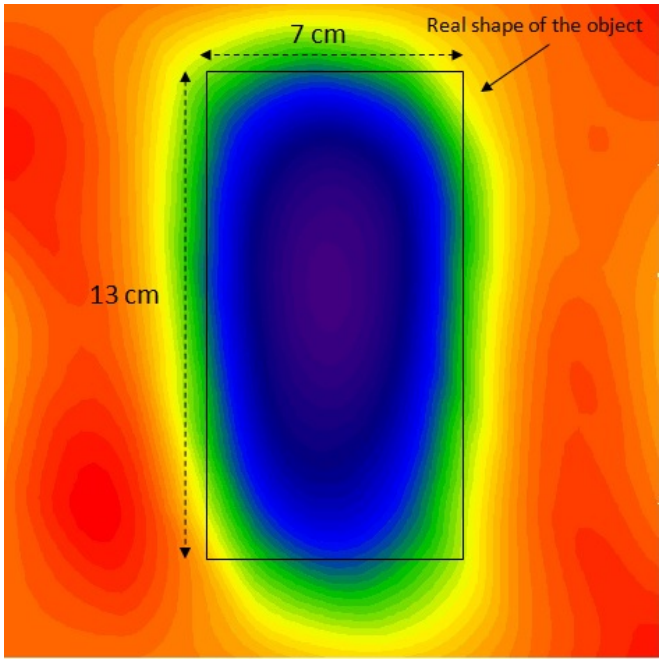

Figure 6.6: Image of the void tube acquired with capacitance sensors

6.2.4. Measurement of Jet Length

Figure 6.7 shows a typical image of the voidage distribution of the horizontal gas supersonic jet obtained by the capacitance sensors at a nozzle mass flowrate of 0.014 kg/s while the fluidization velocity was 0.1 m/s. The supersonic jet penetration length is

defined here as the distance between the nozzle tip and the farthest point on the supersonic jet axis where the voidage is equal to the average of the maximum jet voidage and of the bed voidage at the same height.

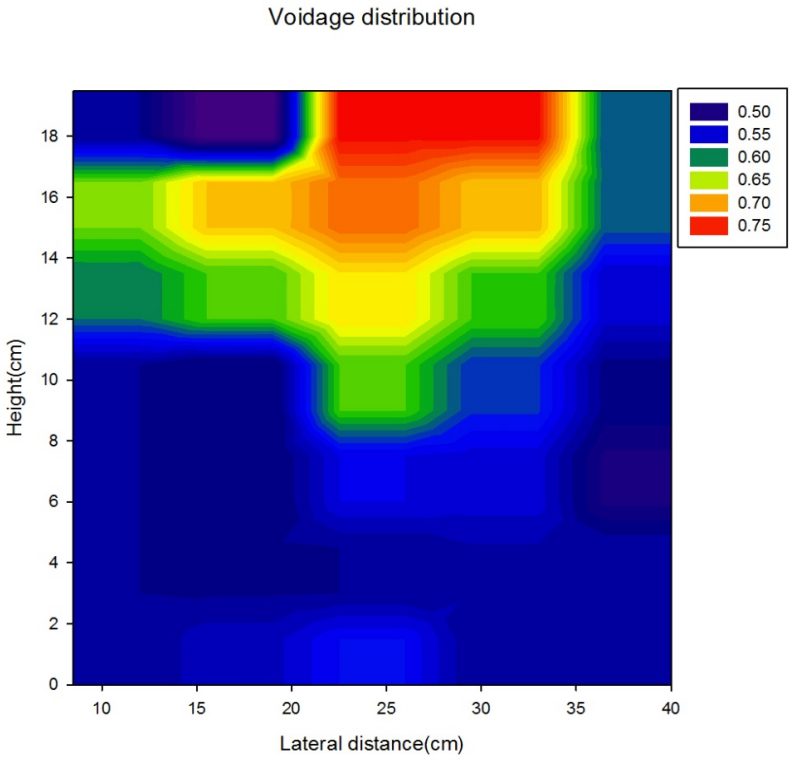

Figure 6.7: Image of voidage distribution of the gas–solid fluidized bed with horizontal gas supersonic jet penetration obtained by ECT at mass flowrate of 0.007 kg/s and fluidization velocity of 0.1m/s

Since the horizontal resolution of the image is 6 pixels, a polynomial curve fitting of order 5 was used to specify the voidage at any point in the row and enable the accurate calculation of supersonic jet length.

6.2.5. Measurement of Bubble Velocity

The average bubble velocity at the same superficial gas velocity was measured through imaging of the voids with capacitance sensors. For each image of 30 pixels, the center of bubbles was obtained by fitting polynomials to the measured voidages from each sensor and calculating the local minima. The bubble velocity was calculated from the vertical displacement of the bubble center between successive images.

6.3. Results and Discussion

6.3.1. Study of Supersonic Jet Penetration Length

The effect of nozzle mass flowrate on the time-averaged supersonic jet penetration length is shown in Figure 6.8, which compares experimental results with the predictions from four different correlations. This figure demonstrates that the jet penetration depth increases with increasing the nozzle mass flowrate, which corresponds to what was found by other researchers (Cruz, 2011). The best agreement is with Benjelloun's correlation. It should be noted that there is no universal definition for jet penetration length. Besides, invasive measurement methods as used in most of correlations can affect the measured jet length values. So the way that a jet penetration length is defined and the method used for jet penetration measurement may cause the measured jet penetration length values become closer to a specific correlation.

To study the impact of nozzle size, some experiments have been performed with two nozzle throat sizes, 2.4 and 2.8 mm. Figure 6.9 shows that increasing the nozzle size increases the supersonic jet penetration depth, as expected from the correlations listed in Table 6.1.

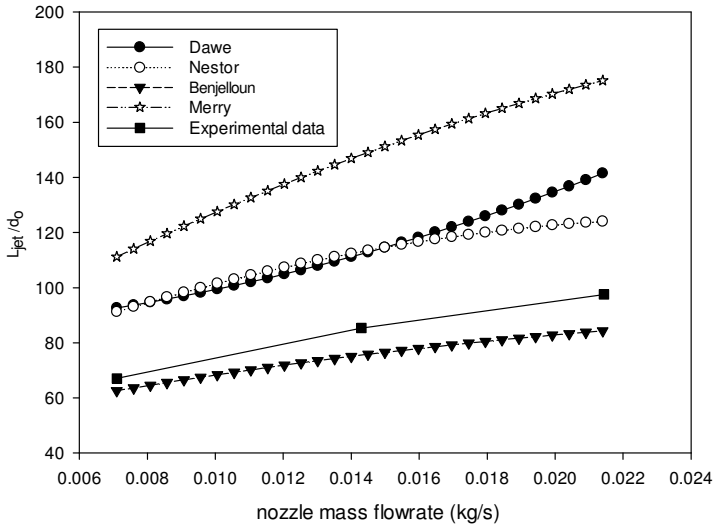

Figure 6.8: Comparison between measured supersonic jet penetration depth and correlations

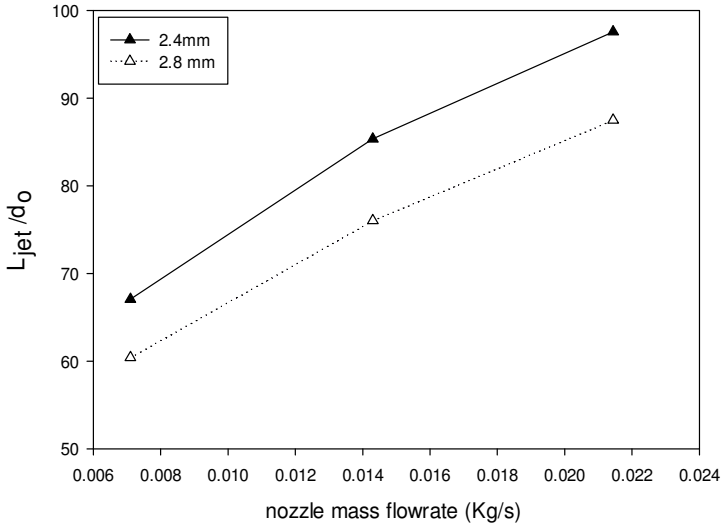

Figure 6.9: Jet penetration length versus gas mass flux for different nozzle diameters

Another parameter which has impact on the jet penetration length is the density of the injected gas. The jet penetration length was therefore measured with N_2, He and CO_2 attrition gases. Figure 6.10 shows that a less dense gas penetrates further at constant mass flowrate because of its higher velocity and momentum, as expected from the correlations in Table 6.1.

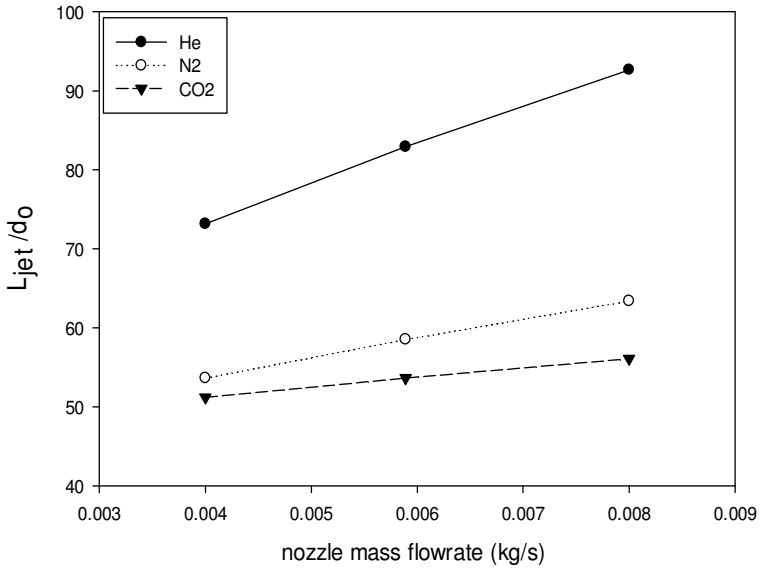

Figure 6.10: Jet penetration length versus gas mass flux for different gas densities

The superficial gas fluidization velocity is also an important factor that can affect the jet penetration length (Wang, 2010). To investigate the effect of superficial gas velocity on the jet penetration length, the bed was fluidized at three different fluidization velocities and, in each case, the injection performed with three different gas mass fluxes. Figure 6.11 shows that the jet penetration length increases with increasing fluidization velocity, as expected from the correlations.

Figure 6.12 shows that the supersonic jet length slightly increases with increasing upward nozzle angle and decreases when nozzle angle increases downward. This result is in fair agreement with correlations for inclined subsonic jets (Hong, 1997).

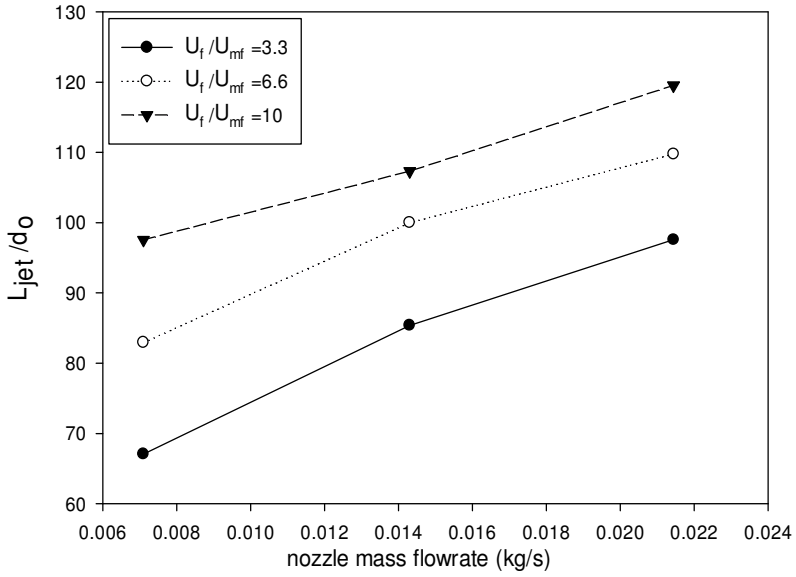

Figure 6.11: Jet penetration length versus gas mass flux for different fluidization velocities

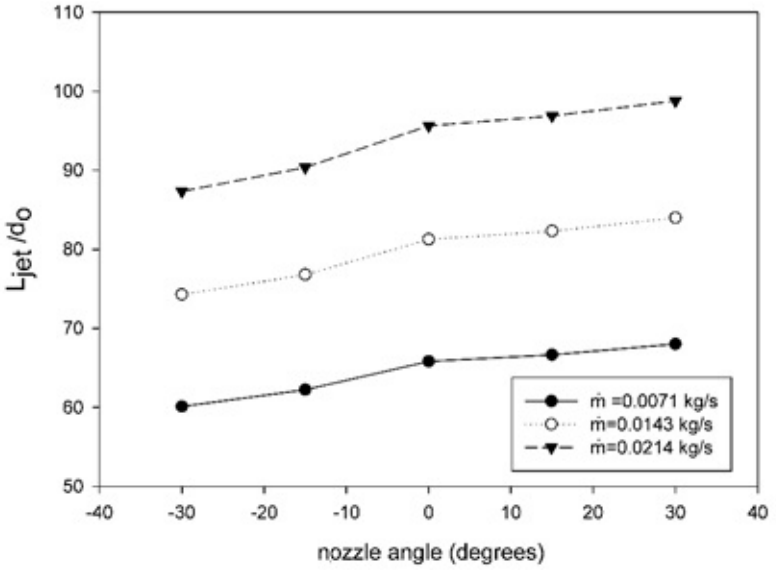

Figure 6.12: Jet penetration length versus nozzle angle with respect to the horizontal

Figure 6.13 compares the measured jet penetrations with the predictions from Benjelloun et al. (Benjelloun, 1997), for all the measured supersonic jet lengths at different nozzle mass flowrates, nozzle gas densities and nozzle sizes. As shown in Figure 6.13, measured

and predicted values of jet length are close but all predicted values are below the line of equality.

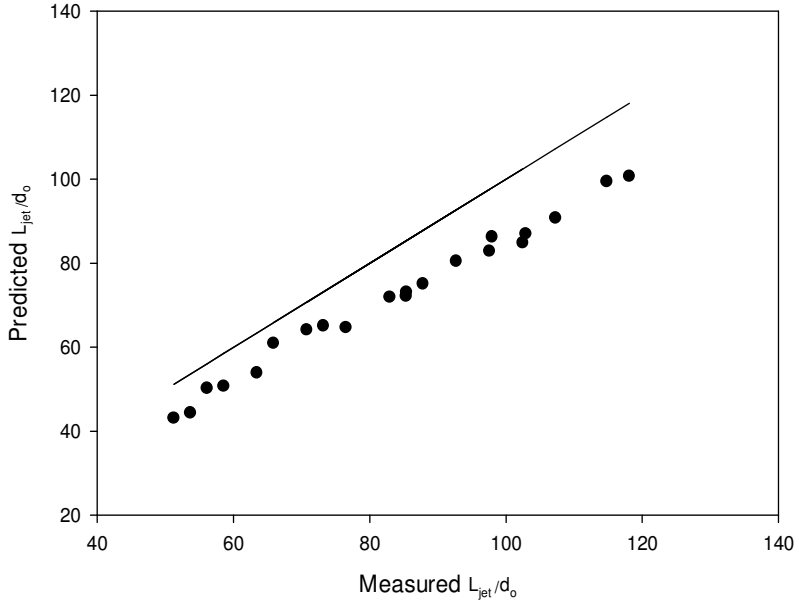

Figure 6.13: Comparison between values predicted with Benjelloun's correlation and all measured horizontal supersonic jet lengths at different nozzle sizes, nozzle mass flowrates and nozzle gas densities

The constant coefficient of Benjelloun's correlation was, thus, adjusted to get a better fit of the experimental data:

$$\frac{L_{jet}}{d_0} = 6.38\left[\frac{\rho_e U_0^2}{(\rho_p - \rho_f) g d_0}\right]^{0.27}$$

(6.2)

Figure 6.14 compared the measured jet penetrations with the predictions from the modified correlation in equation 6.2.

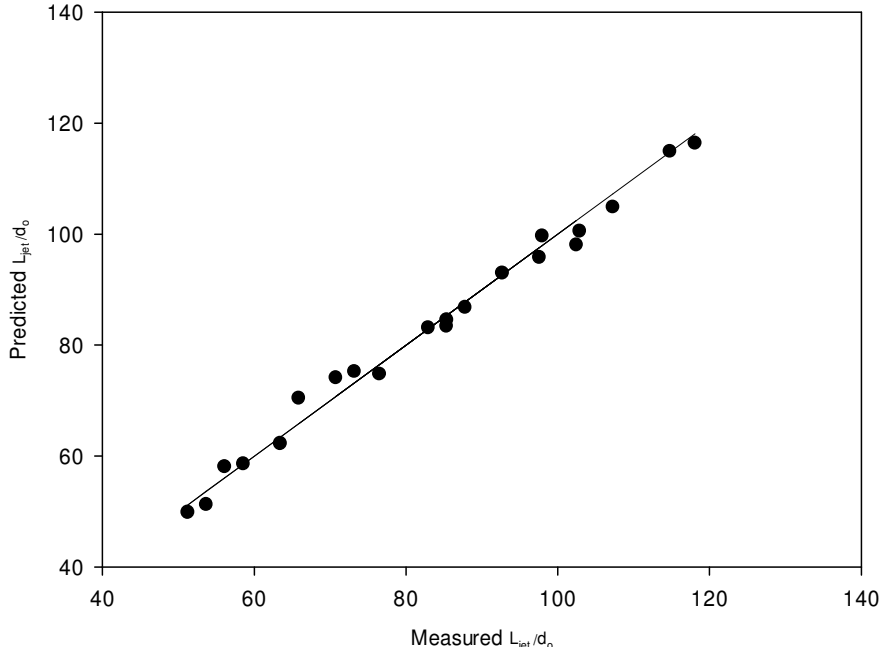

Figure 6.14: Comparison between values predicted with the adjusted correlation and all measured horizontal supersonic jet lengths at different nozzle sizes, nozzle mass flowrates and nozzle gas densities

6.3.2. Study of fluctuations of the supersonic jet length

With capacitance imaging of the jet as discussed in section 2.4, one can measure the supersonic jet length at each image and generate a time series of jet lengths. Distributions of supersonic jet lengths are symmetric around the mean, since the supersonic jet length moves through a cyclic sequence of left-central-right-central positions which is consistent with other studies for downward subsonic jets (Shen, 1991). Figure 6.15 shows the q-q plot of the distribution of supersonic jet lengths for different fluidization velocities and nozzle inclination angles: it compares the quantiles for the measured distribution to the quantiles for the Gaussian distribution.

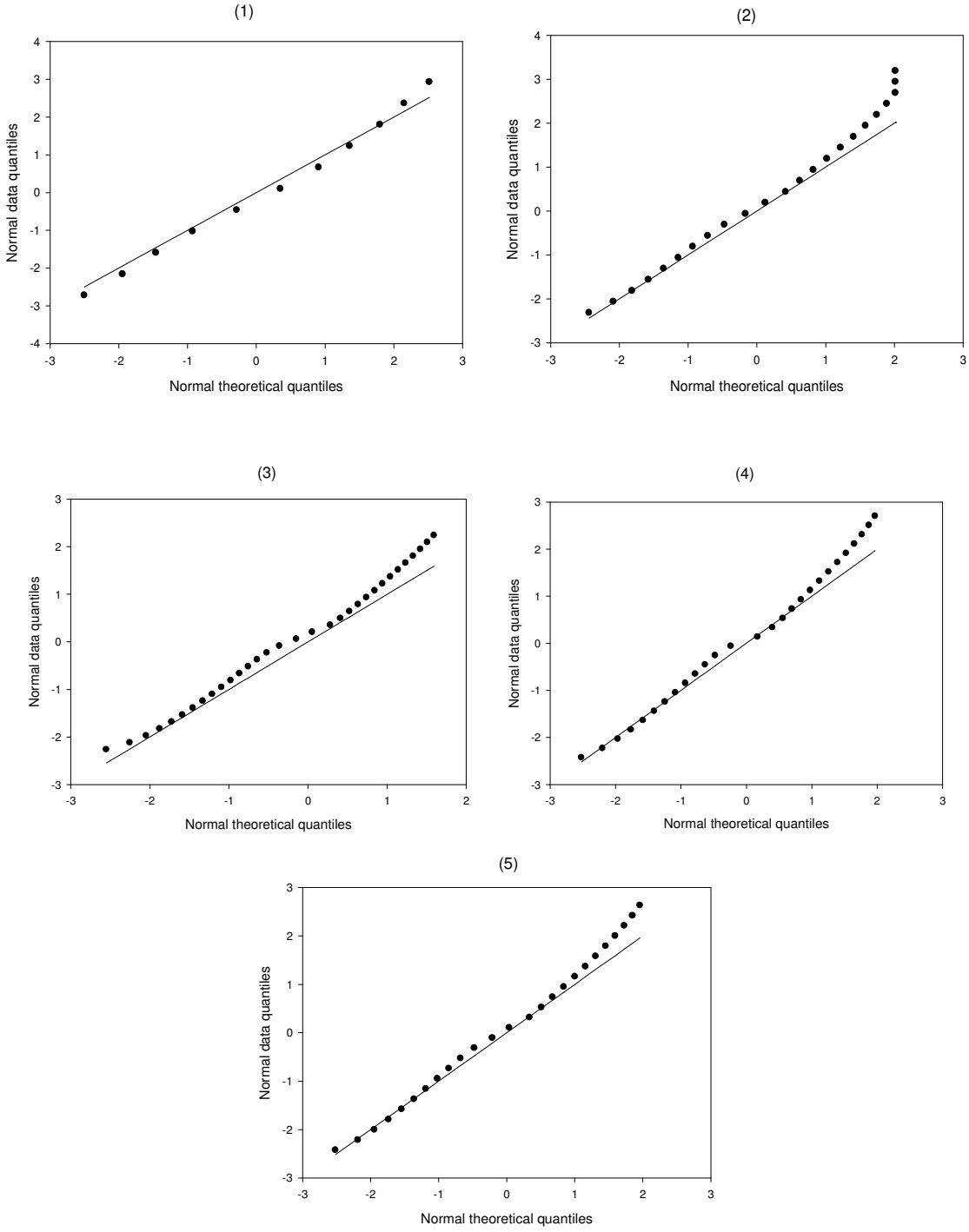

Figure 6.15: q-q plot of jet penetration length distribution at constant nozzle mass flowrate :(1), (2), (3) with horizontal nozzle and U_f = 0.1, 0.2, 0.3 m/s and (4), (5) with inclined nozzle $\alpha=15^o,-15^0$ while U_f = 0.1m/s

Since the distribution of supersonic jet length can be approximated with the Gaussian distribution according to Figure 6.15, it can be fully determined from its mean and its

coefficient of variation. The mean or time-averaged jet penetration can be obtained from the correlation developed in section 6.3.1.

Capacitance imaging was performed on the horizontal supersonic jet of nitrogen issuing from a 2.4 mm nozzle while the bed was fluidized with a fluidization velocity of 0.1 m/s. The length of supersonic jet was calculated for each image and the generated time series was zero centered and normalized. Voidage measured with electrodes at the second row above the distributor (Figure 6.4) was also zero centered and normalized. Then the cross correlation integral between the length of the supersonic jet and the voidage measured with electrodes above the distributor (below the jet) was calculated as a function of the time lag between the two measurements. Figure 6.16 shows the results of this cross correlation. Figure 6.17 shows the maximum cross correlation between length of horizontal supersonic

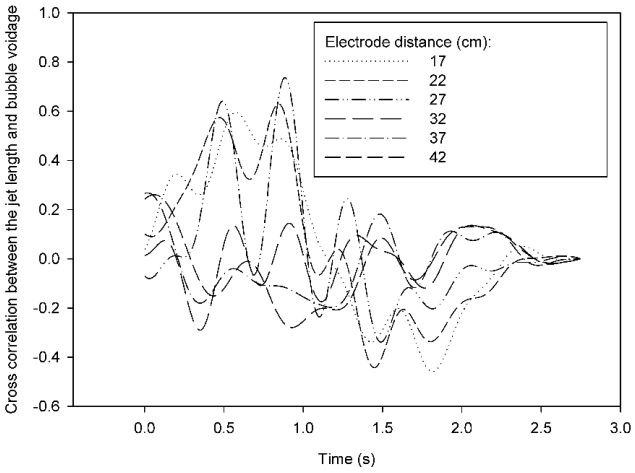

Figure 6.16: Cross correlation between voidages of horizontal supersonic jet and voidages measured with electrodes below the jet with different horizontal distance from the nozzle tip versus time lag (U_f = 0.1 m/s; Nitrogen injected with horizontal nozzle with d_o = 2.4 mm)

jet and voidage measured with electrodes below the jet versus the distance from the nozzle tip. As shown in Figure 6.17, voidages measured with electrodes with distances of 17, 22 and 27 cm from the nozzle are better cross-correlated with the supersonic jet length than voidages measured with electrodes farther from the nozzle. The relatively

high values of the maximum cross correlation integral for the locations corresponding to the jet indicate that the rising gas bubbles hitting the jet from below are the main cause of the jet length fluctuations.

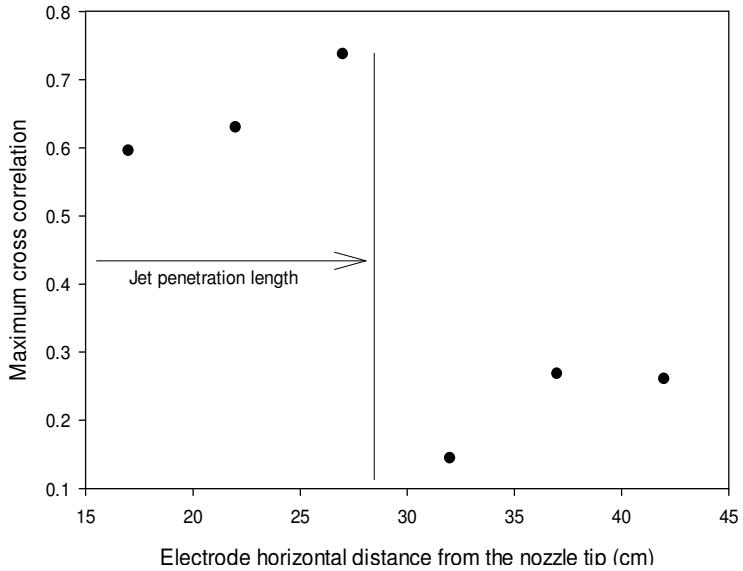

Figure 6.17: Maximum cross correlation between voidages of horizontal supersonic jet and voidages measured with electrodes below the jet versus horizontal distance from nozzle tip (U_f = 0.1 m/s; Nitrogen injected with horizontal nozzle with d_o = 2.4 mm)

The time associated with maximum cross correlation between jet length and voidages close to nozzle, in Figure 6.16, is much larger than the time a bubble needs to travel to the jet location. This indicates that the jet expanded relatively slowly when hit from below by a bubble.

The thrust of the nozzle is calculated using the conditions at nozzle tip:

$$F = \dot{m}U_o + (p_e - p_o)A_e \tag{6.3}$$

The effect of thrust of the nozzle at different nozzle inclination angles and fluidization velocity on the supersonic jet fluctuation has been investigated. The coefficient of variation of supersonic jet length was calculated at different nozzle thrusts, nozzle inclination angles, injected gas densities and fluidization velocities by dividing the

standard deviation of jet length distribution by its mean. Figure 6.18 shows that the coefficient of variation of the supersonic jet length decreases with increasing nozzle thrust, for various nozzle inclinations.

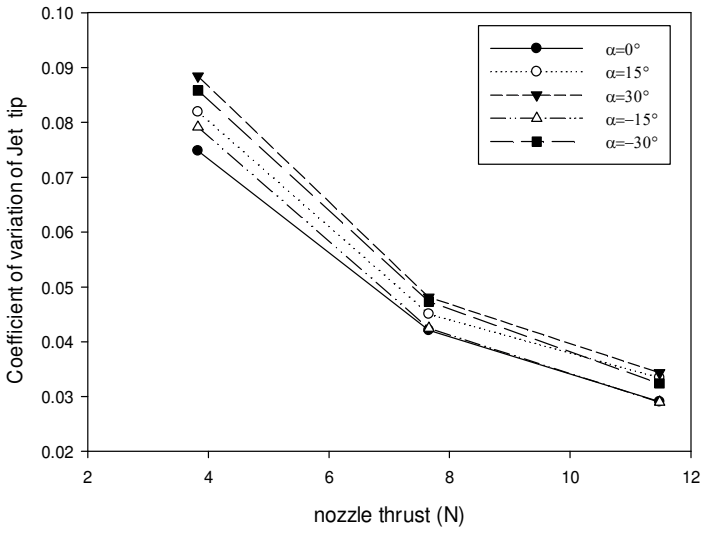

Figure 6.18: Coefficient of variation of supersonic jet length versus nozzle thrust and nozzle inclination angle

When the nozzle thrust increases, the momentum of the supersonic jet increases and this, in turn, reduces the perturbations from the bubbles: the supersonic jet thus becomes more stable. Figure 6.18 also shows that the coefficient of variation of the supersonic jet length increases with increasing nozzle inclination in either upward or downward directions. This is caused by the decrease in the horizontal component of the nozzle thrust caused by the nozzle inclination, which reduces the horizontal stability of the jet when perturbed by gas bubbles.

Figure 6.19 shows that the coefficient of variation of the supersonic length increases almost linearly with increasing fluidization velocity. This stems from the increase in the

size and momentum of the gas bubbles, which results in more frequent and stronger perturbations of the supersonic jet.

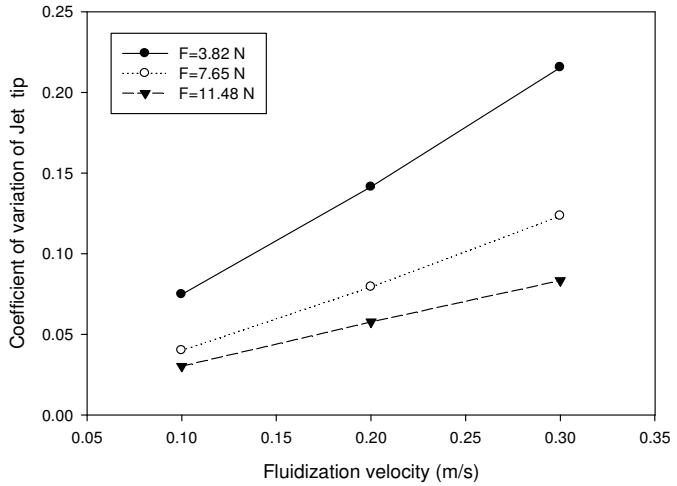

Figure 6.19: Coefficient of variation of horizontal supersonic jet length versus fluidization velocity and nozzle thrust

Figure 6.20 shows that the measured bubble velocity increases almost linearly with increasing fluidization velocity, which explains the increase in the coefficient of variation of the jet length with increasing fluidization velocity.

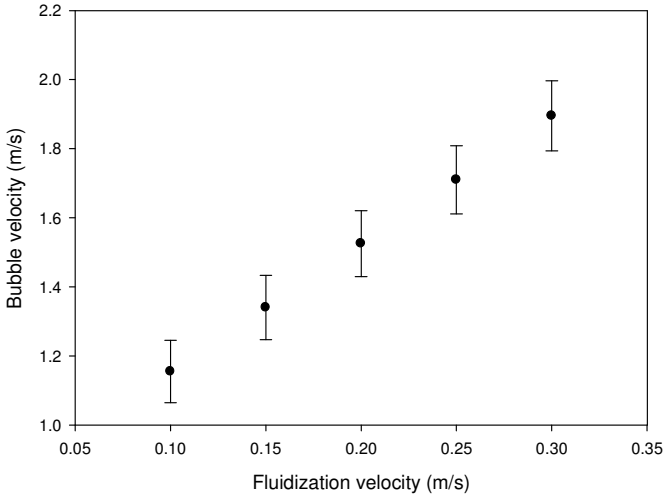

Figure 6.20: Bubble velocity with 95% confidence interval versus fluidization velocity

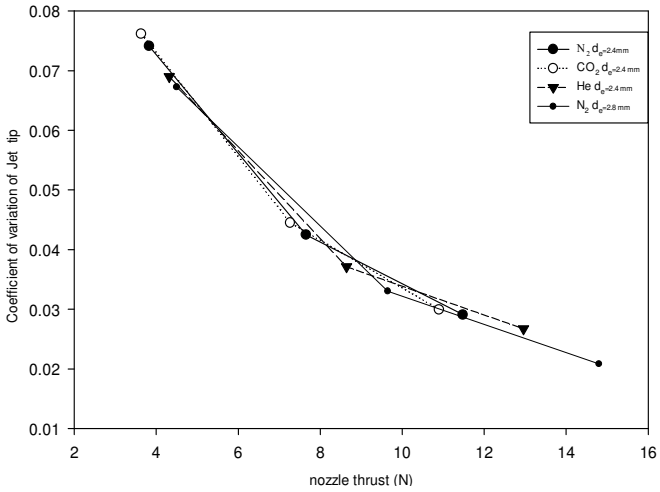

Figure 6.21: Coefficient of variation of supersonic jet length versus nozzle thrust with different injection gases and nozzle diameters

According to Figure 6.21, there was no considerable change in the coefficient of variation of the supersonic jet length when the gas molecular weight or the nozzle size was changed while keeping the nozzle thrust constant. This confirms that the nozzle thrust is the most important nozzle parameter for the jet length fluctuations.

6.3.3. Empirical correlation for supersonic jet fluctuations

Since no correlation has yet been proposed for supersonic gas jet fluctuations, a new empirical correlation is developed. Assuming that the coefficient of variation of the supersonic jet tip depends on the horizontal component of the jet thrust (F cos(α)) and on the flowrate of gas bubbles (Uf – Umf) in the fluidized bed, the generic form of relationship can be expressed as:

$$CV\left(L_{jet}\right) = 1.81\,\frac{(U_f - U_{mf})^{0.76}}{(F\cos(\alpha_{jet}))^{0.86}} \qquad (6.4)$$

Where CV represents the coefficient of variation, F represents the thrust of the nozzle and α is the nozzle inclination angle. The correlation fits the experimental data with a R-value

of 0.99. Figure 6.22 shows the excellent agreement between the predicted coefficient of variation and all the experimental values obtained in this study.

6.4. Conclusions

The effects of fluidization velocity, nozzle gas mass flux, nozzle gas density, nozzle diameter and nozzle inclination on the penetration length of a supersonic jet were investigated using capacitance sensors, a non-invasive measurement method.

The measured time-averaged jet penetration was predicted well with the modified Benjelloun's correlation for subsonic jets. The fluctuations of the supersonic jet length were analyzed and a new correlation was developed accounting for the effects of injection gas mass flowrate, nozzle inclination angle and fluidization velocity. The results demonstrate that the jet is more stable at higher nozzle thrusts, lower nozzle inclination angles and lower fluidization velocities. Nozzle size and gas composition do not have a significant impact on the coefficient of variation of the jet length, for a constant thrust.

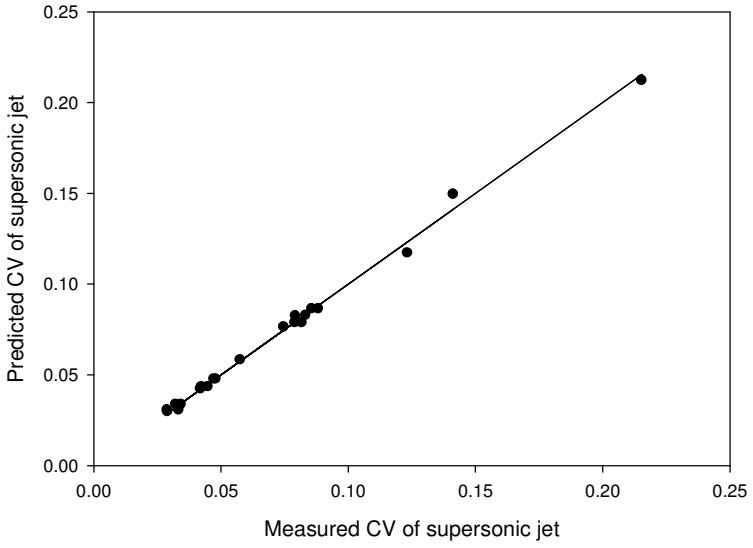

Figure 6.22: Predicted CV of supersonic jet versus measured CV of supersonic jet at different nozzle thrust, nozzle inclination angles and fluidization velocities

6.5. References

Ariyapadi S, Berruti F, Briens C, McMillan J, Zhou D, Horizontal penetration of gas-liquid spray jets in gas-solid fluidized beds, Intl. J. Chem. Reactor Eng. 2(1) (2004)1542-6580

Benjelloun F, Liegeois R, Vanderschuren J, Penetration length of horizontal gas jets into atmospheric fluidized beds, Proc. Fluidization-VIII, J-F. Large and C.

Cruz N, Briens C, Berruti F, Effect of thrust on supersonic gas jet penetration in gas-solid fluidized beds, Powder Technology, 214(1) (2011) 38-46.

Dawe M, Briens C, Berruti F, Study of Horizontal Sonic Gas Jets in Gas-Solid Fluidized Beds, The 12th International Conference on Fluidization - New Horizons in Fluidization Engineering,4(96) (2007).

Dunlop D. D, Griffin J. L. I, Moser J. J. F, Chemical Engineering Progress, 54(8) (1958) 39-42.

Guohua L, Jiyu Z, Bijiang Z, The behavior of gas flow ejected from two vertical nozzles in a fluidized bed, Chinese Journal of Chemical Engineering 5(3) (1997) 280–286.

Hong R, Li H, Li H, Wang Y, Studies on inclined jet penetration length in a gas-solid fluidized bed, 92(3) (1997) 205-212

Hong R.Y, Guo Q.J, Luo G.H, Zhang J.Y, Ding J, On the jet penetration height in fluidized beds with two vertical jets, Powder Technology 133(1-3) (2003) 216–227.

Laguerie Eds., Engineering Foundation, N.Y. (1995) 239-246.

Liu M, Zhang Y, Bi H, Grace J.R, Zhu Y, Non-intrusive determination of bubble size in a gas-solid fluidized bed: An evaluation, Chemical Engineering Science 65(11) (2010) 3485–3493.

Luo G.H, Zhang J.Y, Zhang B.J, The behavior of gas flow ejected from two vertical nozzles in a fluidized bed, Chinese Journal of Chemical Engineering 3 (1997) 280–285.

Merry J.D, Penetration of a horizontal gas jet into a fluidized bed, Trans. Instn Chem. Eng. 49 (1971)189-195

Shen Z, Briens C.L, Bergougnou M.A, Jet presence probability in a two-dimensional fluidized bed, Powder Technology, 67 (1991) 93-101

Vaccaro S, Musmarra D, Petrecca M, Evaluation of the jet penetration depth in gas-fluidized beds by pressure signal analysis, Int. J. Multiphase Flow 23(4) (1997) 683-698.

Wang F, Yu Z, Marashdeh Q, Fan L., Horizontal gas and gas/solid jet penetration in a gas–solid fluidized bed, Chemical Engineering Science 65(11) (2010) 3394–3408.

Xie C.G, Huang S.M, Hoyle B.S, Thorn R, Lenn C, Snowden D, Beck M.S, "Electrical capacitance tomography for flow imaging: system model for development of image reconstruction algorithms and design of primary sensors." IEE Proc. G, 139(1) (1992) 89-98.

Zhong W.Q, Zhang M.Y, Jet penetration depth in a two-dimensional spout fluidized bed, Chemical Engineering Science 60 (2005) 315–327.

CHAPTER 7: EFFECT OF BOGGING ON GAS AND GAS-LIQUID JET FLUCTUATIONS

7.1. Introduction

Bogging can degrade some fluidized bed processes. In a fluidized bed, bogging usually happens when particles become cohesive due to injected liquid or a high bed temperature that melts some of the bed material. This results in uneven distribution of the gas, poor solid mixing and defluidized zones (Briens, 1999). Bogging can decrease the yield of reaction in different ways including affecting the particle size distribution, bed hydrodynamics and fluctuations of the jet cavity formed by liquid atomized into the bed.

In many processes where liquid is injected into a fluidized bed, good liquid distribution on the bed particles is essential to achieve high yields of valuable products and maintain good reactor operability. The effect of feed jet fluctuations on the liquid distribution can be inferred from previous works. Several studies have explored how wet agglomerates are formed when liquid is injected into a fluidized bed. Ariyapadi et al. studied the structure of gas-liquid jets in fluidized beds and calculated the penetration distance and jet expansion angle using digital X-ray imaging (Ariyapadi, 2003). Ariyapadi et al. observed that agglomerates form at the tip of the jet cavity, which suggests that horizontal fluctuations of the gas-liquid jet cavity plays an important role in agglomerate formation (Ariyapadi, 2003). McMillan studied the local quality of solid-liquid mixing in the fluidized bed on a short time scale (McMillan, 2007). She observed that a liquid rich

region forms at the core of the jet cavity, while solid particles exist mainly at the annular region of the jet, and the quality of the liquid distribution can be improved by enhancing radial mixing within the jet cavity, which is affected by jet fluctuations. Saha et al. studied the formation of agglomerates when a high velocity, pure gas attrition jet interacts with the gas-liquid jet (Saha, 2007). He found that the agglomerate size can be reduced by using smaller attrition jets around the periphery of the main gas-liquid jet.

The above mentioned studies suggest that gas-liquid jet fluctuations is of importance to decrease the size of the agglomerates that are formed when liquid is atomized into a fluidized bed. Although several works have been published to investigate the effect of bogging on bed hydrodynamics, there has not been a study to investigate the effect of bogging on liquid-solid jet fluctuations.

The objective of this paper is, thus, to study the effect of bogging on the fluctuations of gas and gas-liquid jets under various conditions.

7.2. Experimental

7.2.1. Experimental set up

Experiments were conducted in a 1.97 m high fluidized bed with a trapezoidal cross sectional area, as shown in Figure 7.1. Coke particles with a Sauter mean diameter of 144 μm and a total mass of 42 kg were used for all the experiments. The bed was fluidized with air at a superficial velocity ranging from 0.1 to 0.2 m/s.

The tip of the nozzle for all experiments was located 0.245 m above the porous plate gas distributor, and penetrated into the bed 0.06 m from the wall. The bed height was approximately 0.29 m when defluidized, and around 0.35 m when the fluidization velocity was 0.2 m/s. The minimum fluidization velocity was 0.03 m/s for all experiments.

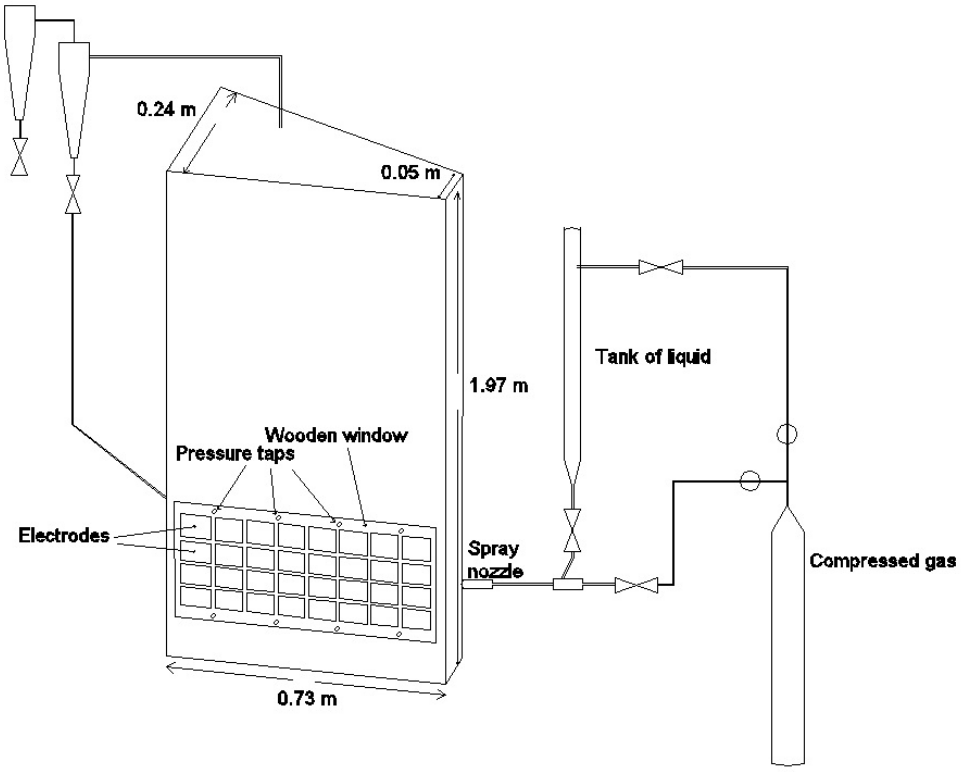

Figure 7.1: Experimental set up

Attrition nozzles were used for gas jet experiments. Two attrition nozzles were tested to determine the effect of nozzle scale on the jet penetration length. Both nozzles were convergent-divergent, Laval-type nozzles with a diameter at the nozzle throat of either 2.4 mm or 2.8 mm, as shown in Figures 7.2 and 7.3. The gas flowrate was ranging between 7 and 22 g/s. For experiments with the gas-liquid jet, a TEB Nozzle with a throat diameter of 2 mm were used (Figure 7.4). The flowrate of liquid was 16 g/s while the gas to liquid ratio was 2% and the injection time was 10 s.

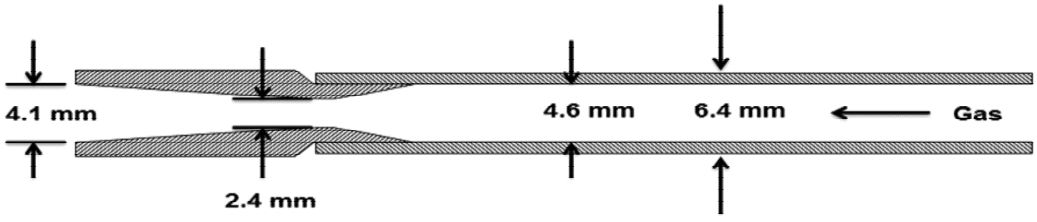

Figure 7.2: Laval type nozzle, d_{th} =2.4 mm

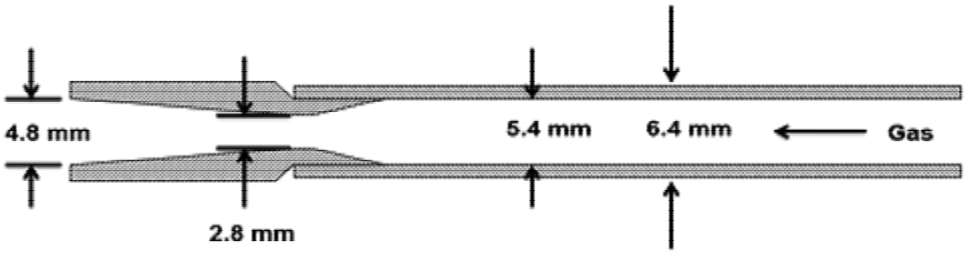

Figure 7.3: Laval type nozzle, d_{th} =2.8 mm

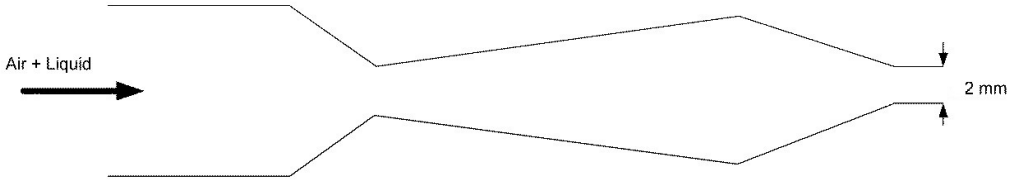

Figure 7.4: Schematic of gas-liquid Spray nozzle

The capacitance meter used in experiments was an AC based circuit with a differential noise cancelling system. Figure 7.1 shows the configuration of 32 electrodes mounted externally on one side of the fluidized bed, on the outside surface of a wooden window, while on the other side one single electrode covered the entire wall, also installed on the outside surface of a wooden window. This electrode was connected to the signal generator, acting as a transmitter, while the rest of electrodes were connected to the virtual ground of the amplifier, functioning as receivers. The capacitance signals were acquired with a frequency of 100 kHz using an analog to digital converter connected to the 32 electrodes through an amplifier and a multiplexer. The multiplexer connected each electrode for 200 μs and then switched to the next electrode. By taking the rms (root mean square) value of the measurements in each 200 μs time window, the capacitance measured by each electrode was sampled at 6.4 ms intervals.

Measurements were performed as Voltesso oil was progressively added to the fluidized bed. Voltesso oil simulates, at room temperature, the properties of heavy oil at the temperature of Fluid CokersTM. Voltesso, which has a negligible vapor pressure at room temperature, was used to provide a constant liquid background during each experiment. Voltesso was mechanically mixed with particles to ensure that all the liquid coated

individual particles and that no coke-Voltesso agglomerates were formed. To study the effect of bogging on the gas jet, pure nitrogen was injected into the fluidized bed of coke particles with different concentrations of Voltesso oil. To study the effect of bogging on the gas-liquid jet, Varsol liquid was atomized with nitrogen into the fluidized bed with different concentrations of Voltesso oil. The mass of Varsol that was not trapped in wet agglomerates at the end of the Varsol injection could be obtained from the capacitance measurements, using a method described in chapter 3.

7.2.2. Measurement of Local Voidage

Coke particles in the fluidized bed have a considerable dielectric constant and can concentrate an electric field within themselves. Using capacitance sensors, the voidage distribution within the fluidized bed could be determined based on the difference in dielectric constant between coke particles and the fluidization gas. The average bed voidage was calculated at different fluidization velocities from the bed pressure drop measured with pressure transducers at different heights within the bed, using Equation 7.1:

$$\frac{\Delta p}{z} = \rho_p(1-\varepsilon)g \qquad (7.1)$$

The bed capacitance was measured at different fluidization velocities and was normalized with respect to the defluidized bed capacitance. Figure 6.5 shows that the average normalized bed capacitance is a linear function of the average bed voidage. The local bed voidage can, thus, be obtained from the normalized capacitance of any electrode, using the linear relationship of Figure 6.5.

7.2.3. Measurement of jet length

Figure 6.7 shows a typical image of the voidage distribution of the horizontal gas supersonic jet obtained by the capacitance sensors method at a nozzle mass flowrate of 0.014 kg/s while the fluidization velocity was 0.1 m/s. The supersonic jet penetration length is defined here as the distance between the nozzle tip and the farthest point on the supersonic jet axis where the voidage is equal to the average of the maximum jet voidage and of the bed voidage at the same height (Figure 6.7). Since the horizontal resolution of

the image is 8 pixels, a polynomial curve fitting of order 7 was used to specify the voidage at any point in the row and enable the accurate calculation of supersonic jet length.

The gas-liquid jet penetration was measured with the same definition of gas jet length but liquid holdup was used instead of gas holdup or voidage. Since in this case, three dielectric materials i.e. gas, liquid and coke particles co-exist at the same time, the dielectric of gas and coke particles merged together by averaging the time series of capacitance over a time period. This time period was 200 ms assuming the gas holdup is constant during 200 ms regarding the bubble frequency which is greater than 5 Hz.

7.3. Distribution of Jet length

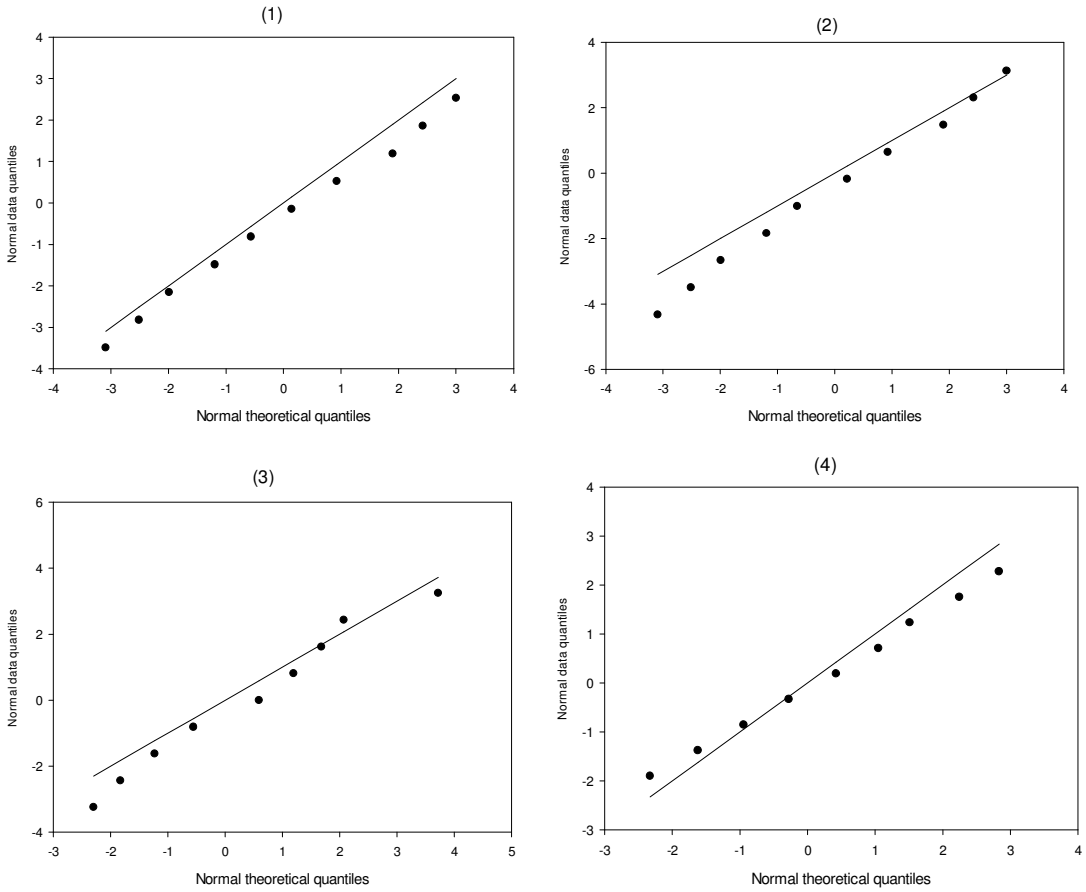

Figure 7.5: q-q plot of 1,2: gas jet length at oil mass fraction of 0.25% and 0.3% 3,4:gas-liquid jet length at oil mass fraction of 0.25% and 0.3% (U_f=0.1m/s)

An earlier study showed that in a dry fluidized bed, the probability distribution of the instantaneous length of a gas or gas-liquid jet follows a Gaussian distribution. Figure 7.5 shows that, in a bogged fluidized bed, the probability is also Gaussian. This means that in both dry and bogged beds, the probability distribution of the instantaneous jet length can be fully characterized with its average and standard deviation.

7.4. Results and Discussion

7.4.1. Effect of Bogging on Gas Jet Length

The effect of bogging and fluidization velocity on the gas and gas-liquid jet was investigated, when the fluidized bed was operated with a constant fluidization velocity and Voltesso oil was added to coke particles in several steps until serious bogging occurred. In each step, the capacitance as well as pressure were measured.

Figure 7.6 shows the average gas jet length measured at different concentrations of Voltesso oil and fluidization velocities. According to Figure 7.6, the average gas jet length is almost constant until the concentration of Voltesso oil reaches 0.2% and it increases gradually with increasing oil concentration past this point.

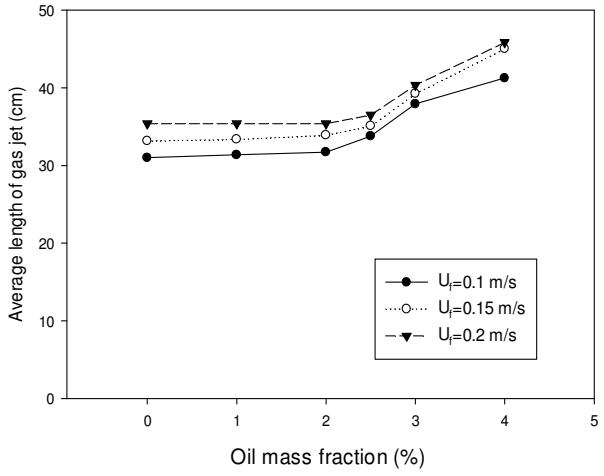

Figure 7.6: Average length of gas jet versus mass fraction of Voltesso oil at different fluidization velocities

To understand the impact of oil concentration in gas jet penetration, the bed density was obtained from the pressure drop between two vertically separated pressure taps within the bed (Figure 7.1), using Equation 7.1. Figure 7.7 shows the measured pressure drop versus Voltesso oil concentration at different fluidization velocities.

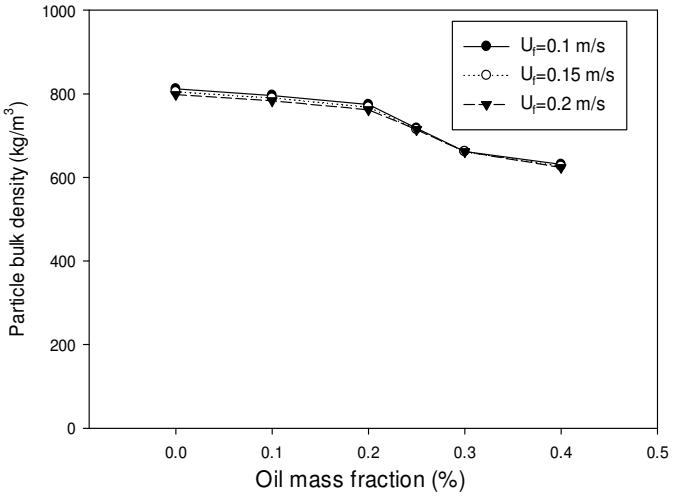

Figure 7.7: Particle bulk density versus mass fraction of Voltesso oil at different fluidization velocities

According to Figure 7.7, the bulk density of particles decreases with increasing Voltesso concentration. The average length of gas jet, therefore, should simultaneously increase according to the correlation published by Hong et al. where $(1-\varepsilon)\rho_p$ represents the bed density (Hong, 1997):

$$\frac{L_{jet}}{d_0} + 3.8 = C\left[\frac{\rho_e U_0^2}{(1-\epsilon)\rho_p g d_p}\right]^{0.327}\left[\frac{\rho_f}{\rho_p}\right]^{1.974}\left[\frac{d_p}{d_0}\right]^{-0.04} \quad (7.2)$$

Figure 7.8 shows the comparison between the measured average gas jet length and the predicted value from Equation 7.2, using the measured bed density. The average penetration length of the gas jet becomes greater than the predicted value after initial point of bogging, suggested that the effect of bogging is not fully captured by the concomitant change in bed density.

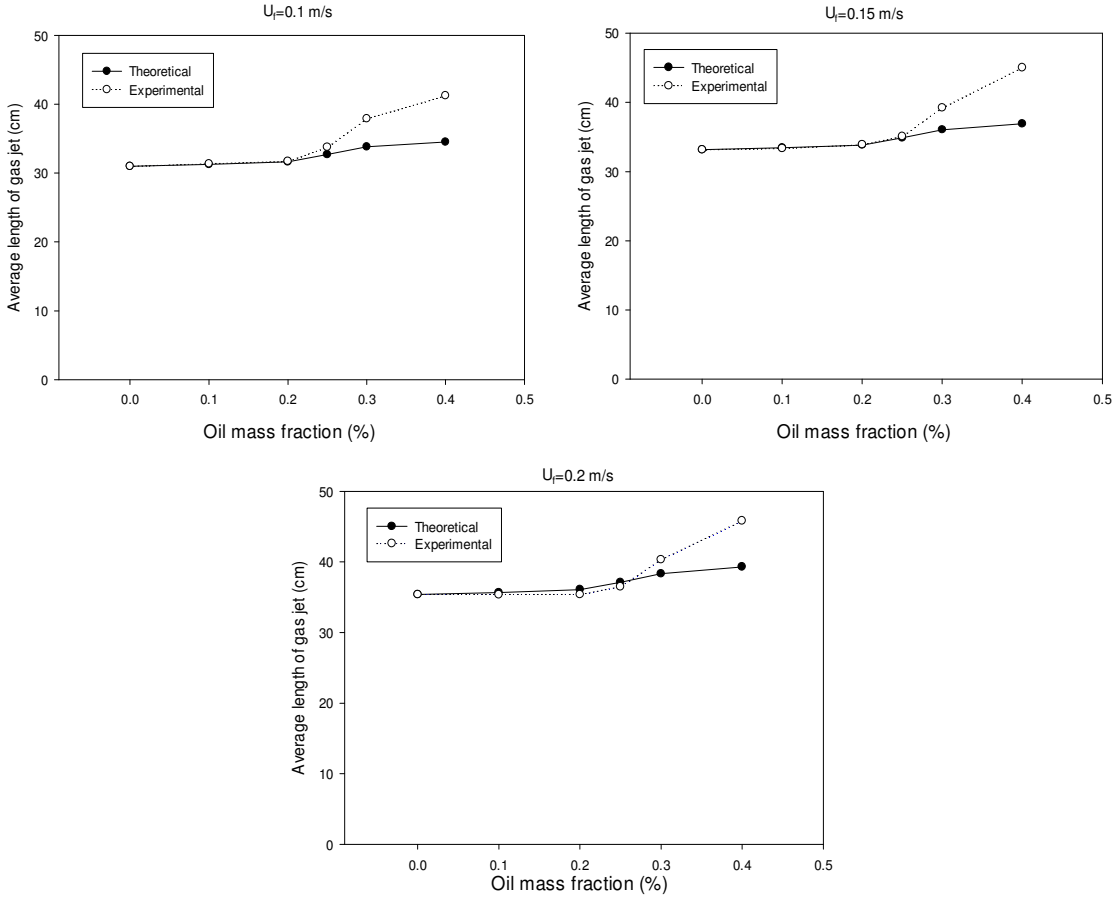

Figure 7.8: Comparison of measured and expected average gas jet length at different fluidization velocities

Figure 7.9 shows the coefficient of variation of gas jet length measured at different Voltesso oil concentrations and fluidization velocities (standard deviation divided by mean). At first, the coefficient of variation of the gas jet length decreases gradually with increasing Voltesso oil fraction, and then drops sharply as bogging conditions are reached, for a Voltesso oil fraction of 0.25%.

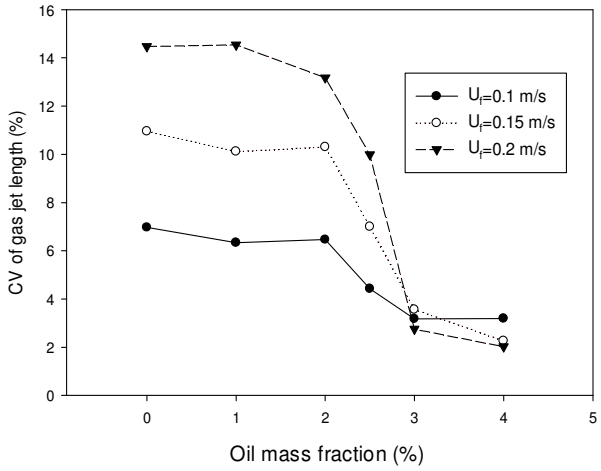

Figure 7.9: CV of gas jet length versus mass fraction of Voltesso oil at different fluidization velocities

This can be explained by the increase in complete fluidization velocity as bogging conditions are reached, as shown in Figure 7.11. The complete fluidization velocity was calculated from the variation in measured bed pressure drop with the superficial gas velocity at different concentrations of Voltesso oil (Figure 7.10).

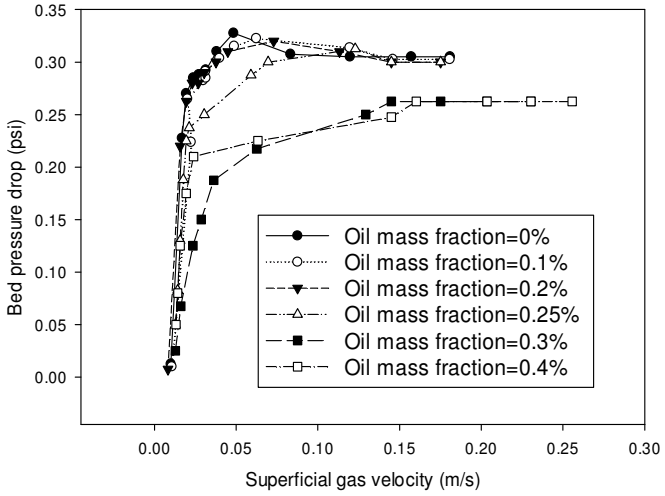

Figure 7.10: Bed pressure drop versus superficial gas velocity at different concentrations of Voltesso oil

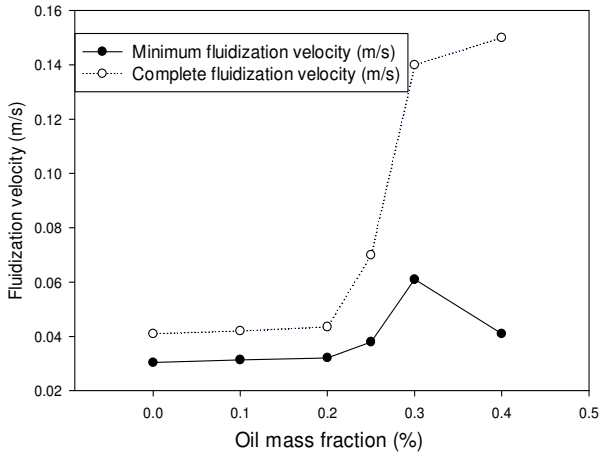

Figure 7.11: Complete and minimum fluidization velocity at different concentrations of Voltesso oil

The correlation developed for CV of the gas jet in the chapter 6 can be used to predict the decrease in the CV of the gas jet.

$$CV\left(L_{jet}\right) = 1.81\frac{(U_f - U_{mf})^{0.76}}{(Fcos(\alpha))^{0.86}}$$

(7.3)

Where CV represents the coefficient of variation, F represents the thrust of the nozzle and α is the nozzle inclination angle. In this correlation, the complete fluidization velocity has been used instead of the minimum fluidization velocity since the minimum fluidization velocity is difficult to measure In beds of cohesive particles. Figure 7.12 compares the predicted coefficient of variation calculated using Equation 7.3 and its measured value, for the gas jet. Before the initial point of bogging, values are close but under fully bogged conditions, predicted values are less than the experimental values, presumably because of partial defluidization and uneven gas distribution.

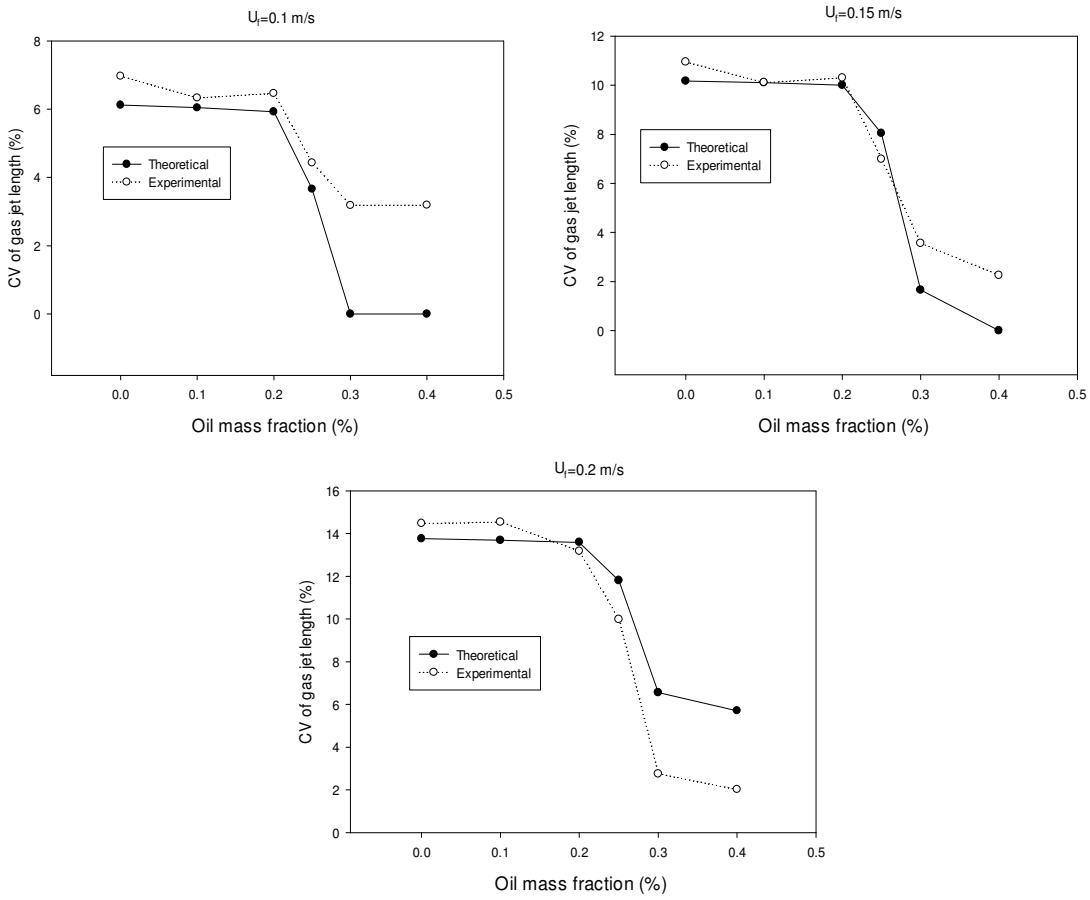

Figure 7.12: Comparison of measured and expected CV of gas jet length at different fluidization velocities

7.4.2. Effect of Bogging on Gas-Liquid Jet Length

Figure 7.13 shows the gas-liquid jet length versus time at different concentrations of Voltesso oil. In the dry bed and at low Voltesso oil concentrations, the jet length varies substantially with time in an apparent periodic fashion with a strong random component. When the Voltesso oil is higher than the minimum concentration for bogging (0.25 wt%), the gas-liquid jet length is higher at the beginning of the injection and decreases as the increasing liquid concentration caused by the injected liquid increases the degree of bogging in the bed.

Figure 7.14 shows the effect of bogging on the time-averaged length of the gas-liquid jet. The length of gas-liquid jet slightly decreases under bogging conditions. This is the opposite of what was observed with the gas jet (Figure 7.6) and may be explained by the

increase in effective particle size due to formation of more agglomerates at the time of Varsol injections. The mass of injected Varsol that was trapped in agglomerates was calculated by measuring the free Varsol with capacitance sensors (chapter 3).

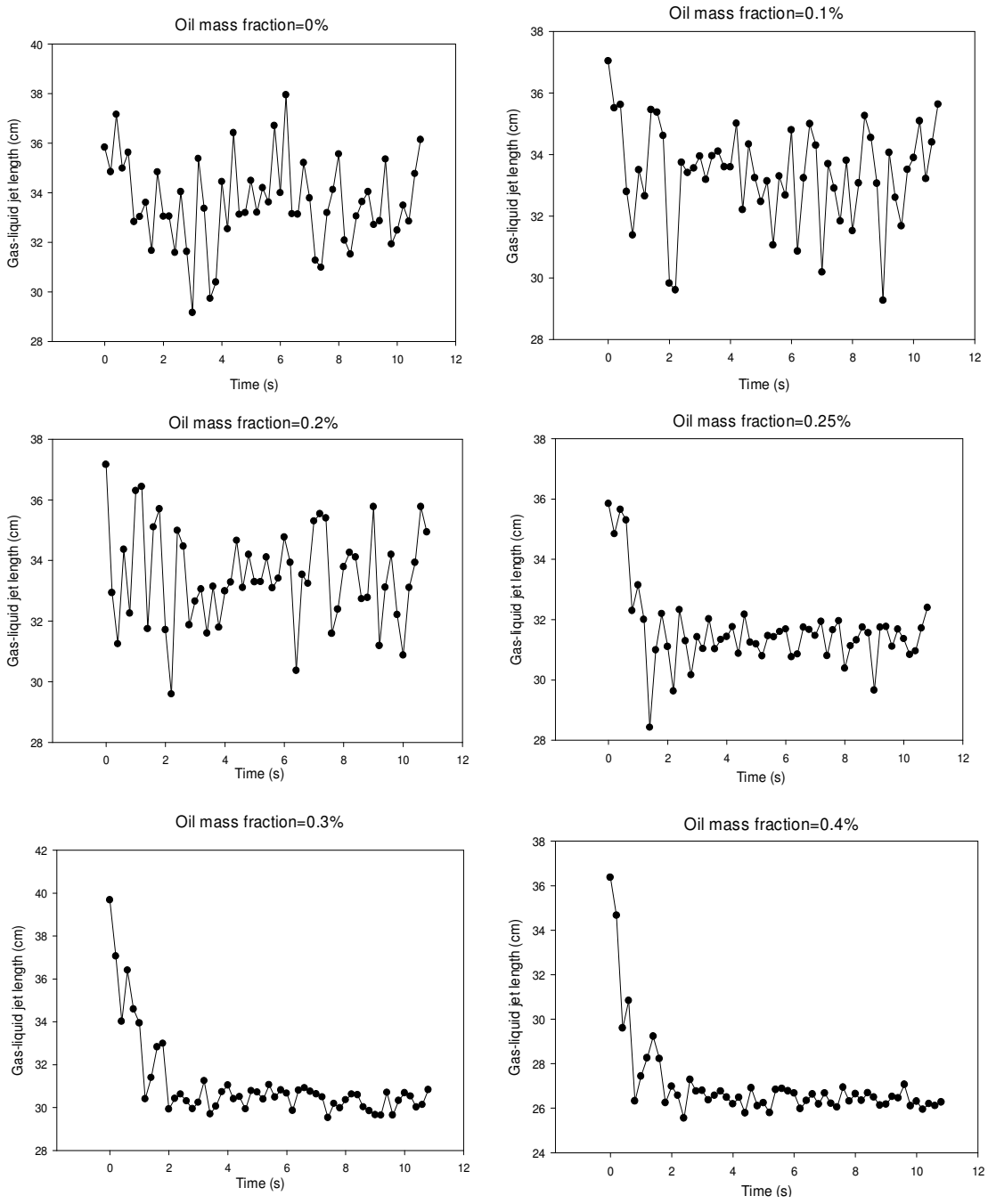

Figure 7.13: Gas-liquid jet length versus time at different concentrations of Voltesso oil (U_f=0.1 m/s)

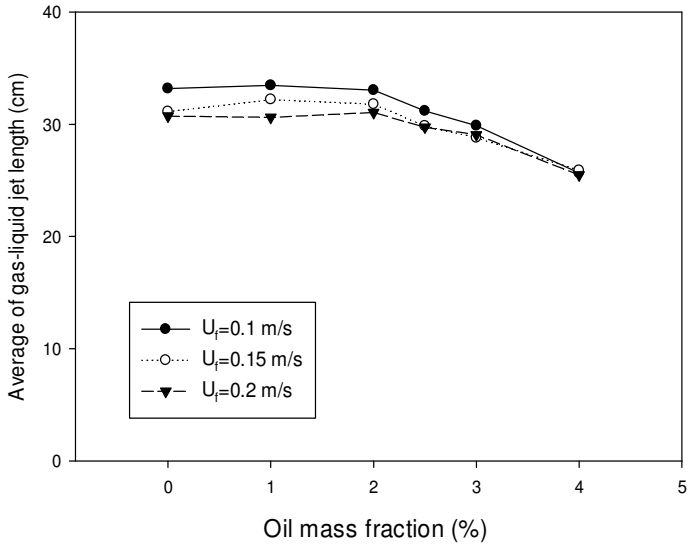

Figure 7.14: Average length of gas-liquid jet versus mass fraction of Voltesso oil at different fluidization velocities

Figure 7.15 shows that the mass of Varsol that was not trapped in agglomerates decreased with increasing Voltesso oil fraction, indicating the detrimental impact of bogging on the distribution of the sprayed liquid on the bed particles (House, 2004).

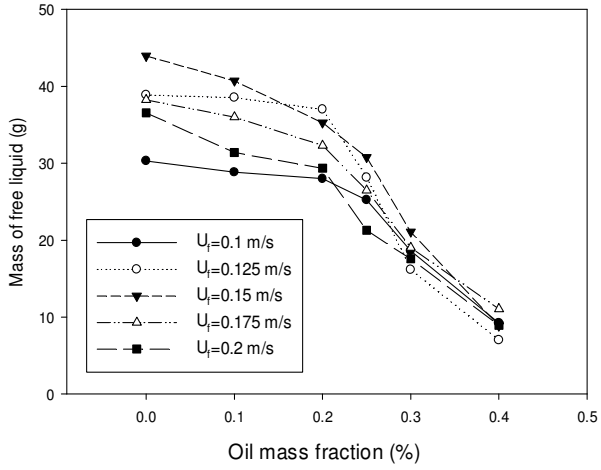

Figure 7.15: Measured mass of free injected Varsol liquid versus mass fraction of Voltesso oil at different fluidization velocities

Figure 7.16 shows the effect of bogging on the coefficient of variation of the gas-liquid jet length. According to the Figure 7.16, the coefficient of variation of the gas-liquid jet length decreases with increasing in Voltesso oil mass fraction.

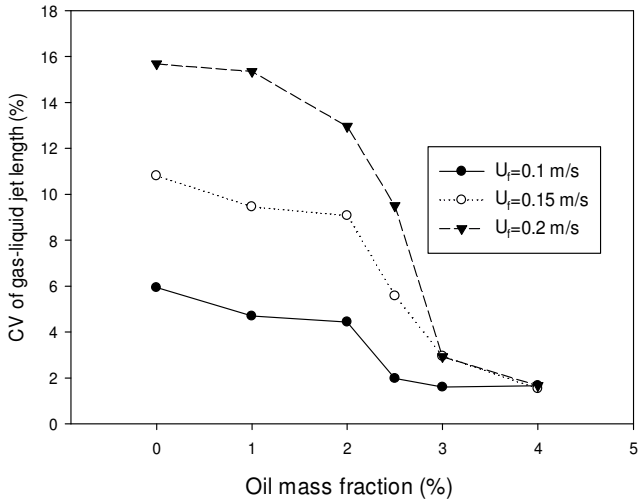

Figure 7.16: CV of length of liquid-gas jet versus mass fraction of Voltesso oil at different fluidization velocities

As with the CV of gas jet, a sharp decrease occurs at the 0.25% Voltesso oil fraction that corresponds to the initial point of bogging. The decrease in the CV of gas-liquid jet can be explained by the increase in the complete fluidization velocity and the concomitant decrease in the bubble flow rate as shown in the Figure 7.10. Figure 7.17 shows that there was good agreement between the measured CV of the gas-liquid jet length and values predicted using Equation 7.3.

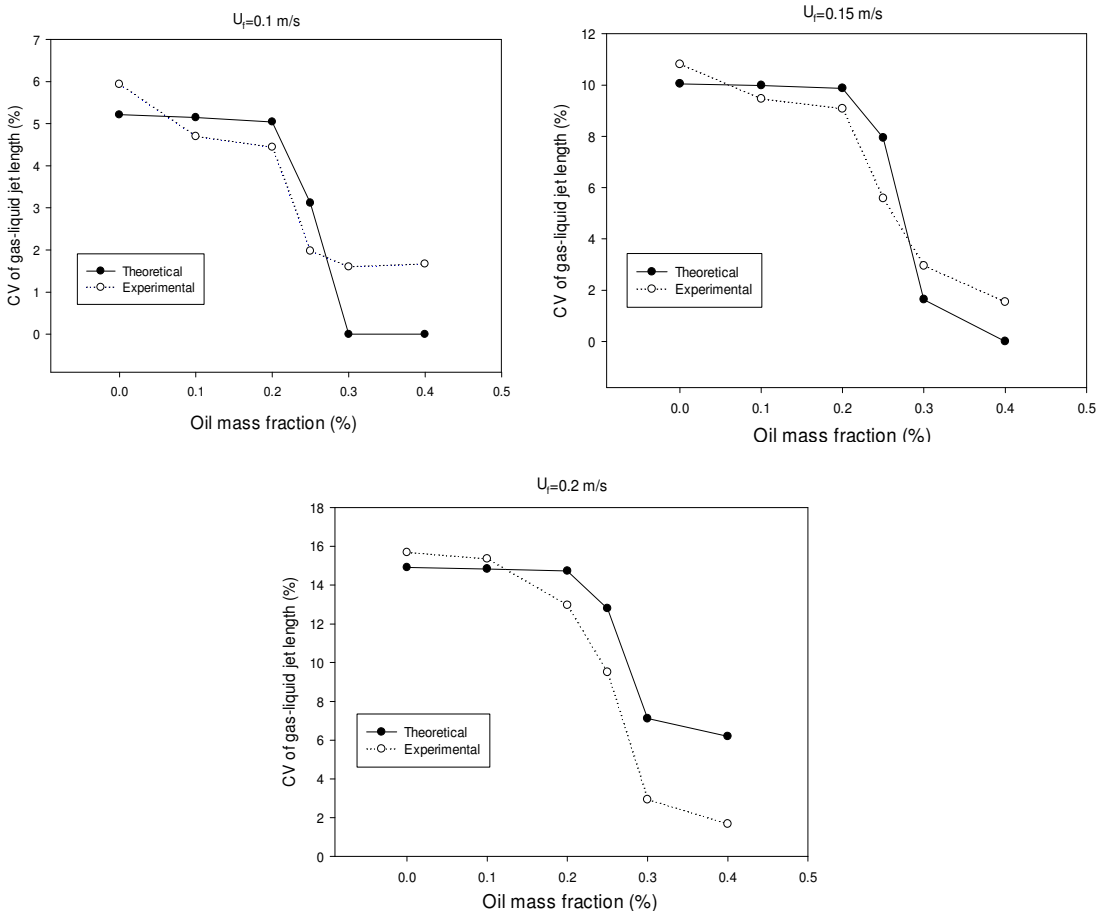

Figure 7.17: Comparison of measured and expected CV of liquid-gas jet length at different fluidization velocities

7.4.3. Effect of Bogging on the Frequency of Jet Fluctuations

The frequency of the jet fluctuations is reported as the dominant frequency from the frequency spectrum of the jet length fluctuations. Bubble frequency was also obtained using the same technique from the time series of measured capacitance below the jet. Figure 7.18 shows the frequency of fluctuations of gas jet and gas liquid jet at different concentrations of Voltesso oil. The frequency of the fluctuations of the gas jet is considerably higher than the frequency of fluctuations of the gas-liquid jet. The main explanation for the difference between the two types of jets, since both their time-averaged jet length and its coefficient of variation are similar, is the difference in the injected gas flowrates: 7 to 22 g/s for gas jet and 0.32 g/s for gas-liquid jet.

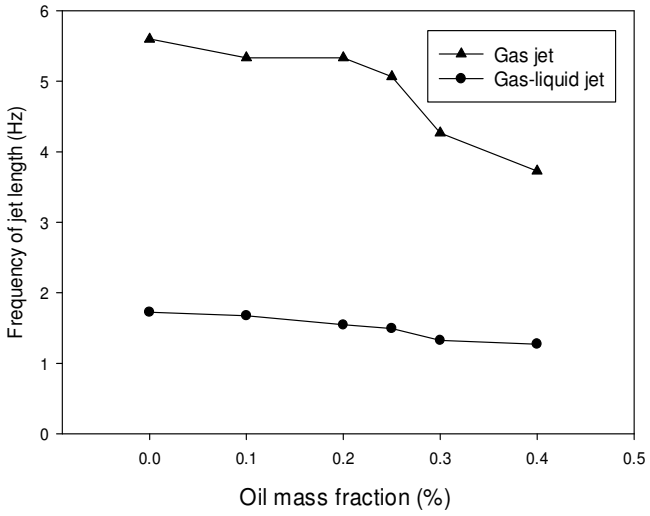

Figure 7.18: Frequency of fluctuations of gas jet and gas-liquid jet length at different Voltesso oil mass fractions (U_f=0.1 m/s)

As it can be seen in the Figure 7.18, both frequencies decreases with the increase in Voltesso oil mass fraction. The underlying reason can be explained with mass balance Equation for the gas flow rate if the jet boundary be considered as the control volume for a specific period of time:

$$F_b + F_g = N_b \times V_b \quad (7.4)$$

Where F_b represents the gas flow rate enters the jet as bubbles, F_g represents the gas flow rate of nozzle, N_b is number of bubbles release from the jet and V_b represents the average volume of bubbles release from the jet. Since the bubble frequency decreases with the increase in Voltesso oil concentration as it is shown in Figure 7.19, assuming the negligible change in bubble size and nozzle gas flow rate, the frequency of jet length fluctuations should decrease.

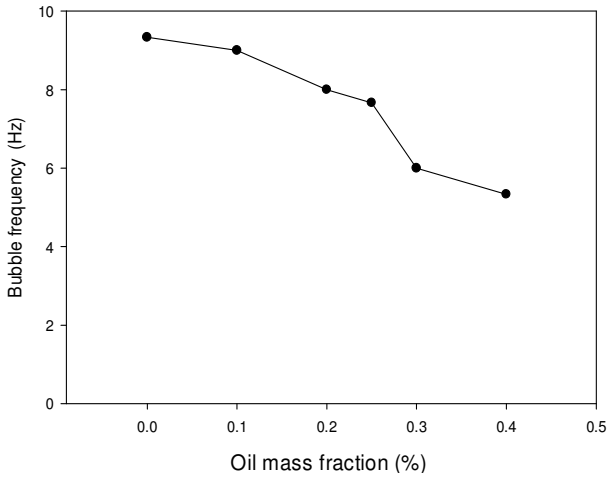

Figure 7.19: Bubble frequency at different Voltesso oil mass fractions (Uf=0.1 m/s)

7.5. Conclusion

Bogging increases the average length of gas jets but decreases the average length of liquid jets, while the amplitude of the jet fluctuations decreases with bogging in both cases.

The frequency of jet fluctuations decreases with increasing oil mass fraction in the bed due to the concomitant decrease in bubble frequency. Results were interpreted with published correlations for jet length in the fluidized bed.

7.6. References

Ariyapadi, S., Holdsworth, D., Norley, C, Berruti, F., Briens, C, "Digital X-Ray imaging technique to study the horizontal injection of gas-liquid jets into fluidized beds" Int. J. Chem. React. Eng., 1 (A56), 1114 (2003).

Briens C.L, Briens L.A, Barthel E, Le Blevec J.M, Tedoldi A, Margaritis A. "Detection of local fluidization characteristics using the V statistic" Powder Technology 102(1): 95-103 (1999).

Hamidi, M. Berruti, F. Briens, C. McMillan, J. “Bogging Detection in a Fluidized Bed Using Plannar Capacitance Sensors” The 14th International Conference on Fluidization – From Fundamentals to Products (2013)

Hamidi, M. Berruti, F. Briens, C. McMillan, J. “Study of supersonic jets fluctuations in gas-solid fluidized beds with capacitance sensors” (2014)

Hong, R. Li, H. Li, H. Wang,Y., “Studies on inclined jet penetration length in a gas-solid fluidized bed”, 92(3) 205-212 (1997).

House, P.K., Saberian, M., Briens, C.L., Berruti, F., Chan, E. “Injection of a liquid spray into a fluidized bed: particle–liquid mixing and impact on fluid coker yields” Ind. Eng. Chem. Res. 43, 5663–5669 (2004)

McMillan, J., “Characterization of the interactions between high velocity jets and fluidized particles”, Ph.D. dissertation, The University of Western Ontario, London, Canada. 2007.

Saha, M., “simultaneous particle agglomeration and attrition in the fluidized bed”, Ph.D. dissertation, The University of Western Ontario, London, Canada. 2007.

CHAPTER 8: CONCLUSIONS AND RECOMMENDATIONS

8.1. Conclusions

Thanks to sophisticated cancelation of capacitive and inductive coupling noise, a new capacitance sensor can image jets, bubbles and evaluate the distribution of liquid on the solid particles. This non-invasive sensor enables the measurement of voids as well as "free liquid", i.e. liquid that is not trapped within agglomerates in a fluidized bed. The rate at which liquid is released from breaking agglomerates can be measured with this sensor.

Bogging greatly affects liquid distribution. The changes in liquid caused by bogging were found to correlate well with changes in particle cohesivity that, in turn, affect the properties of the gas bubbles.

Several methods have been developed to detect the onset of bogging:

- The standard deviation of bubble frequencies, as measured with the new capacitance sensors.
- A new bogging index based on the wavelet decomposition of pressure fluctuations, which performs better than other methods using pressure fluctuations. The new bogging index was developed from the observed changes with bogging of sound transmission at different frequencies through the fluidized bed.
- The measured speed of sound in a fluidized bed. A theoretical model confirmed that the changes in bubbles properties that result from bogging affect the transmission of sound through the fluidized bed.

The new capacitance sensors were used to study jet cavity fluctuations in fluidized beds. Two types of jets were investigated: the supersonic gas jets used for particle attrition in fluidized beds and the jets formed when liquid is atomized with a gas into a fluidized bed. A new correlation was developed to predict the fluctuations of the jet penetration in fluidized beds. Bogging greatly affects jet fluctuations, as suggested by correlations developed in this thesis.

8.2. Recommendations

The following directions are suggested for future research:

1. For evaluation of developed bogging detection methods, more experiments are suggested to investigate the effect of temperature on each bogging index.
2. For the standard deviation of bubble frequency, more experiments are suggested to study the effect of bed scale up.
3. For the correlation developed for supersonic jet fluctuations, experiments with 3D capacitance tomography are suggested to measure the fluctuations of supersonic jet length at all dimensions.

APPENDIX A

This appendix shows measured bubble frequency at locations of 8 side electrodes in the fluidized bed (Figure 3.1) at different concentrations of Voltesso oil. Electrode 1 is the closest one to the nozzle while electrode 8 is the farthest one from the nozzle.

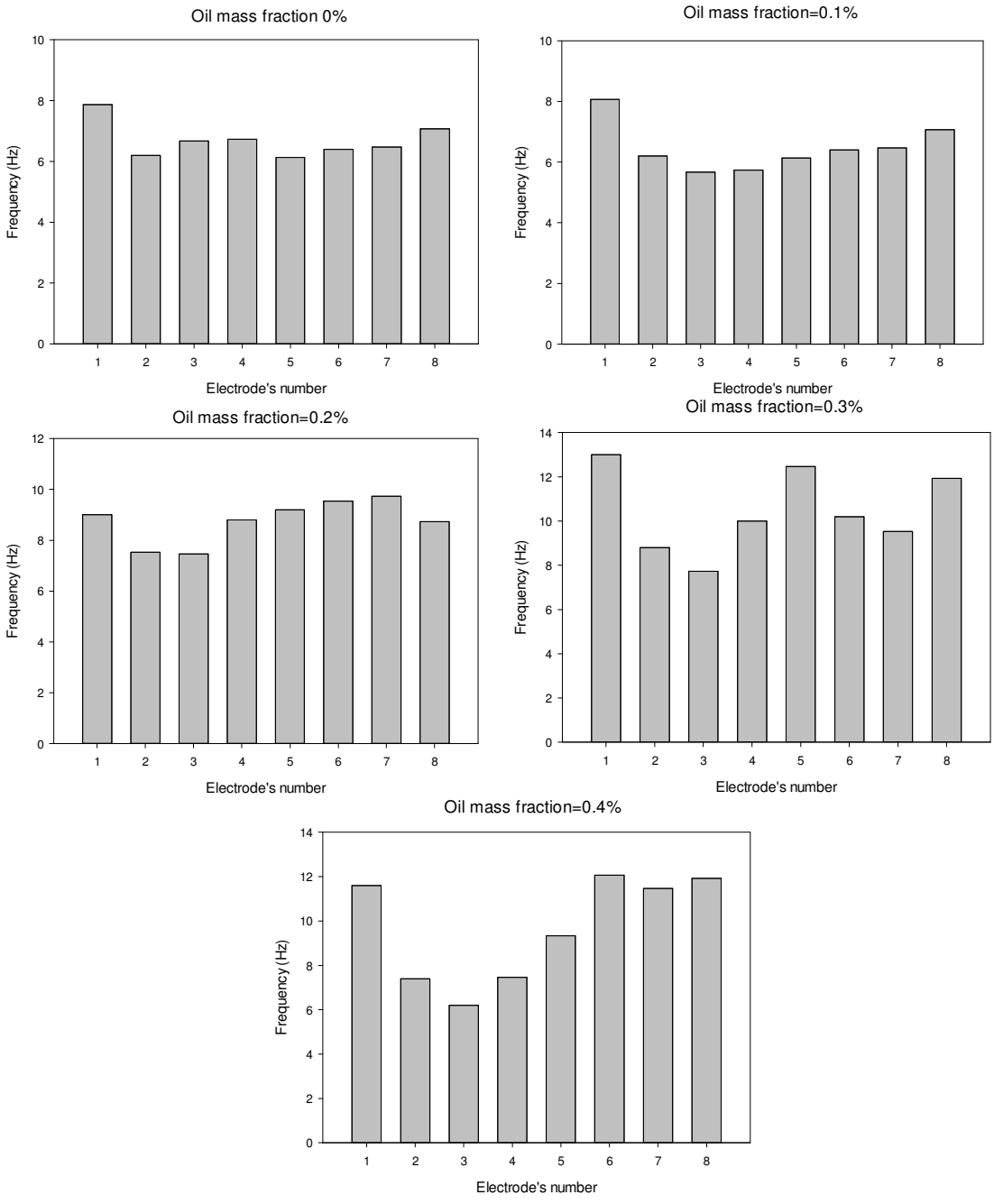

Bubble frequency versus concentrations of Voltesso oil (U_f=0.1 m/s)

APPENDIX B

Kolmogorov- Smirnov test

The Kolmogorov–Smirnov test is a statistical test of the equality of one-dimensional continuous probability distributions. The Kolmogorov–Smirnov test can be used to compare a sample probability distribution with a reference probability distribution, or to compare two sample probability distributions. The Kolmogorov–Smirnov statistic is defined as a statistical distance between the cumulative probability distribution functions of two samples. The null hypothesis for the test is that the samples are taken from the same probability distribution.

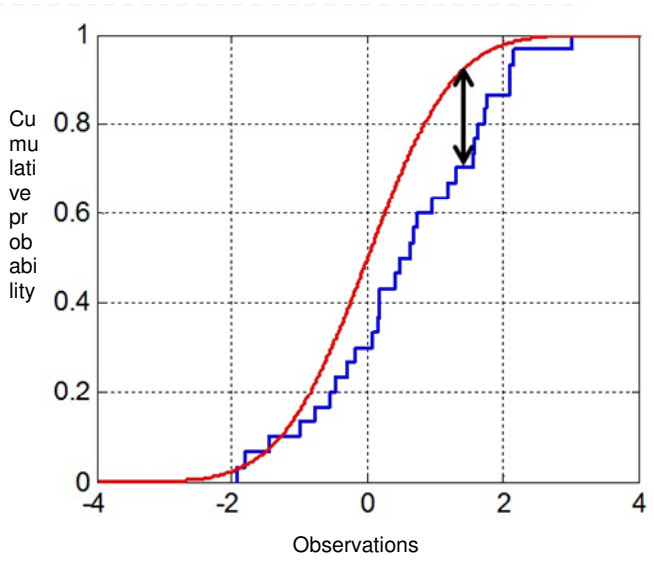

Kolmogorov - Smirnov test - two cumulative probability distributions are shown with red and blue lines while the black arrow is the Kolmogorov- Smirnov statistic

For $F_{1,n}$ and $F_{2,n'}$ as the cumulative probability distribution functions of the first and the second sample respectively, the Kolmogorov-Smirnov statistic is defined as

$$D_{n,n'} = \sup_x |F_{1,n}(x) - F_{2,n'}(x)|,$$

Where $\sup_x$ is the supremum function. The null hypothesis is rejected at level α if

$$D_{n,n'} > c(\alpha)\sqrt{\frac{n+n'}{nn'}}.$$

The value of c(α) is given in the table below for each level of α

α	0.10	0.05	0.025	0.01	0.005	0.001
c(α)	1.22	1.36	1.48	1.63	1.73	1.95

VITAE

Name:	Majid Hamidi
Post-Secondary Education and Degrees	Western University London, Ontario, Canada 2010-2014 Ph.D., Chemical Engineering
	Sharif University of technology Tehran, Iran 2003-2005 M.Sc., Electrical Engineering
	Iran University of Science and Technology Tehran, Iran 1999—2003 B.Sc., Electrical Engineering
Related Work	Teaching Assistant and Research Assistant Western University, London, Canada 2010-2014

Publications:

Hamidi, M. Berruti, F. Briens, C. McMillan, J. “Bogging Detection in a Fluidized Bed Using Plannar Capacitance Sensors” The 14th International Conference on Fluidization – From Fundamentals to Products (2013)

Mohagheghi, M., M. Hamidi, C. Briens, F. Berruti and J. McMillan. "Study of the Effectof Local Hydrodynamics on Liquid Distribution in a Gas-Solid Fluidized Bed using a Capacitance Method." *Fuel*. Retrieved 12 April 2013.

Mohagheghi, M., M. Hamidi, C. Briens, F. Berruti and J. McMillan. "The Effects of Liquid Properties and Bed Hydrodynamics on the Distribution of Liquid on Solid Fluidized Particles in a Cold-Model Fluidized Bed." *Powder Technology* 256:5-12. Retrieved 19 June 2014.